Electronic Supplementary Information (ESI)

Vanadium(V) complexes derived from triphenylphosphonium and hydrazides: Cytotoxicity evaluation and interaction with biomolecules

Francisco Mainardi Martins[a], Bernardo Almeida Iglesias[b], Otávio Augusto Chaves[c,d], Jean Lucas Gutknecht da Silva[e], Daniela Bitencourt Rosa Leal[e] and Davi Fernando Back[1]*

[a]Laboratory of Inorganic Materials, Department of Chemistry, CCNE, UFSM, Santa Maria - RS - Brazil - 97105-900.

[b]Laboratory of Bioinorganic and Porphyrin Materials, Department of Chemistry, CCNE, UFSM, Santa Maria - RS - Brazil - 97105-900.

[c]CQC-IMS, Department of Chemistry, University of Coimbra, Rua Larga s/n, Coimbra, Portugal - 3004-535.

[d]Laboratory of Immunopharmacology, Centro de Pesquisa, Inovação e Vigilância em COVID-19 e Emergências Sanitárias (CPIV), Oswaldo Cruz Institute (IOC), Oswaldo Cruz Foundation (Fiocruz), Rio de Janeiro – RJ – Brazil - 21040-361.

[e]Laboratory of Experimental and applied immunobiology, CCNE, Santa Maria - RS - Brazil - 97105-900.

Corresponding author: E-mail: davi.f.back@ufsm.br. Fax number: +55 (55) 3220-8031.

Electronic Supplementary Information caption

S1 Synthesis procedures and spectroscopic data of 5-(chloromethyl)-2-hydroxybenzaldehyde, **[AH]Cl**, **[H_2L1]Cl**–**[H_2L5]Cl,** and **C1**–**C5**

S1.1 5-(chloromethyl)-2-hydroxybenzaldehyde

For this synthesis, an experimental procedure already published was used, but with some modifications.[1] In a 250 mL round bottom flask, 8 g of paraformaldehyde and 60 mL of hydrochloric acid were added. Under constant magnetic stirring, 150 mmol of salicylaldehyde (18.32 g; 15.65 mL) and a few drops of sulfuric acid were added, evidencing the initial formation of a beige colored solid. This reaction mixture was maintained under constant magnetic stirring and under heating in an oil bath at 50 °C for 48 hours (Scheme 1).

After this period, the solid formed was separated by filtration and the solid was washed with 200 mL of deionized water. The solid was solubilized with dichloromethane. After filtration and evaporation of the solvent at room temperature, a light beige solid was obtained. This solid was solubilized in a 1:1 (v/v) acetonitrile (MeCN) and dichloromethane (CH_2Cl_2) mixture. By slow evaporation of the solvent at room temperature, light beige single crystals suitable for X-ray diffraction were obtained. The purity of the compound was sufficient to proceed to the following reactions.

(23.30 g, 91.1 %). mp 79 °C (from MeCN/CH_2Cl_2). ν_{max}/cm^{-1} (FT-IR) 3209br (OH), 3069w $(C–H)_{aromatic}$, 2966w $(C–H)_{aliphatic}$, and 1650s (C=O). ν_{max}/cm^{-1} (FT-Raman) 3071w $(C–H)_{aromatic}$, 2967w $(C–H)_{aliphatic}$, and 1651s (C=O). δ_H(600 MHz; $CDCl_3$; Me_4Si) 4.58 (2 H, s, CH_2), 6.97, 6.98 (1 H, d, $CH_{aromatic}$), 7.53–7.55 (1 H, m, $CH_{aromatic}$), 7.57, 7.57 (1 H, d, $CH_{aromatic}$), 9.87 (1 H, s, $CH_{aldehyde}$), and 11.05 (1 H, s, OH). δ_C(151 MHz; $CDCl_3$; Me_4Si) 45.24, 118.28, 120.33, 129.21, 133.64, 137.31, and 161.57.

S1.2 (3-formyl-4-hydroxybenzyl)triphenylphosphonium chloride (**[AH]Cl**)

For this synthesis, an experimental procedure already published was used, but with some modifications.[2,3] This reaction was carried out in a system under an inert atmosphere of argon. In a 100 mL round bottom flask, 5.00 mmol of 5-(chloromethyl)-2-hydroxybenzaldehyde (0.853 g) was dissolved in 20 mL of toluene. Under magnetic stirring and heating in an oil bath at 80 °C, 5.50 mmol of triphenylphosphane (1.443 g) dissolved in 20 mL of toluene was added slowly via a dropping funnel. As a result, a light beige precipitate initially forms. The reaction system was heated to 100 °C and the conditions of temperature, stirring and inert atmosphere were maintained for 6 hours (Scheme 1).

After this, the solid was separated by filtration and purified by washing with 30 mL of hot toluene and 10 mL of diethyl ether. After drying at open atmosphere, the solid was solubilized in methanol (MeOH). After slow evaporation of the solvent at room temperature, light yellow single crystals suitable for X-ray diffraction were obtained.

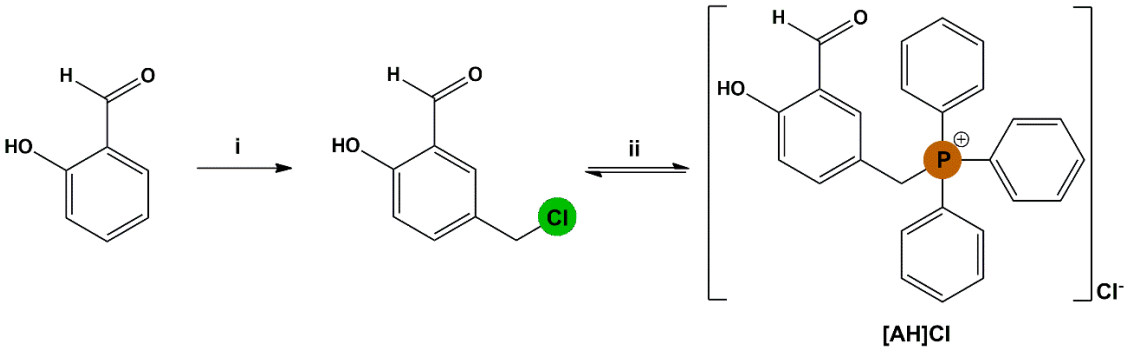

i = Paraformaldehyde, HCl, H_2SO_4 (drops), 50 °C, 48 hours
ii = Triphenylphosphane, toluene, argon, 100 °C, 6 hours

Scheme S1 Synthesis of 5-(chloromethyl)-2-hydroxybenzaldehyde and **[AH]Cl**.

(1.93 g, 89.2 %). mp 246 °C (decomposition, from MeOH). ν_{max}/cm^{-1} (FT-IR) 3022w $(C–H)_{aromatic}$, 2963w $(C–H)_{aliphatic}$, and 1674s (C=O). ν_{max}/cm^{-1} (FT-Raman) 3063s $(C–H)_{aromatic}$, 2964w $(C–H)_{aliphatic}$, and 1664s (C=O). δ_H(600 MHz; DMSO-d_6) 5.15, 5.18 (2 H, d, CH_2), 7.02, 7.04 (1 H, d, $CH_{aromatic}$), 7.07–7.09 (1 H, m, $CH_{aromatic}$), 7.21–7.22 (1 H, t,

$CH_{aromatic}$), 7.67–7.76 (12 H, m, $CH_{aromatic}$), 7.88–7.91 (3 H, m, $CH_{aromatic}$), 10.16 (1 H, s, $CH_{aldehyde)}$, and 11.27 (1 H, s, OH). δ_C(151 MHz; DMSO-d_6) 27.10, 27.41, 117.42, 117.96, 117.99, 118.01, 122.48, 122.50, 130.07, 130.15, 134.02, 134.08, 135.08, 135.09, 137.95, 137.98, 160.94, 160.96, and 189.35. $\delta^{31}{}_P$(243 MHz; DMSO-$d_{6;}$ PPh_3) 22.02.

S1.3 Synthesis and spectroscopic data of the ligands **[H_2L1]Cl**–**[H_2L5]Cl**

The ligands **[H_2L1]Cl** and **[H_2L5]Cl** have already been synthesized by S. T. Chew and collaborators, however using ethanol as solvent.[3,4] The first one also reported the crystallographic structure of **[H_2L1]Cl.**[3] In a 50 mL round bottom flask, 0.30 mmol of (3-formyl-4-hydroxybenzyl)triphenylphosphonium chloride (**[AH]Cl**, 0.130 g) and 0.30 mmol of the respective hydrazide (benzoic, 0.040 g; nicotinic, 0.041 g; isonicotinic, 0.041 g; 3-hydroxy-2-naphthoic, 0.061 g, and 4-fluorobenzoic, 0.046g) were solubilized in 20 mL of methanol. The mixture was maintained under constant magnetic stirring and heating in an oil bath at 70°C for 6 hours (Scheme 2).

After this, the resulting yellow or orange (**[H_3L4]Cl**) mixture was filtered to remove any residual precipitate and the solution was added to small vials. After slow evaporation of methanol at room temperature, light yellow single crystals suitable for X-ray diffraction of ligands, with exception of **[H_3L4]Cl**, were obtained. The crystalline material was washed with 2 mL of ethanol and 10 mL of diethyl ether. **[H_3L4]Cl** was purified by silica gel column chromatography with 85:15 (v/v) acetonitrile/methanol mixture as eluent.

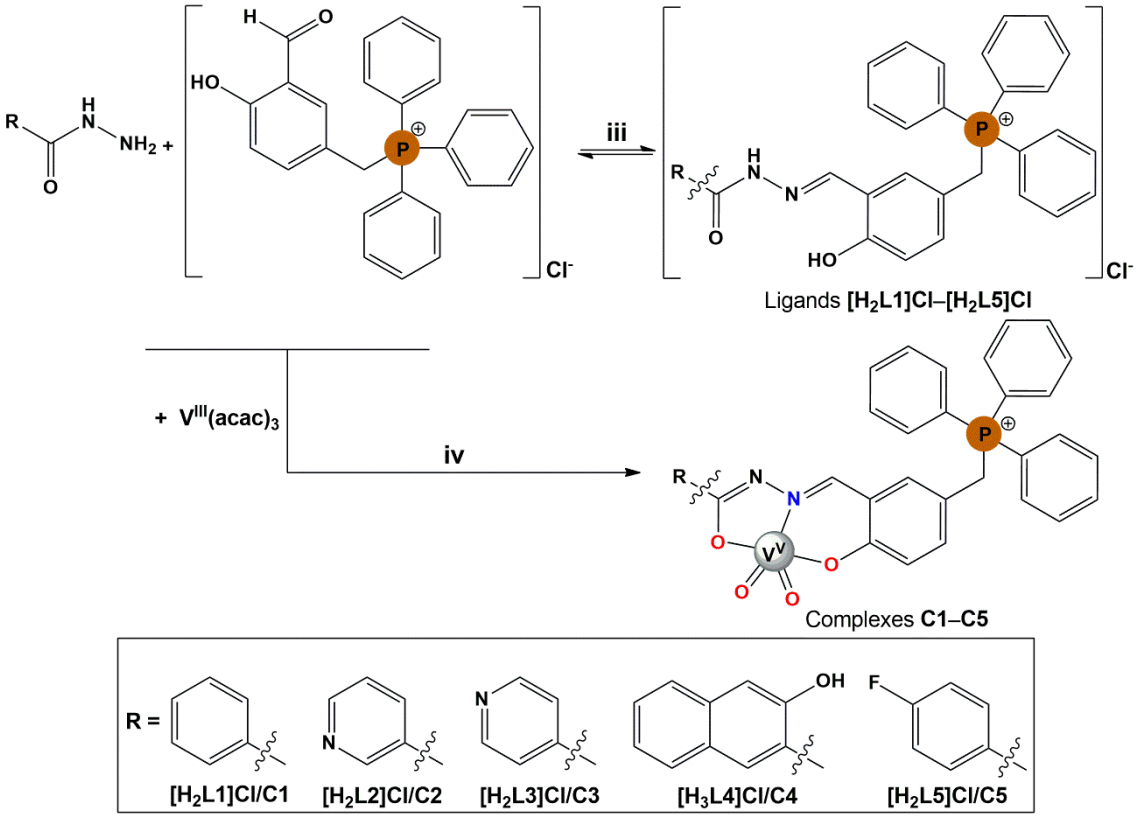

iii = Methanol, 70 °C, 6 hours
iv = Triethylamine or 1,8-diazabicyclo[5.4.0]undec-7-ene, methanol, 70 °C, 2 hours

Scheme S2 General synthesis of ligands **[H_2L1]Cl**–**[H_2L5]Cl** and complexes **C1**–**C5**

S1.3.1 Ligand {(*E*)-{3-[(2-benzoylhydrazono)methyl]-4-hydroxybenzyl}triphenylphosphonium chloride (**[H_2L1]Cl**)

Derived from benzoic hydrazide. (0.093 g, 56.3 %). mp 247 °C (from MeOH). (Found: C, 71.92; H, 5.10; N, 5.08. Calc. for $C_{33}H_{28}ClN_2O_2P$: C, 71.93; H, 5.12; N, 5.08 %). ν_{max}/cm^{-1} (FT-IR) 3388br (O–H), 3055w (C–H)$_{aromatic}$, 2948w (C–H)$_{aliphatic}$, 1664s (C=O), and 1615m (C=N). ν_{max}/cm^{-1} (FT-Raman) 3062w (C–H)$_{aromatic}$, 1663w (C=O), and 1616m (C=N). δ_H(600 MHz; DMSO-d_6) 5.16, 5.18 (2 H, d CH_2), 6.84–6.88 (2 H, m, $CH_{aromatic}$), 7.19 (1 H, s, $CH_{aromatic}$), 7.50–7.53 (2 H, t, $CH_{aromatic}$), 7.58–7.61 (1 H, m, $CH_{aromatic}$), 7.68–7.77 (12 H, m, $CH_{aromatic}$), 7.89–7.91 (3 H, t, $CH_{aromatic}$), 8.03, 8.04 (2 H, d, $CH_{aromatic}$), 8.66 (1 H, s, N=CH), 11.49 (1 H, s, OH), and 12.53 (1 H, s, NH). δ_C(151 MHz; DMSO-d_6) 27.32, 27.62, 116.92, 117.57, 118.05, 118.11, 118.14, 119.27, 119.29, 127.83, 128.46, 130.06, 130.14, 131.41, 131.45, 131.98, 132.59, 133.11, 133.14, 134.04, 134.10, 135.08, 135.09, 146.81, 157.30, 157.31, and 162.70. $\delta^{31}{}_P$(243 MHz; DMSO-d_6; PPh_3) 21.85.

S1.3.2 Ligand {(*E*)-{4-hydroxy-3-[(2-nicotinoylhydrazono)methyl]benzyl}triphenylphosphonium chloride (**[H_2L2]Cl**)

Derived from nicotinic hydrazide. (0.060 g, 36.2 %) mp 249 °C (from MeOH). (Found: C, 69.62; H, 4.91 N, 7.58. Calc. for $C_{32}H_{27}ClN_3O_2P$: C, 69.63; H, 4.93; N, 7.61 %). ν_{max}/cm^{-1} (FT-IR) 3048m $(C–H)_{aromatic}$, 2795m $(C–H)_{aliphatic}$, 1670s (C=O), and 1627m (C=N). ν_{max}/cm^{-1} (FT-Raman) 3059m $(C–H)_{aromatic}$, 1669m (C=O), and 1628s *v*(C=N). δ_H(600 MHz; DMSO-d_6) 5.13, 5.16 (2 H, d, CH_2), 6.84–6.88 (2 H, m, $CH_{aromatic}$), 7.23 (1 H, s, $CH_{aromatic}$), 7.55–7.57 (1 H, m, $CH_{aromatic}$), 7.67–7.77 (12 H, m, $CH_{aromatic}$), 7.89–7.91 (3H, t, $CH_{aromatic}$), 8.37–8.39 (1 H, m, $CH_{aromatic}$), 8.65 (1 H, s, N=CH), 8.76 (1 H, d, $CH_{aromatic}$), 9.15 (1 H, s, $CH_{aromatic}$), 11.32 (1 H, s, OH), and 12.66 (1 H, s, NH). δ_C(151 MHz; DMSO-d_6) 27.35, 27.66, 116.94, 116.96, 117.58, 118.14, 118.19, 119.33, 119.34, 123.59, 128.49, 130.11, 130.19, 131.20, 131.24, 133.35, 133.37, 134.05, 134.11, 135.13, 135.14, 135.60, 147.07, 148.86, 152.46, 157.30, 157.32, and 161.37. δ^{31}_P(243 MHz; DMSO-d_6; PPh_3) 21.82.

S1.3.3 Ligand {(*E*)-{4-hydroxy-3-[(2-isonicotinoylhydrazono)methyl]benzyl}triphenylphosphonium chloride (**[H_2L3]Cl**)

Derived from isonicotinic hydrazide. (0.087 g, 52.5 %) mp 274 °C (decomposition, from MeOH). (Found: C, 69.61; H, 4.92; N, 7.60. Calc. for $C_{32}H_{27}ClN_3O_2P$: C, 69.63; H, 4.93; N, 7.61 %). ν_{max}/cm^{-1} (FT-IR) 2796w $(C–H)_{aliphatic}$, 1679s (C=O), and 1627m (C=N). ν_{max}/cm^{-1} (FT-Raman) 3058w $(C–H)_{aromatic}$, 1677w (C=O), and 1628m (C=N). δ_H(600 MHz; DMSO-d_6) 5.08, 5.11 (2 H, 2H, CH_2), 6.80, 6.81 (1 H, d, $CH_{aromatic}$), 6.84–6.87 (1 H, m, $CH_{aromatic}$), 7.26–7.26 (1 H, t, $CH_{aromatic}$), 7.66–7.69 (6 H, m, $CH_{aromatic}$), 7.74–7.77 (6 H, m, $CH_{aromatic}$), 7.85, 7.86 (2 H, d, $CH_{aromatic}$), 7.89–7.91 (3 H, t, $CH_{aromatic}$), 8.54 (1 H, s, N=CH), 8.78, 8.79 (2 H, d, $CH_{aromatic}$), 11.13 (1 H, s, OH), and 12.36 (1 H, s, NH). δ_C(151 MHz; DMSO-d_6): 27.32, 27.64, 116.94, 116.96, 117.57, 119.37, 119.38, 121.71, 130.11, 130.19, 131.04, 131.08, 133.46, 133.49, 134.05, 134.11, 135.13, 135.15, 139.81, 147.39, 150.36, 157.29, 157.31, and 161.24. δ^{31}_P(243 MHz; DMSO-d_6; PPh_3) 21.82.

S1.3.4 Ligand {(*E*)-{4-hydroxy-3-{[2-(3-hydroxy-2-naphthoyl)hydrazono]methyl}benzyl}triphenylphosphonium chloride (**[H_3L4]Cl**)

Derived from 3-hydroxy-2-naphtoic hydrazide. (0.045 g, 24.3 %). mp 178 °C (from MeCN/MeOH). (Found: C, 71.95; H, 4.86; N, 4.51. Calc. for $C_{37}H_{30}ClN_2O_3P$: C, 72.02; H, 4.90; N, 4.54 %). ν_{max}/cm^{-1} (FT-IR) 3054w $(C–H)_{aromatic}$, 2937w $(C–H)_{aliphatic}$, 1663s (C=O), and 1624s (C=N). δ_H(600 MHz; DMSO-d_6) 5.15, 5.18 (2 H, d, CH_2), 6.87 (2 H, s, $CH_{aromatic}$), 7.25 (1 H, s, $CH_{aromatic}$), 7.32–7.35 (1 H, t, $CH_{aromatic}$), 7.38 (2 H, s, $CH_{aromatic}$), 7.48–7.50 (2 H, t, $CH_{aromatic}$), 7.68–7.75 (12 H, m, $CH_{aromatic}$), 7.88–7.91 (3 H, m, $CH_{aromatic}$), 8.62 (1 H, s, $CH_{aromatic}$), 8.64 (1 H, s, N=CH), 11.48 (1 H, s, OH), and 12.36 (1 H, s, NH). δ_C(151 MHz; DMSO-d_6) 27.35, 27.66, 110.59, 116.96, 117.59, 118.15, 119.39, 119.41, 119.68, 123.63, 125.79, 126.67, 128.27, 128.74, 129.97, 130.09, 130.17, 130.48, 131.24, 131.27, 133.31, 133.34, 134.05, 134.11, 135.11,135.98, 147.09, 154.69, 157.40, 157.42, and 164.12. δ^{31}_P(243 MHz; DMSO-d_6; PPh_3) 21.82.

S1.3.5 Ligand {(*E*)-{3-{[2-(4-fluorobenzoyl)hydrazono]methyl}-4-hydroxybenzyl}triphenylphosphonium chloride (**[H_2L5]Cl**)

Derived from 4-fluorobenzoic hydrazide. (0.036 g, 21.1 %). mp 168 °C (from MeOH). (Found: C, 69.64; H, 4.78; N, 4.92. Calc. for $C_{33}H_{27}ClFN_2O_2P$: C, 69.66; H, 4.78; N, 4.92 %). ν_{max}/cm^{-1} (FT-IR) 3388br (O–H), 3056w $(C–H)_{aromatic}$, 2994w $(C–H)_{aliphatic}$, 1667s (C=O), and 1624m (C=N). ν_{max}/cm^{-1} (FT-Raman) 3061w $(C–H)_{aromatic}$, 1668w (C=O), and 1612s (C=N). δ_H(600 MHz; DMSO-d_6) 5.14, 5.16 (2 H, d, CH_2), 6.83–6.87 (2 H, m, $CH_{aromatic}$), 7.19 (1 H, t, $CH_{aromatic}$), 7.34–7.37 (2 H, t, $CH_{aromatic}$), 7.67–7.77 (12 H, m, $CH_{aromatic}$), 7.89–7.91 (3 H, t, $CH_{aromatic}$), 8.10–8.13 (2 H, m, $CH_{aromatic}$), 8.64 (1 H, s, N=CH), 11.43 (1 H, s, OH), and 12.55 (1 H, s, NH). δ_C(151 MHz; DMSO-d_6) 27.35, 27.65, 115.42, 115.57, 116.94, 117.58, 118.15, 119.28, 119.30, 129.09, 129.11, 130.09, 130.17, 130.60, 130.66, 131.40, 131.44, 133.20, 133.23, 134.05, 134.11, 135.12, 135.13, 146.86, 157.30, 157.32, 161.70, 163.48, and 165.14. δ^{19}_F(565 MHz; DMSO-d_6) -107.99. δ^{31}_P(243 MHz; DMSO-d_6; PPh_3) 21.83.

S1.4 Synthesis of the complexes **C1**–**C5**

In a 50 mL round bottom flask, 0.10 mmol of the respective hydrazide (benzoic, 0.014 g; nicotinic, 0.014 g; isonicotinic, 0.014 g; 3-hydroxy-2-naphthoic, 0.020 g, and 4-fluorobenzoic, 0.016 g) and 0.10 mmol of (3-formyl-4-hydroxybenzyl)triphenylphosphonium chloride (**[AH]Cl**, 0.043 g) were solubilized in 10 mL of methanol. The solution was maintained under constant magnetic stirring and heating in an oil bath at 70°C for 30 minutes. After this period, 0.10 mmol of tris(acetylacetonate)vanadium(III) ($V(acac)_3$, 0.035 g) was added at 70°C. Then, triethylamine (Et_3N) or 1,8-diazabicyclo[5.4.0]undec-7-ene (DBU) was added to the reaction 70°C. The deprotonate agent and the amount used for each complex is described along with its spectroscopic data. The reaction system was maintained under the same stirring and heating conditions at 70°C for more 2 hours (Scheme 1).

After this period, the resulting brown mixture was filtered to remove any residual precipitate and the supernatant was added to small vials. After slow evaporation of methanol at room temperature, brown single crystals suitable for X-ray diffraction were obtained. The crystalline materials were separated and washed with ethanol and methanol (5mL each) and the material was dried at 50 °C for 24 hours.

S1.4.1 Complex $[VO_2(L1)]\cdot 2H_2O$ (**C1**)

Derived from benzoic hydrazide. Et_3N (0.20 mmol, 0.020 g, 28 µL) was used. (0.040 g, 61.5 %). mp 182°C (decomposition, from MeOH). (Found: C, 62.66; H, 4.78; N, 4.42. Calc. for $C_{33}H_{26}N_2O_4PV\cdot 2H_2O$: C, 62.60; H, 4.71; N, 4.40 %). ν_{max}/cm^{-1} (FT-IR) 3480br (O–H), 3054w $(C–H)_{aromatic}$, 2959w $(C–H)_{aliphatic}$, 1616m (C=N), 931–915s (V=O), and 829s (V=O). ν_{max}/cm^{-1} (FT-Raman) 3058w $(C–H)_{aromatic}$ and 1616w (C=N). δ_H(600 MHz; DMSO-d_6) 5.06, 5.08 (2 H, d, CH_2), 6.62, 6.63 (1 H, d, $CH_{aromatic}$), 6.84, 6.86 (1 H, d, $CH_{aromatic}$), 7.10 (1 H, s, $CH_{aromatic}$), 7.43–7.50 (3 H, m, $CH_{aromatic}$), 7.69–7.77 (12 H, m, $CH_{aromatic}$), 7.90–7.92 (3 H, t, $CH_{aromatic}$), 7.97, 7.98 (2 H, d, $CH_{aromatic}$), and 8.62 (1 H, s, N=CH). $\delta^{31}{}_P$(600 MHz; DMSO-d_6, PPh_3) 21.13. $\delta^{51}{}_V$(158 MHz; DMSO-d_6; $VOCl_3/C_6D_6$) -537.08.

S1.4.2 Complex $[VO_2(L2)]\cdot CH_3OH\cdot 4H_2O$ (**C2**)

Derived from nicotinic hydrazide. Et_3N (0.20 mmol, 0.020 g, 28 µL) was used. (0.036 g, 51.3 %). mp 183 °C (decomposition, from MeOH). (Found: C, 57.47; H, 5.31; N, 5.95. Calc. for $C_{32}H_{25}N_3O_4PV\cdot CH_3OH\cdot 4H_2O$: C, 57.33; H, 5.23; N, 5.89 %). ν_{max}/cm^{-1} (FT-IR) 3396br (O–H), 3058w $(C–H)_{aromatic}$, 2902w $(C–H)_{aliphatic}$, 1614m (C=N), 918s (V=O), and 827s (V=O). ν_{max}/cm^{-1} (FT-Raman) 3060w $(C–H)_{aromatic}$ and 1616m (C=N). δ_H(600 MHz; DMSO-d_6) 5.07, 5.09 (2 H, d, CH_2), 6.62, 6.64 (1 H, d, $CH_{aromatic}$), 6.85, 6.86 (1 H, d, $CH_{aromatic}$), 7.13 (1 H, s, $CH_{aromatic}$), 7.48–7.50 (1 H, m, $CH_{aromatic}$), 7.69–7.77 (12 H, m, $CH_{aromatic}$), 7.90–7.92 (3 H, t, $CH_{aromatic}$), 8.25, 8.26 (1 H, d, $CH_{aromatic}$), 8.68 (2 H, m, $CH_{aromatic}$ and N=CH overlapping), and 9.12 (1 H, s, $CH_{aromatic}$). δ^{31}_P(243 MHz; DMSO-d_6; PPh_3) 21.17. δ^{51}_V(158 MHz; DMSO-d_6; $VOCl_3/C_6D_6$) -536.97.

S1.4.3 Complex $[VO_2(L3)]\cdot 3H_2O\cdot MeOH$ (**C3**)

Derived from isonicotinic hydrazide. Et_3N (0.20 mmol, 0.020 g, 28 µL) was used. (0.028 g, 42.4 %). mp 198 °C (decomposition, from MeOH). (Found: C, 57.98; H, 5.15; N, 6.14. Calc. for $C_{32}H_{25}N_3O_4PV\cdot 3H_2O\cdot MeOH$: C, 57.95; H, 5.12; N, 6.09 %). ν_{max}/cm^{-1} (FT-IR) 3386br (O–H), 3065w $(C–H)_{aromatic}$, 2945w $(C–H)_{aliphatic}$, 1617s *v*(C=N), 923–892s (V=O), and 849–835s (V=O). ν_{max}/cm^{-1} (FT-Raman) 1617w (C=N). δ_H(600 MHz; DMSO-d_6) 5.07, 5.10 (2 H, d, CH_2), 6.63, 6.64 (1 H, 1H, $CH_{aromatic}$), 6.87, 6.88 (1 H, d, $CH_{aromatic}$), 7.15 (2 H, s, $CH_{aromatic}$), 7.69–7.77 (12 H, m, $CH_{aromatic}$), 7.85 (2 H, s, $CH_{aromatic}$); 7.89–7.92 (3 H, t, $CH_{aromatic}$), and 8.70 (3 H, s, $CH_{aromatic}$ and N=CH overlapping). δ^{31}_P(243 MHz; DMSO-d_6; PPh_3) 21.19. δ^{51}_V(158 MHz; DMSO-d_6; $VOCl_3/C_6D_6$) -536.62.

S1.4.4 Complex $[VO_2(HL4)]\cdot 2CH_3OH$ (**C4**)

Derived from 3-hydroxy-2-naphtoic hydrazide. DBU (0.10 mmol, 0.015 g, 15 µL) was used. (0.035 g, 48.2 %). mp 198 °C (decomposition, from MeOH). (Found: C, 64.42; H, 4.91; N, 3.82. Calc. for $C_{37}H_{28}N_2O_5PV\cdot 2CH_3OH$: C, 64.46; H, 4.99; N, 3.86 %). ν_{max}/cm^{-1} (FT-IR) 3651m (O–H), 3346br (O–H), 3065w $(C–H)_{aromatic}$, 2912w $(C–H)_{aliphatic}$, 1614s (C=N), 941–870s (V=O), and 851–826s (V=O). ν_{max}/cm^{-1} (FT-Raman) 3061w $(C–H)_{aromatic}$

and 1615m (C=N). δ_H(600 MHz; DMSO-d_6) 5.10, 5.12 (2 H, d, CH_2), 6.65, 6.67 (1 H, d, $CH_{aromatic}$), 6.87 (1 H, m, $CH_{aromatic}$), 7.21 (1 H, s, $CH_{aromatic}$), 7.30–7.33 (3 H, m, $CH_{aromatic}$), 7.47–7.49 (1 H, t, $CH_{aromatic}$), 7.71–7.76 (12 H, m, $CH_{aromatic}$), 7.91 (3 H, m, $CH_{aromatic}$), 7.95, 7.96 (1 H, d, $CH_{aromatic}$), 8.49 (1 H, s, $CH_{aromatic}$), 8.89 (1 H, s, N=CH), and 11.98 (1 H, s, $OH_{naphtoic}$. δ^{31}_P(243 MHz; DMSO-d_6; PPh_3) 21.20. δ^{51}_V(158 MHz; DMSO-d_6; $VOCl_3/C_6D_6$) -543.29.

S1.4.5 Complex $[VO_2(L5)]\cdot CH_3OH\cdot H_2O$ (**C5**)

Derived from 4-fluorobenzoic hydrazide. DBU (0.20 mmol, 0.030 g, 30 µL) was used. (0.037 g, 55.7 %). mp 175 °C (decomposition, from MeOH). (Found: C, 61.42; H, 4.67; N, 4.21. Calc. for $C_{33}H_{25}FN_2O_4PV\cdot CH_3OH\cdot H_2O$: C, 61.45; H, 4.70; N, 4.22 %). ν_{max}/cm^{-1} (FT-IR) 3021w $(C–H)_{aromatic}$, 2886w $(C–H)_{aliphatic}$, 1615s (C=N), 931–884s (V=O), and 853–811s (V=O). ν_{max}/cm^{-1} (FT-Raman) 3065w $(C–H)_{aromatic}$ and 1617m (C=N). δ_H(600 MHz; DMSO-d_6) 5.06, 5.08 (2 H, d, CH_2), 6.61, 6.63 (1 H, d, $CH_{aromatic}$), 6.85, 6.86 (1 H, d, $CH_{aromatic}$), 7.10 (1 H, s, $CH_{aromatic}$), 7.26–7.28 (2 H, t, $CH_{aromatic}$), 7.69–7.77 (12 H, m, $CH_{aromatic}$), 7.89–7.92 (3 H, t, $CH_{aromatic}$), 8.00-8.03 (2 H, t, $CH_{aromatic}$), and 8.61 (1 H, s, N=CH). δ^{19}_F(158 MHz; DMSO-d_6) -110.01. δ^{31}_P(243 MHz; DMSO-d_6; PPh_3) 21.15. δ^{51}_V(158 MHz; DMSO-d_6; $VOCl_3/C_6D_6$) -536.68.

Table S1 Crystal data and structure refinement for **[AH]Cl**, **[H_2L2]Cl**, and **[H_2L3]Cl**

Compound	**[AH]Cl**	**[H_2L2]Cl**	**[H_2L3]Cl**
Empirical formula	$C_{52}H_{44}Cl_2O_4P_2$	$C_{32}H_{27}ClN_3O_2P$	C32 H27 Cl N3 O2 P
Formula weight	865.71	551.99	551.99
Temperature (K)	100(2)	100(2)	100(2)
Wavelength (Å)	0.71073 (Mo–Kα)	0.71073 (Mo–Kα)	0.71073 (Mo–Kα)
Crystal system, space group	Triclinic, P-1	Monoclinic, $P2_1/c$	Monoclinic, $P2_1/c$
a(Å) *b* (Å) *c* (Å)	9.7713(5) 13.1128(6) 17.6654(9)	11.6944(5) 10.2221(4) 23.3093(8)	11.5892(4) 10.1708(4) 23.3468(8)
α (º) β(º) γ (º)	105.387(2) 92.247(2) 90.731(2)	90.00 102.2020(20) 90.00	90.00 101.7700(10) 90.00
Volume (Å^3)	2180.01(19)	2723.47(18)	2694.06(17)
Z; C. density (mg m^{-3})	2, 1.319	4; 1.346	4, 1.361
Absorp. Coeffic. (mm^{-1})	0.269	0.235	0.237
F (000)	904	1152	1152
Crystal size (mm)	0.38 × 0.29 × 0.25	0.25 × 0.05 × 0.04	0.27× 0.12 × 0.10
Theta range for data collection (º)	2.09 to 29.63	2.18 to 28.36	2.19 to 28.33
Limiting indices	13 ≤ *h* ≤ 13, -18 ≤ *k* ≤ 13, -24 ≤ *l* ≤ 24	-15 ≤ *h* ≤ 15, -13 ≤ *k* ≤ 12, -31 ≤ *l* ≤ 28	-15 ≤ *h* ≤ 13, -13 ≤ *k* ≤ 13, -29 ≤ *l* ≤ 31
Reflections collected/unique	43134 / 12285	36928 / 6805	27628 / 6718
Completeness to theta	99.9 %	99.8%	99.8%
Absorption correction	Semi-empirical from equivalents	Semi-empirical from equivalents	Semi-empirical from equivalents
Max. and min. trans.	0.9458 and 0.8483	0.7457 and 0.7121	0.9867 and 0.9488
Data/restraints/ parameters	12163 / 0 / 547	6805/0 / 360	6718 / 0 / 358
Goodness-of-fit on F^2	1.165	1.027	1.022
Indice R_{int}	0.0354	0.1037	0.0656
Final R indices R_1 and $wR_2[I > 2\sigma(I)]$	0.0760 and 0.1480	0.0571 and 0.0934	0.0511 and 0.0979
R indices (all data)	0.0923 and 0.1452	0.1123 and 0.1078	0.0924 and 0.1115
Largest diff. peak and hole e.A^-3	1.017 and -0.442	0.315 and -0.345	0.431 and -0.359

Table S2 Crystal data and structure refinement for **C1**–**C5**

Complex	**C1**	**C2**	**C3**	**C4**	**C5**
Empirical formula	$C_{33}H_{30}N_2O_6PV$	$C_{33}H_{37}N_3O_9PV$	$C_{65}H_{66}N_6O_{15}P_2V_2$	$C_{39}H_{36}N_2O_7PV$	$C_{34}H_{31}FN_2O_6PV$
Formula mass	632.52	701.57	1335.06	726.61	664.52
Temperature (K)	100(2)	100(2)	100(2)	100(2)	100(2)
Wavelength (Å)	0.71073 (Mo–Kα)	0.71073 (Mo–Kα)	0.71073 (Mo–Kα)	0.71073 (Mo–Kα)	0.71073 (Mo–Kα)
Crystal system, space group	Triclinic, $P\bar{1}$	Triclinic, $P\bar{1}$	Triclinic, $P\bar{1}$	Triclinic, $P\bar{1}$	Triclinic, $P\bar{1}$
a (Å) *b*(Å) *c* (Å)	9.8606(4) 10.6648(4) 15.2352(6)	11.2125(3) 12.2196(4) 14.1895(4)	14.3202(4) 15.0874(5) 16.8813(4)	10.8358(5) 11.2449(4) 14.9567(8)	9.9185(5) 10.6629(4) 15.2191(8)
α (º) β (º) γ (º)	87.9290(10) 89.6510(10) 75.6100(10)	67.9900(10) 78.4230(10) 65.2980(10)	114.3870(10) 94.1470(10) 99.4190(10)	77.0930(10) 83.962(2) 72.1210(10)	88.136(2) 88.887(2) 75.909(2)
Volume (Å^3)	1550.87(11)	1635.27(8)	3237.11(16)	1689.29(13)	1560.20(13)
Z; Calculated density (mg m^{-3})	2; 1.354	2; 1.425	2; 1.370	2; 1.428	2; 1.415
Absorp. coefficient (mm^{-1})	0.418	0.411	0.409	0.396	0.424
F (000)	656	732	1388	756	688
Crystal size (mm)	0.34 × 0.14 × 0.13	0.26 × 0.21 × 0.15	0.31 × 0.17 × 0.15	0.29 × 0.13 × 0.09	0.22 × 0.19 × 0.11
Theta range for data collection (º)	2.34 to 29.62	1.94 to 28.34	2.03 to 28.30	1.94 to 28.73	1.97 to 28.31
Limiting indices	-13 ≤ *h* ≤ 13, -11 ≤ *k* ≤ 14, -21 ≤ *l* ≤ 21	-14 ≤ *h* ≤ 13, -16 ≤ *k* ≤ 16, -18 ≤ *l* ≤ 16	-19 ≤ *h* ≤ 19, -20 ≤ *k* ≤ 20, -22 ≤ *l* ≤ 20	-14 ≤ *h* ≤ 14, -12 ≤ *k* ≤ 15, -20 ≤ *l* ≤ 20	-13 ≤ *h* ≤ 13, -14 ≤ *k* ≤ 10, -20 ≤ *l* ≤ 20
Reflections collected/unique	45636/8713	30241/8131	60181/16017	54534/8758	31886/7748
Completeness to theta	99.5%	99.6%	99.5%	99.8%	99.7%
Absorption correction	Semi-empirical from equivalents	Semi-empirical from equivalents	Semi-empirical from equivalents	Semi-empirical from equivalents	Semi-empirical from equivalents
Max. and min. trans.	0.9076 and 0.8174	0.9509 and 0.9106	0.9512 and 0.8938	0.9552 and 0.8837	0.7457 and 0.6744
Data/restraints/ parameters	8713/1/388	8131/0/440	16017/2/813	8758/0/459	7748/1/408
Goodness-of-fit on F^2	1.028	1.027	1.039	1.026	1.054
Indice R_{int}	0.0295	0.0251	0.0606	0.0578	0.0378

Final R indices R_1 and $wR_2[I > 2\sigma(I)]$	0.0836 and 0.1449	0.0390 and 0.0938	0.1021 and 0.1442	0.0467 and 0.1042	0.0627 and 0.1816
R indices (all data)	0.0913 and 0.1520	0.0478 and 0.0984	0.1504 and 0.1706	0.0710 and 0.1141	0.0803 and 0.1935
Largest diff. peak and hole	1.169 and -1.604	0.991 and -0.572	1.946 and -1.926	1.322 and -0.452	1.842 and -0.842

Table S3 Values of selected bond lengths and angles of synthetized complexes **C1**–**C5**

Selected bond length values of complexes **C1**–**C5** (Å)					
Bond	**C1**	**C2**	**C3**	**C4**	**C5**
V^{V}–N(imine)	2.148(3)	2.1489(13)	2.156(4) 2.120(5)	2.1377(17)	2.146(2)
V^{V}–O(phenolate)	1.932(2)	1.9062(12)	1.911(3) 1.884(4)	1.9263(14)	1.928(2)
V^{V}–O(enolate)	1.984(2)	1.9773(12)	1.973(3) 1.971(4)	1.9875(14)	1.983(2)
V^{V}=O(oxido)	1.621(2) 1.636(2)	1.6296(12) 1.6298(12)	1.610(4) 1.656(4) 1.462(6) 1.893(8)	1.6157(16) 1.6423(15)	1.619(2) 1.644(2)
N(imine)–N(amide)	1.403(3)	1.4108(18)	1.402(5) 1.402(5)	1.395(2)	1.405(3)
C–N(amide)	1.302(4)	1.300(2)	1.321(5) 1.293(7)	1.296(2)	1.309(4)
C–O(enolate)	1.299(4)	1.2994(19)	1.295(6) 1.289(6)	1.317(2)	1.300(4)
Values of bond angles of the coordination spheres of the complexes **C1**–**C5** (°)					
Angle	**C1**	**C2**	**C3**	**C4**	**C5**
N(imine)–V^{V}–O(phenolate)	82.33(10)	82.51(5)	81.54(14) 83.73(17)	82.26(6)	82.43(9)
N(imine)–V^{V}–O(enolate)	73.36(9)	73.45(5)	73.20(14) 74.18(16)	73.91(6)	73.65(9)
N(imine)–V^{V}=O(oxido)	112.38(12) 137.30(12)	116.19(6) 133.03(6)	104.50(18) 144.72(18) 112.5(3) 154.4(4)	122.98(8) 126.22(7)	113.45(11) 136.44(11)
O(phenolate)–V^{V}–O(enolate)	149.47(10)	154.15(5)	146.60(15) 156.96(19)	156.12(6)	150.37(9)
O(oxido)=V^{V}–O(phenolate)	93.69(12) 103.50(12)	96.61(6) 100.95(6)	94.77(18) 105.60(17) 90.1(3) 105.9(3)	97.03(7) 97.87(7)	93.64(10) 103.44(11)
O(oxido)=V^{V}–O(enolate)	91.94(12) 102.69(11)	93.00(6) 98.15(6)	93.53(17) 101.68(18) 92.3(3) 97.0(2)	95.94(7) 96.25(7)	91.89(10) 102.01(10)
O(oxido)=V^{V}=O(oxido)	109.89(13)	110.09(7)	110.2(2) 91.5(5)	110.45(8)	109.66(12)

Table S4 Values of selected bond lengths and angles of dioxidovanadium(V) complexes from the literature for comparison with **C1**–**C5**

Selected bond length values of complexes from literature (Å)					
Bond	**5**	**6**	**7**	**5**	**8***
V^{V}–N(imine)	2.146(6)	2.1588(12)	2.1236(14)	2.1505(12)	2.128(10) 2.117(9)
V^{V}–O(phenolate)	1.903(5)	1.9179(10)	1.9027(13)	1.9017(12)	1.889(9) 1.884(9)
V^{V}–O(enolate)	1.956(5)	1.9731(10)	1.9884(12)	1.9822(11)	1.957(8) 1.961(8)
V^{V}=O(oxido)	1.610(5) 1.636(5)	1.6208(11) 1.6465(10)	1.6183(14) 1.6263(14)	1.6106(14) 1.6358(13)	1.572(8) 1.648(7) 1.562(8) 1.661(8)
N(imine)–N(amide)	1.398(8)	1.3999(16)	1.4067(18)	1.3921(17)	1.429(12) 1.431(13)
C–N(amide)	1.300(9)	1.3055(18)	1.291(2)	1.3105(19)	1.308(15) 1.319(15)
C–O(enolate)	1.302(8)	1.3095(16)	1.309(2)	1.3008(18)	1.331(13) 1.315(14)
Values of bond angles of the coordination spheres of complexes from literature (°)					
Angle	5	6	7	5	8*
N(imine)–V^{V}–O(phenolate)	82.1(2)	83.08(4)	82.79(5)	81.79(5)	82.5(4) 82.8(4)
N(imine)–V^{V}–O(enolate)	73.2(2)	72.90(4)	73.74(5)	73.53(4)	73.9(3) 74.1(4)
N(imine)–V^{V}=O(oxido)	106.8(2) 143.1(3)	102.75(5) 147.12(5)	121.76(8) 130.78(7)	112.22(7) 136.99(7)	107.7(4) 144.2(4) 109.2(4) 142.0(4)
O(phenolate)–V^{V}–O(enolate)	148.0(2)	144.37(5)	155.67(6)	151.65(5)	149.0(4) 150.9(4)
O(oxido)=V^{V}–O(phenolate)	94.0(3) 104.4(3)	96.46(5) 105.42(5)	97.17(7) 101.49(7)	96.32(6) 100.97(7)	96.0(4) 100.4(5)

					96.3(4) 100.1(5)
O(oxido)=V^{V}– O(enolate)	93.7(2) 102.0(3)	90.27(5) 105.29(5)	93.44(6) 96.32(7)	92.43(5) 101.14(6)	91.8(4) 105.7(4) 91.5(4) 103.9(5)
O(oxido)=V^{V}= O(oxido)	109.7(3)	108.96(6)	106.57(9)	110.31(9)	107.7(4) 108.4(5)

* = Two independent units of the complex in the asymmetric unit.

Table S5 The β and α angles values and the calculated values of τ, as well as their respective coordination geometries, of **C1**–**C5** and similar complexes in the literature

Complex	**β (°)[a]**	**α (°)[b]**	τ[c]	**Coordination geometry**
C1	149.52(10)	137.29(12)	0.20	Distorted square based pyramid
C2	154.16(5)	133.08(6)	0.35	Distorted square based pyramid
C3*	146.47(18), 156.9(2)	144.6(2), 154.5(5)	0.03, 0.04	Slightly distorted square based pyramid
C4	156.13(6)	126.22(7)	0.50	Distorted between square based pyramid and trigonal bipyramid
C5	150.37(9)	136.44(11)	0.23	Distorted square based pyramid
5	148.0(2)	143.1(3)	0.08	Distorted square based pyramid
6	147.12(5)	144.37(5)	0.04	Distorted square based pyramid
7	155.67(6)	130.78(7)	0.41	Distorted between square based pyramid and trigonal bipyramid
5	151.65(5)	136.99(7)	0.24	Distorted square based pyramid
8*	149.0(4), 150.9(4)	144.2(4), 142.0(4)	0.08, 0.15	Distorted square based pyramid

a = Highest bond angle value; b = Second highest bond angle value; c = Structural index parameter τ (dimensionless); * = Two independent units of the complex in the asymmetric unit.

Table S6 UV–Vis data of complexes **C1**–**C5** in *N,N*-dimethylformamide (DMF) and DMF(5%)/Tris-HCl (pH 7.4) buffered solution

	DMF		**DMF(5%)/Tris-HCl (pH 7.4)**
Complex	**λ, nm (ε, M^{-1} cm^{-1})**		**λ, nm (ε, M^{-1} cm^{-1})**
C1	265 (33440), 325 (20470), 410 (17380)	**C1**	300 (25620), 391 (6260)
C2	265 (48850), 324 (23645), 408 (19470)	**C2**	299 (23560), 390 (5840)
C3	265 (37160), 328 (14745), 414 (11655)	**C3**	300 (17390), 394 (4025)
C4	265 (48310), 325 (27890), 412 (19930)	**C4**	313 (16490), 404 (6740)
C5	264 (51120), 323 (24910), 408 (21555)	**C5**	300 (28825), 389 (7290)

Table S7 Electrochemical data of complexes **C1**–**C5** in dry *N,N*-dimethylformamide solution

Complex	E_{red1} **(V)**	E_{red2} **(V)**	E_{red3} **(V)**	E_{ox1} **(V)**	E_{ox2} **(V)**
C1	–1.63[c]	–1.11[a]	–0.63[a]	+1.06[b]	+1.40[b]
C2	–1.52[a]	–1.38[a]	–0.61[a]	+0.84[b]	-----
C3	–1.79[a]	–1.52[a]	–0.65[a]	+0.26[b]	+1.38[b]
C4	–1.81[a]	–0.60[a]	-----	+0.44[b]	+0.84[b]
C5	–1.74[a]	–0.60[a]	-----	+0.78[b]	-----

[a]Cathodic peak (E_{pc}); [b]Anodic peak (E_{pa}); [c]$E_{1/2} = E_{pc} + E_{pa} / 2$.

Table S8 Molecular docking results for the interaction between HSA and dioxidovanadium(V) complexes in the site III

System	Amino acid residue	Interaction	Distance (Å)
	Leu-115	Hydrophobic	3.53
	Val-116	Hydrophobic	3.60
	Val-116 (backbone)	Hydrogen bond	3.18
	Arg-117	Hydrophobic	3.56
	Tyr-138	Hydrophobic	4.00
	Tyr-138	π-stacking	5.02
HSA:C1	Glu-141	Hydrophobic	3.30
	Ile-142	Hydrophobic	3.67
	Tyr-161	π-stacking	5.01
	Leu-182	Hydrophobic	3.81
	Leu-185	Hydrophobic	3.32
	Arg-186	Hydrophobic	3.97
	Leu-115	Hydrophobic	3.30
	Arg-117	Hydrophobic	3.62
	Arg-117	Hydrogen bond	3.58
	Phe-134	π-stacking	4.42
	Lys-137	Hydrophobic	3.35
HSA:C2	Tyr-138	Hydrophobic	3.50
	Glu-141	Hydrophobic	3.52
	Ile-142	Hydrophobic	3.56
	Tyr-161	Hydrophobic	3.89
	Leu-182	Hydrophobic	3.27
	Leu-182 (backbone)	Hydrogen bond	2.48
	Arg-186 (backbone)	Hydrogen bond	3.49
	Leu-115	Hydrophobic	3.32
	Val-116	Hydrophobic	3.94
	Arg-117	Hydrophobic	3.46
	Tyr-138	Hydrophobic	3.88
	Tyr-138	π-stacking	4.94
HSA:C3	Glu-141	Hydrophobic	3.47
	Ile-142	Hydrophobic	3.67
	Tyr-161	Hydrophobic	3.43
	Leu-182	Hydrophobic	3.85

	Leu-185	Hydrophobic	3.34
	Arg-186	Hydrophobic	3.90
HSA:C4	Arg-117	Hydrophobic	3.44
	Ala-126	Hydrophobic	3.50
	Asn-130	Hydrophobic	3.54
	Thr-133	Hydrophobic	3.86
	Phe-134	Hydrophobic	3.44
	Lys-137	Hydrophobic	3.92
	Tyr-138	π-stacking	5.00
	Glu-141	Hydrophobic	3.25
	Ile-142	Hydrophobic	3.27
	Tyr-161	Hydrophobic	3.42
	Leu-182	Hydrophobic	3.81
	Leu-185	Hydrophobic	3.37
HSA:C5	Leu-115	Hydrophobic	3.69
	Arg-117	Hydrophobic	3.58
	Ala-126	Hydrophobic	3.58
	Phe-134	Hydrophobic	3.24
	Lys-137	Hydrogen bond	3.96
	Lys-137	Hydrophobic	3.14
	Tyr-138	Hydrophobic	3.55
	Glu-141	Hydrophobic	2.91
	Ile-142	Hydrophobic	3.56
	Tyr-161	π-stacking	5.05
	Leu-182	Hydrophobic	3.55
	Leu-185	Hydrophobic	3.74
	Arg-186	Hydrophobic	3.94

Table S9 Cell viability of HaCaT cells exposed to increasing concentrations of **C1**–**C5**. The cell viability was assessed by MTT method following 24 hours of treatment

Complex	**Concentration (μM)**	**Viable cells (5)**

CN	NA	99,9
C1	2,6133	42,4
	1,30665	55,3
	0,653325	72,5
	0,3266625	74,0
C2	2,5656	40,6
	1,2828	48,6
	0,6414	65,9
	0,3207	84,2
C3	2,2709	44,8
	1,13545	45,6
	0,567725	48,4
	0,2838625	48,7
C4	1,6515	76,4
	0,82575	88,0
	0,412875	96,7
	0,2064375	100,0
C5	1,9563	52,5
	0,97815	69,6
	0,489075	93,2
	0,2445375	100,5

NA = Not available. Control cells were exposed to Dulbecco's Modified Eagle's Medium (DMEM). Values represent mean ± standard deviations of three independent experiments carried out in triplicate. Data were analyzed by one-way ANOVA followed by post hoc comparisons (Tukey test). *P<0.05, **P<0.01, and ***P<0.001, significantly different from control cells; H_2O_2 is a positive control of cytotoxicity.

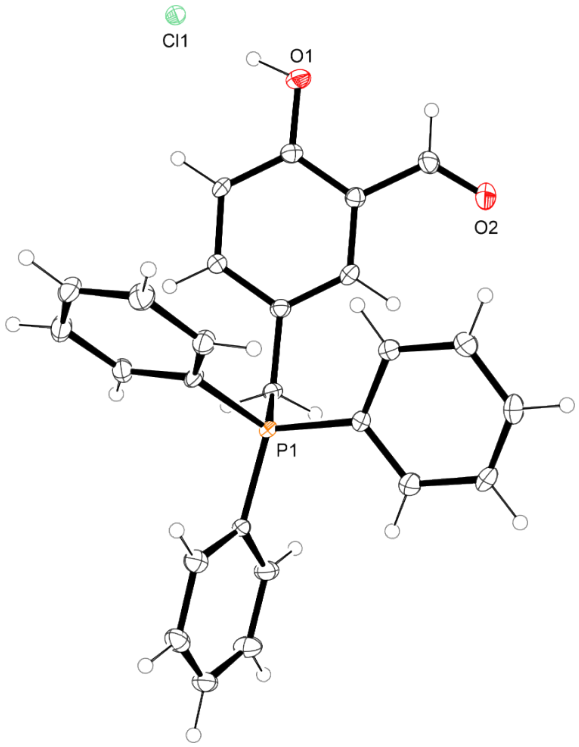

Fig. S1 *ORTEP-3* crystallographic structural projection of (3-formyl-4-hydroxybenzyl)triphenylphosphonium chloride (**[AH]Cl**) in solid state. Thermal ellipsoids are calculated with 50% probability level. Only one independent unit of the asymmetric unit is being represented.

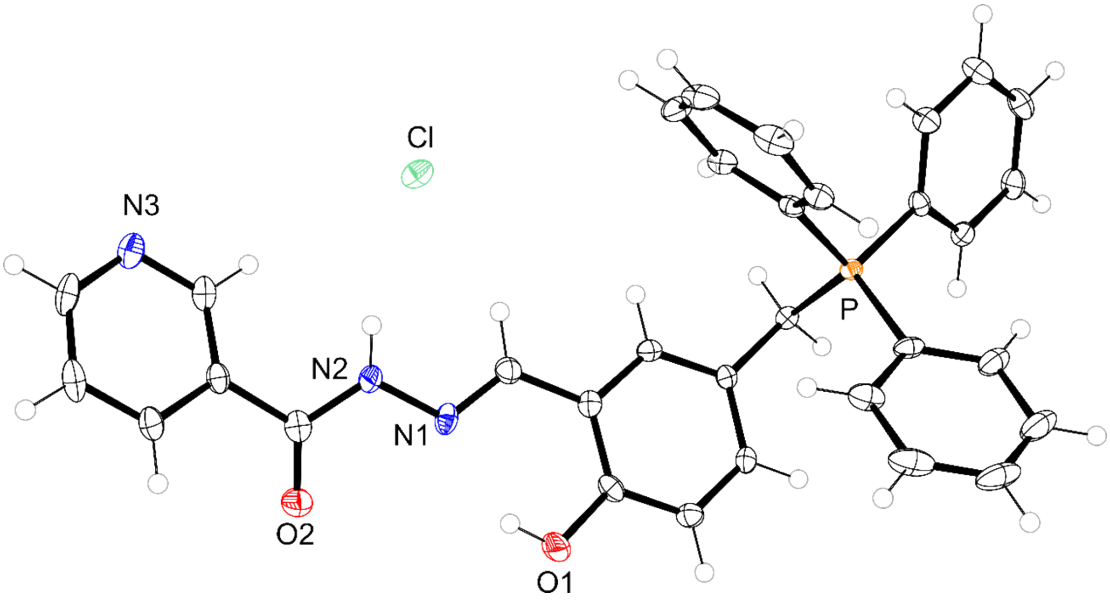

Fig. S2 *ORTEP-3* crystallographic structural projection of **[H_2L2]Cl** in solid state. Thermal ellipsoids are calculated with 50% probability level.

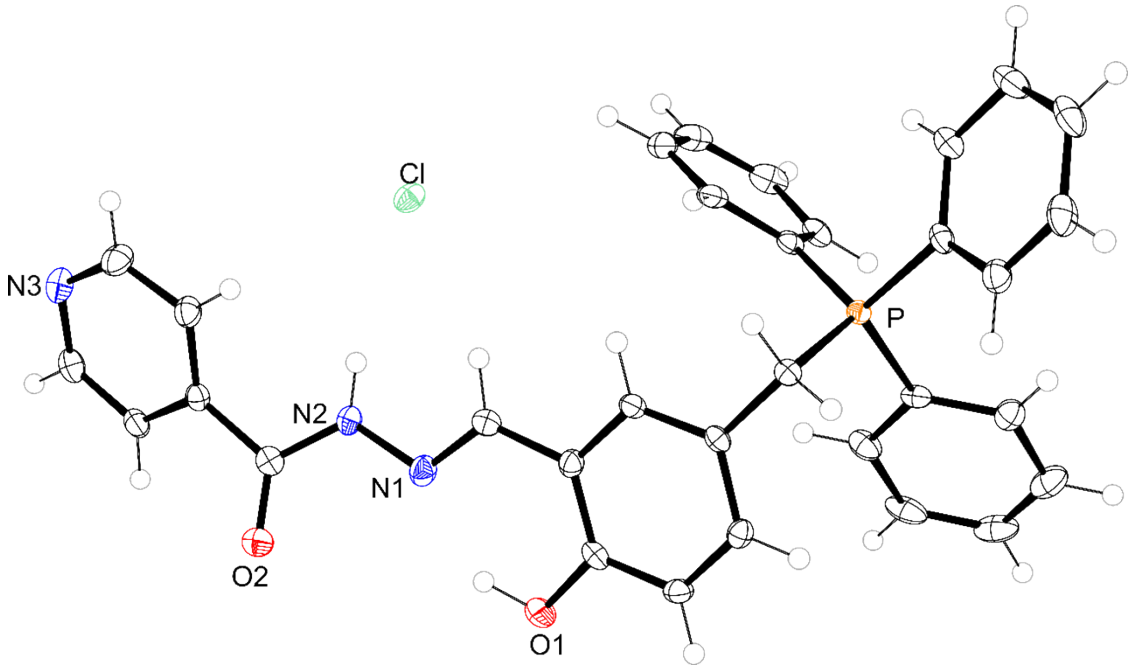

Fig. S3 *ORTEP-3* crystallographic structural projection of **[H_2L3]Cl** in solid state. Thermal ellipsoids are calculated with 50% probability level.

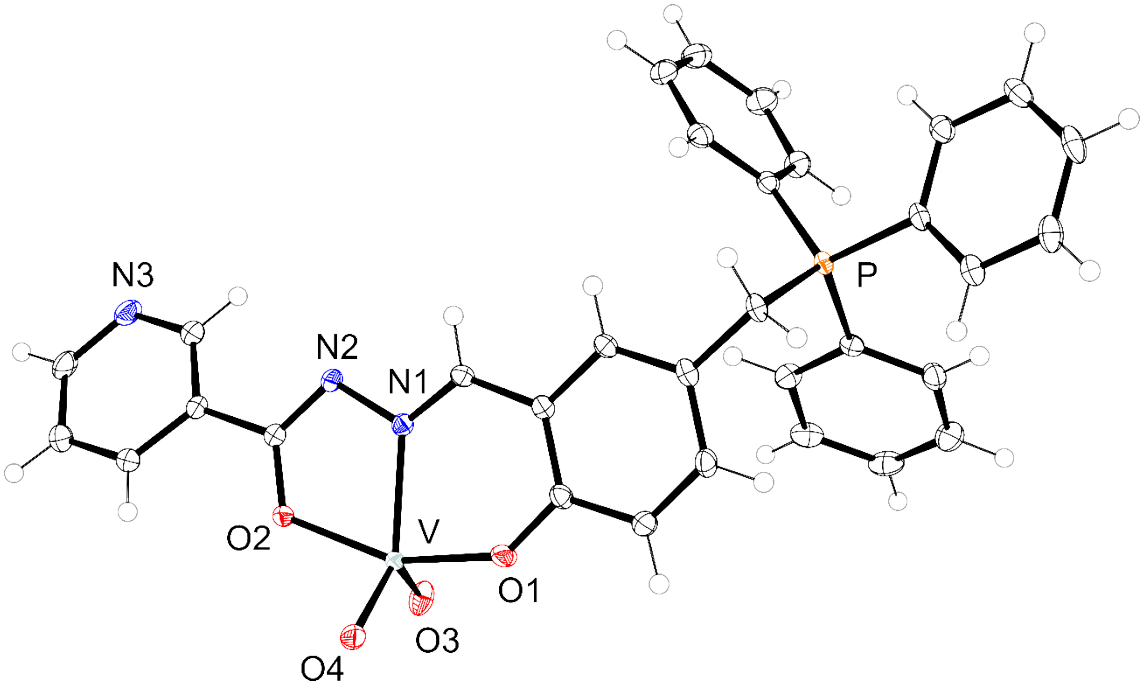

Fig. S4 *ORTEP-3* crystallographic structural projection of **C2** in solid state. Thermal ellipsoids are calculated with 50% probability level. One methanol molecule and four water molecules as crystallization solvates are omitted for better visualization.

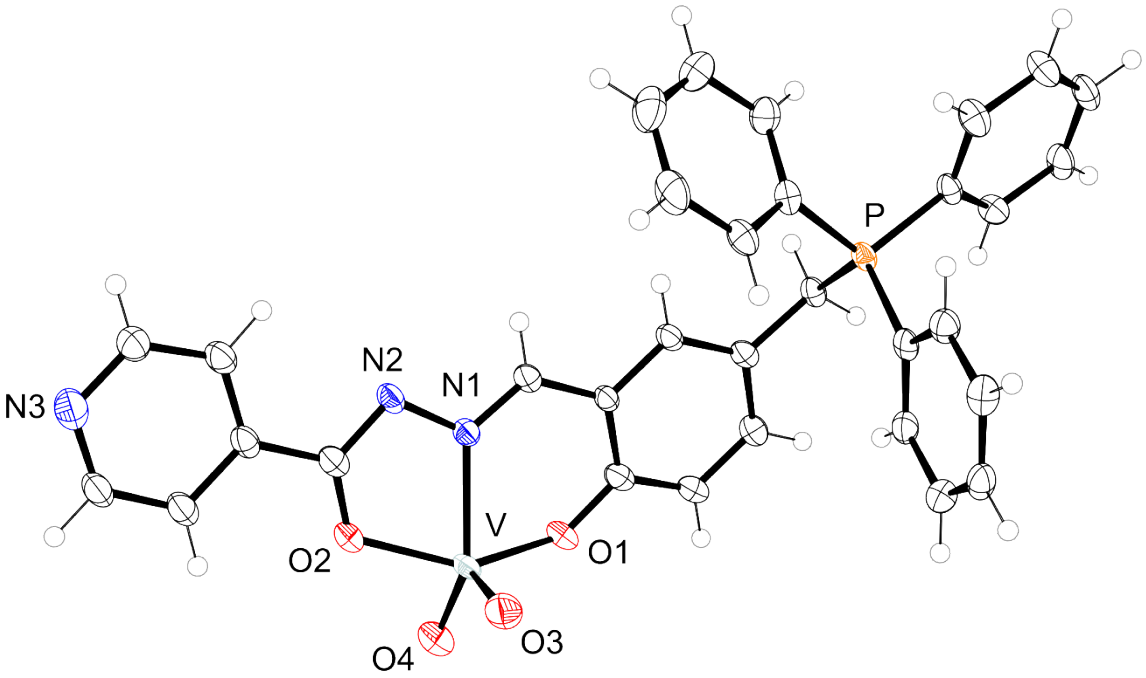

Fig. S5 *ORTEP-3* crystallographic structural projection of one independent unit of the asymmetric unit of **C3** in solid state. Thermal ellipsoids are calculated with 50% probability level. Molecules of water of crystallization are omitted for better visualization.

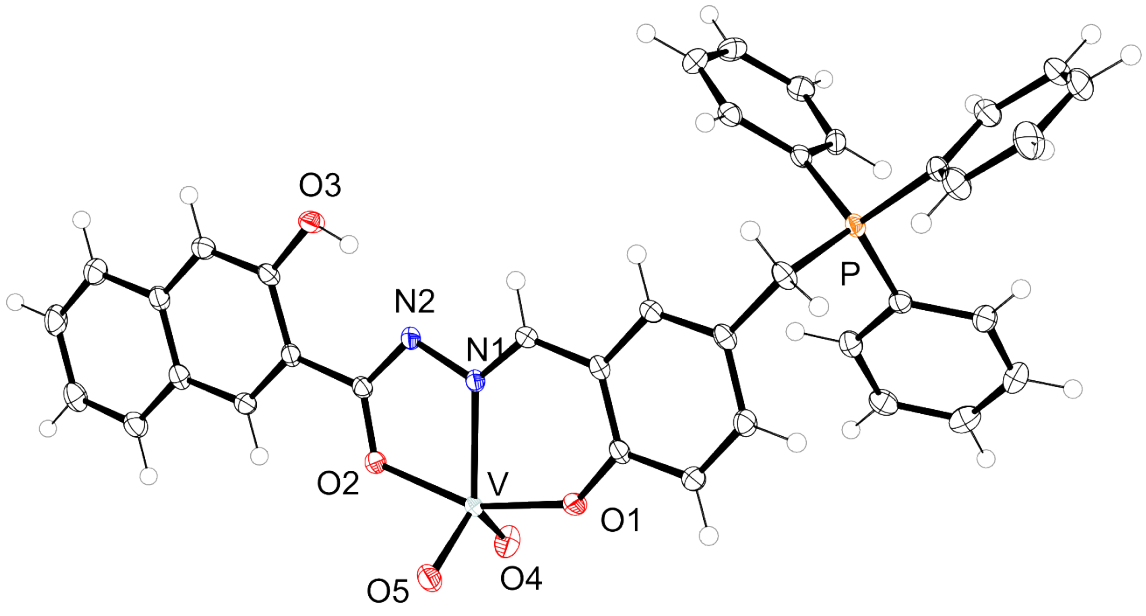

Fig. S6 *ORTEP-3* crystallographic structural projection of **C4** in solid state. Thermal ellipsoids are calculated with 50% probability level. Two methanol molecules as crystallization solvates are omitted for better visualization.

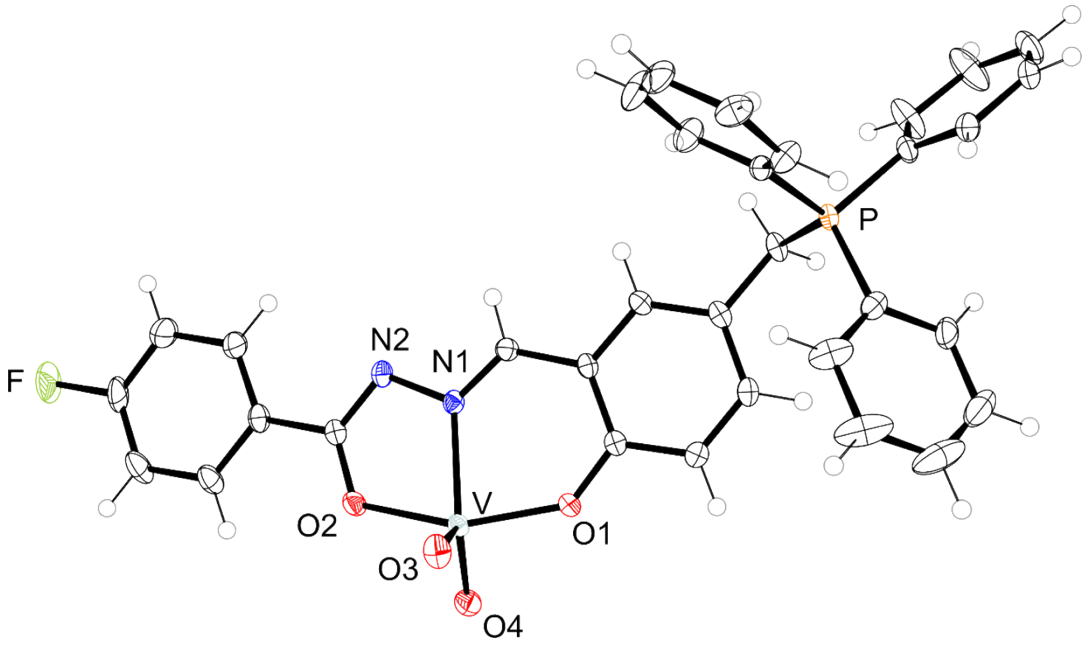

Fig. S7 *ORTEP-3* crystallographic structural projection of **C5** in solid state. Thermal ellipsoids are calculated with 50% probability level. One methanol molecule and one water molecules as crystallization solvates are omitted for better visualization.

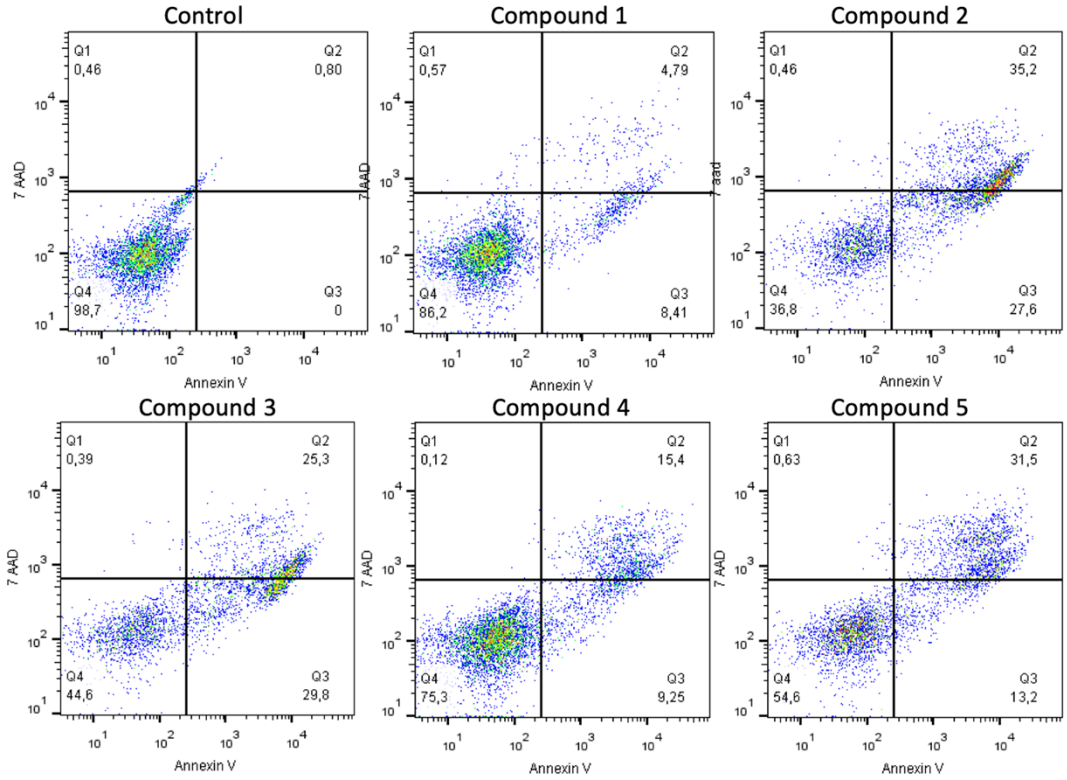

Fig. S8 Effects of **C1**–**C5** compounds in death by early apoptosis, apoptosis, and necrosis of HaCat cells. Flow cytometry is illustrated. Data are shown as mean ± standard deviations of three independent experiments. Two-way ANOVA followed by Tukey's post hoc test was used to assess statistical significance in graph.

FT-IR and FT-Raman spectra of the compounds

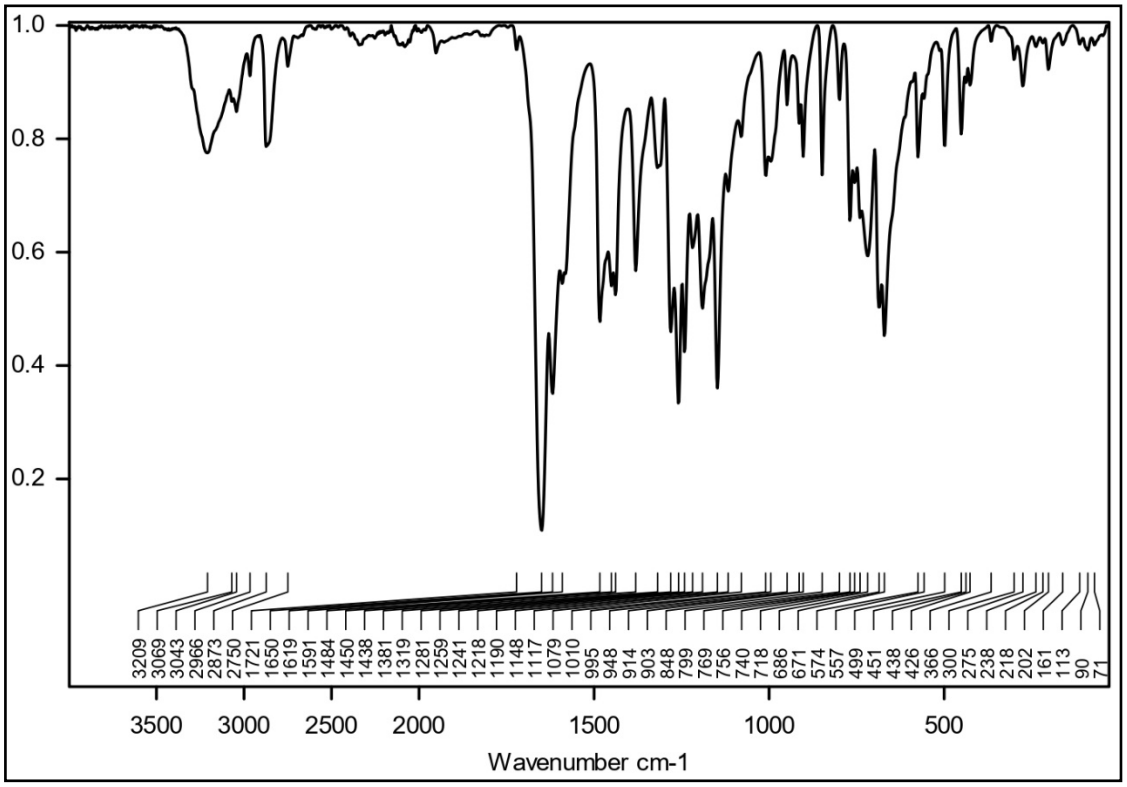

Fig. S9 FT-IR spectrum of 5-(chloromethyl)-2-hydroxybenzaldehyde (ATR).

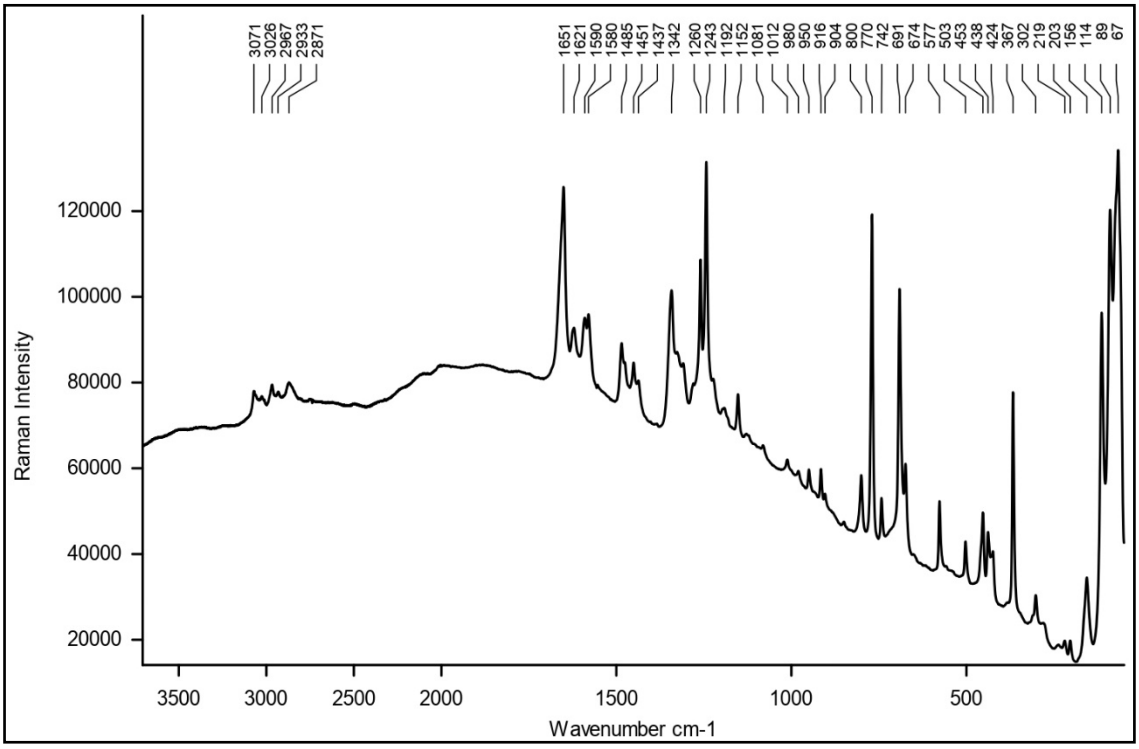

Fig. S10 FT-Raman spectrum of 5-(chloromethyl)-2-hydroxybenzaldehyde (532 nm, 10mW, 10 coaditions of 10 s).

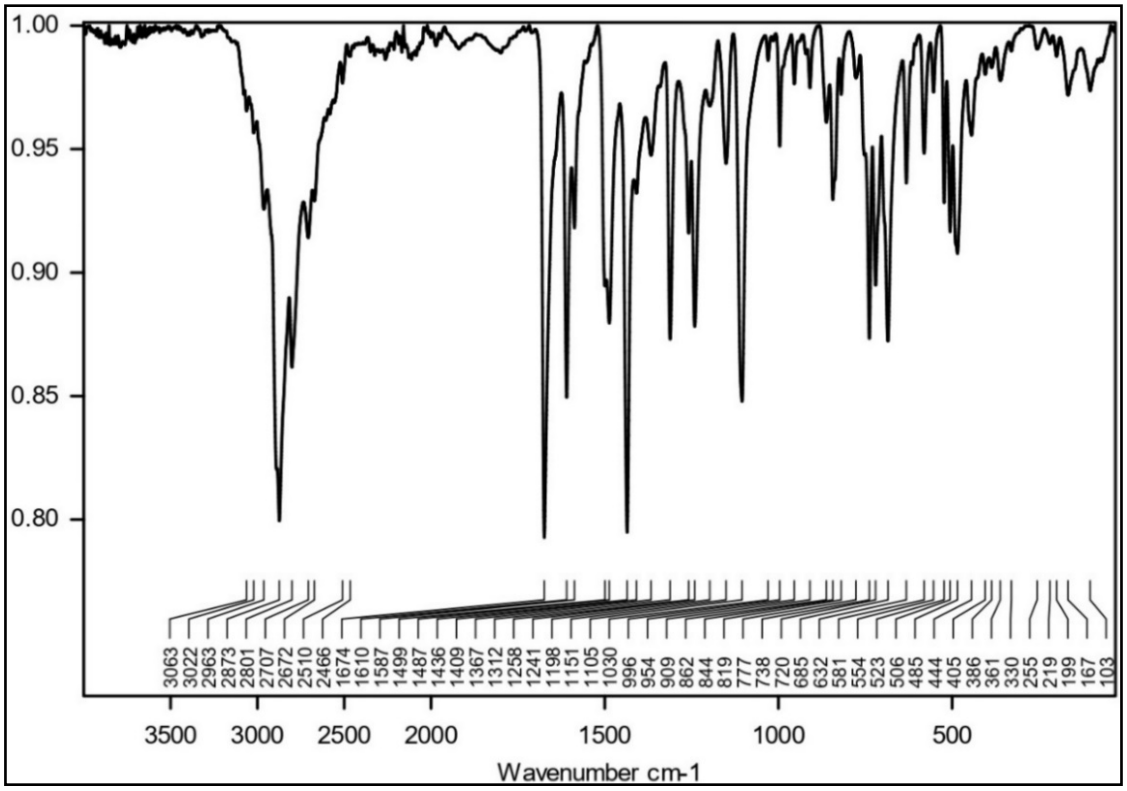

Fig. S11 FT-IR spectrum of **[AH]Cl** (ATR).

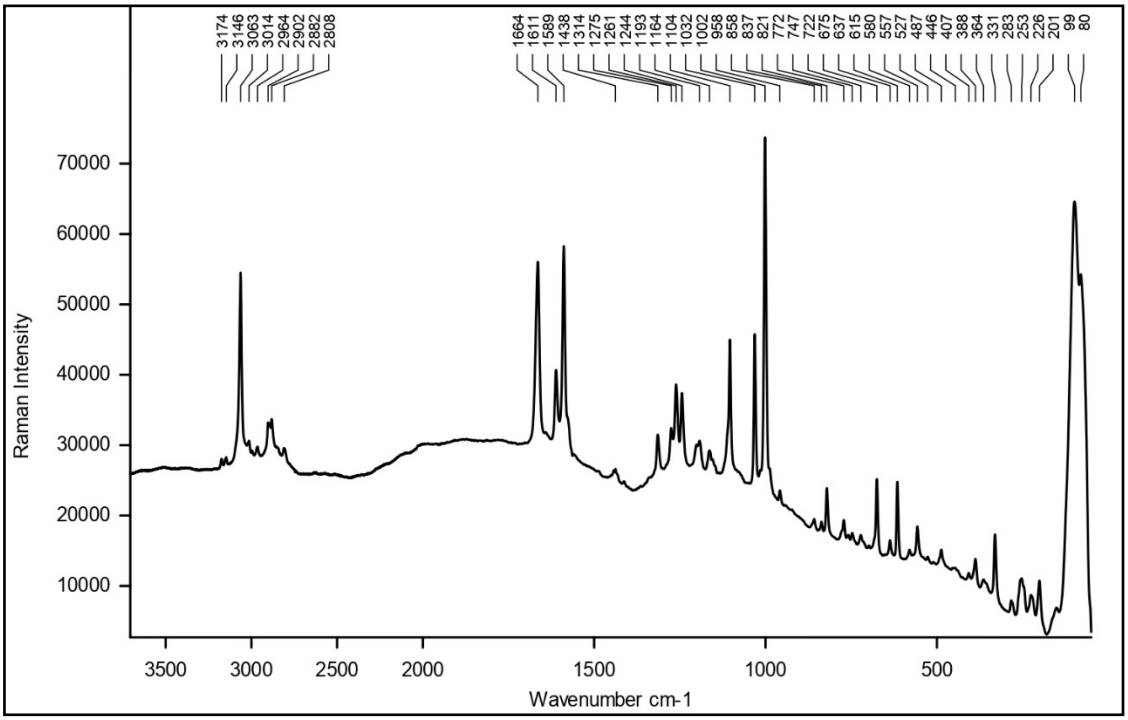

Fig. S12 FT-Raman spectrum of **[AH]Cl** (532 nm, 10mW, 10 coaditions of 10 s).

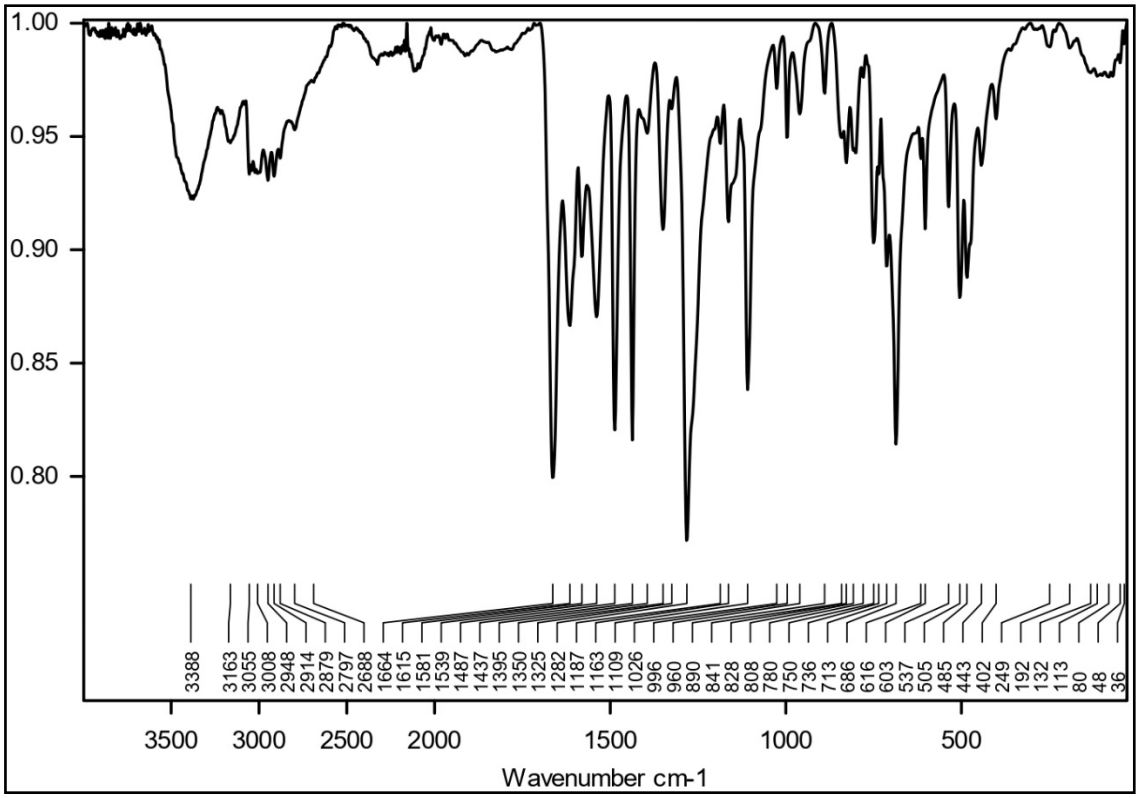

Fig. S13 FT-IR spectrum of **[H_2L1]Cl** (ATR).

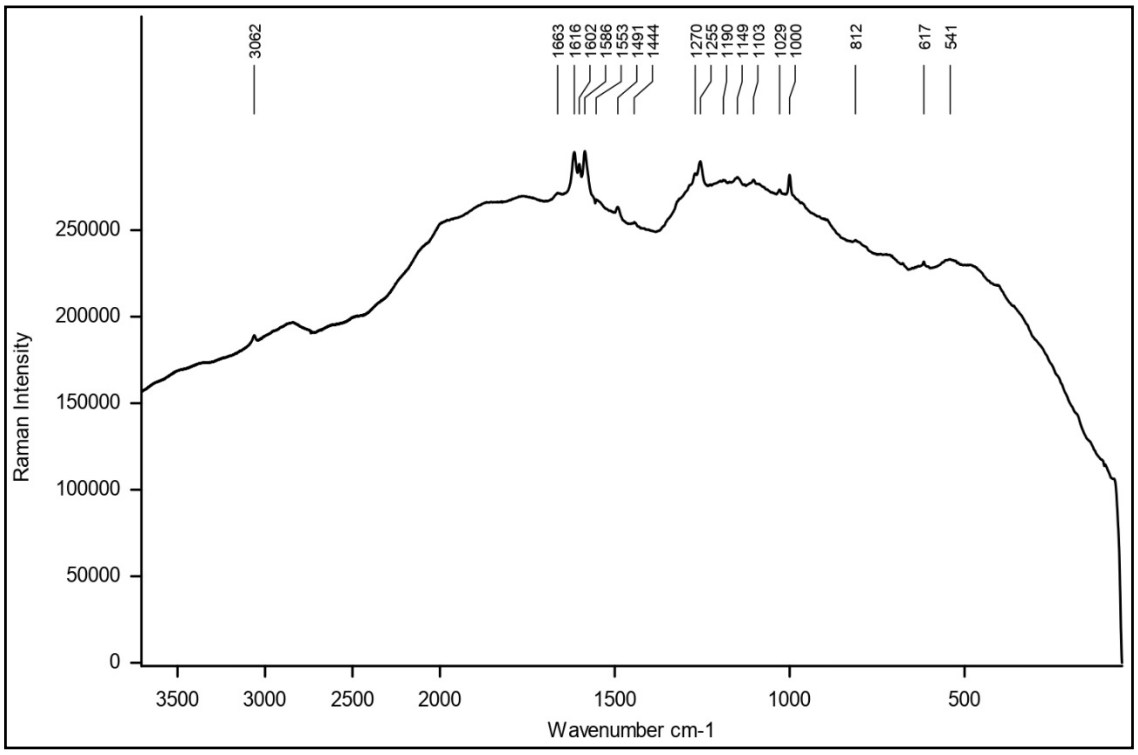

Fig. S14 FT-Raman spectrum of **[H_2L1]Cl** (532 nm, 0.2mW, 10 coaditions of 30 s).

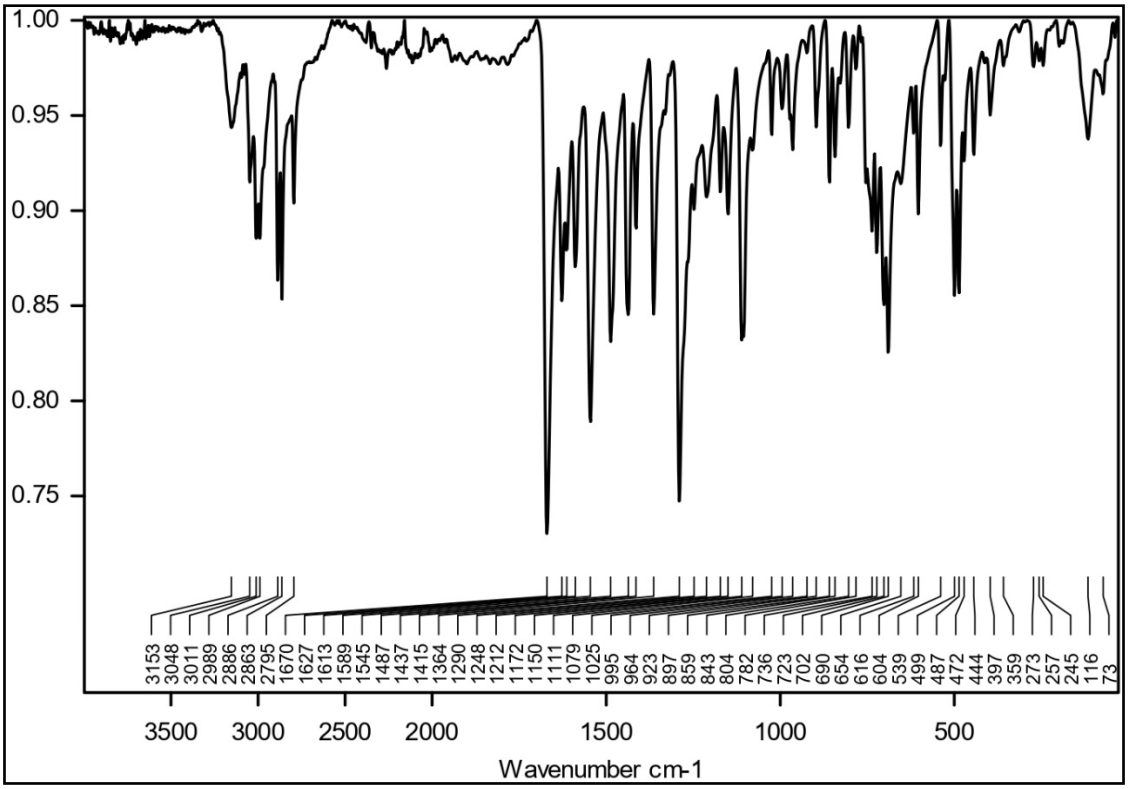

Fig. S15 FT-IR spectrum of **[H_2L2]Cl** (ATR).

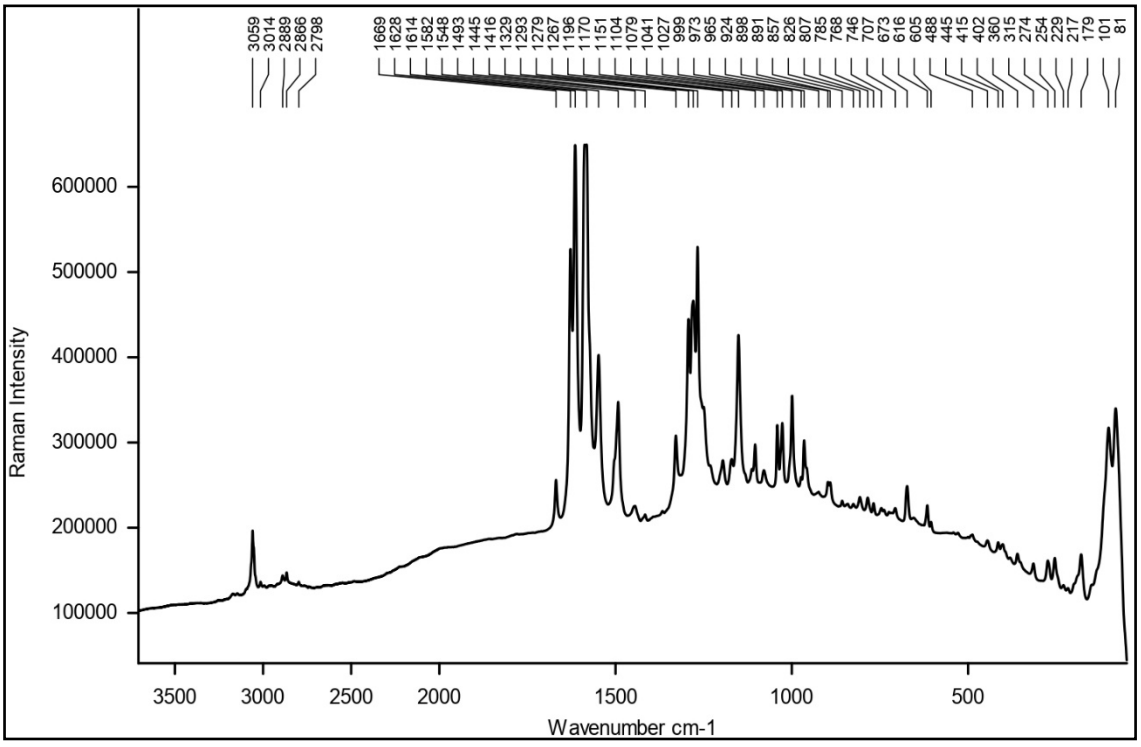

Fig. S16 FT-Raman spectrum of **[H_2L2]Cl** (532 nm, 10mW, 10 coaditions of 10 s).

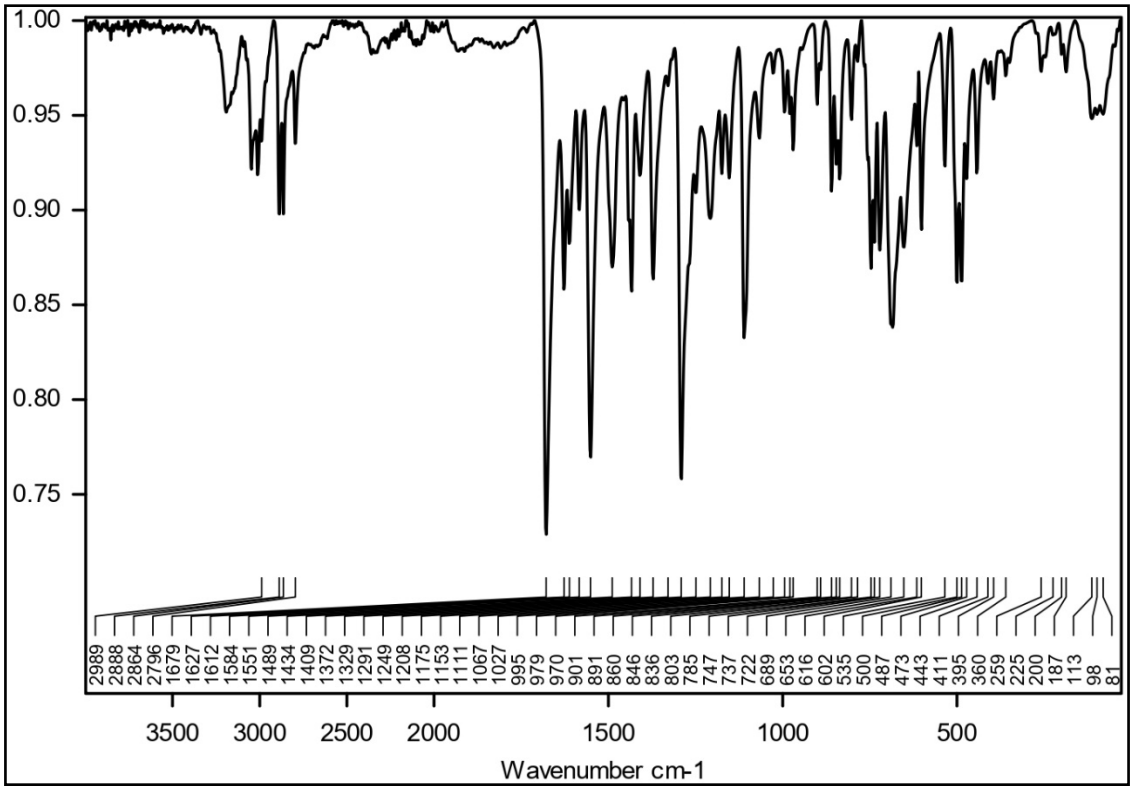

Fig. S17 FT-IR spectrum of **[H_2L3]Cl** (ATR).

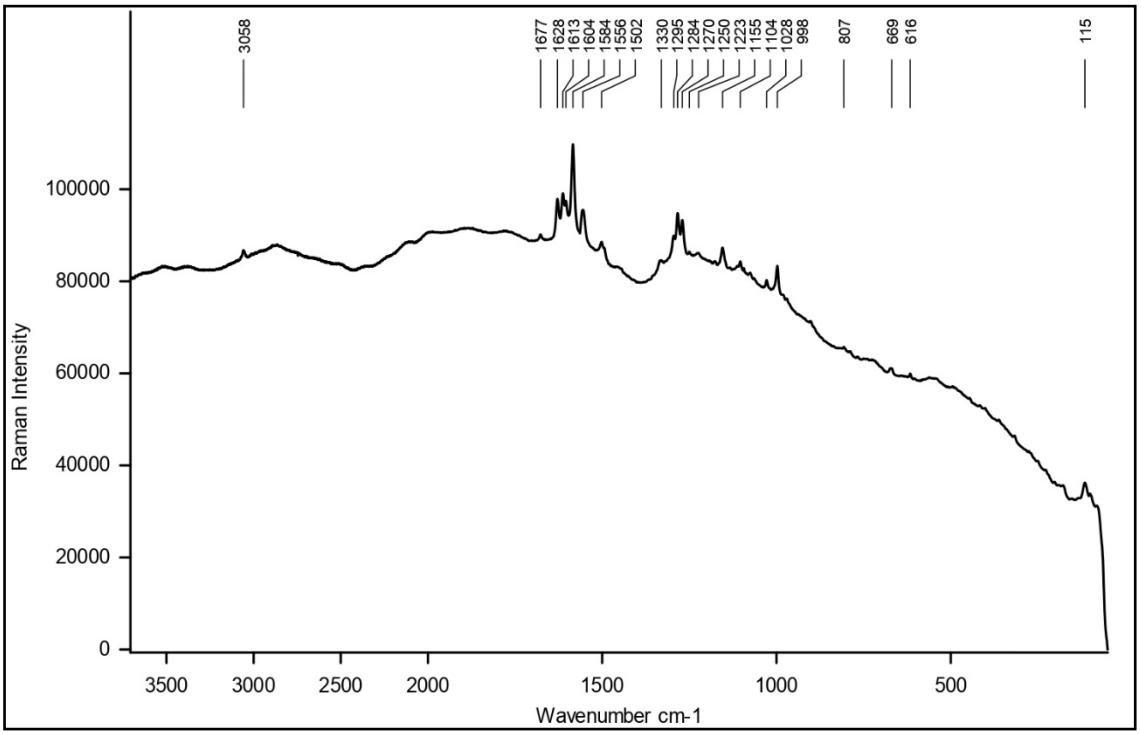

Fig. S18 FT-Raman spectrum of **[H_2L3]Cl** (532 nm, 10mW, 3 coaditions of 10 s).

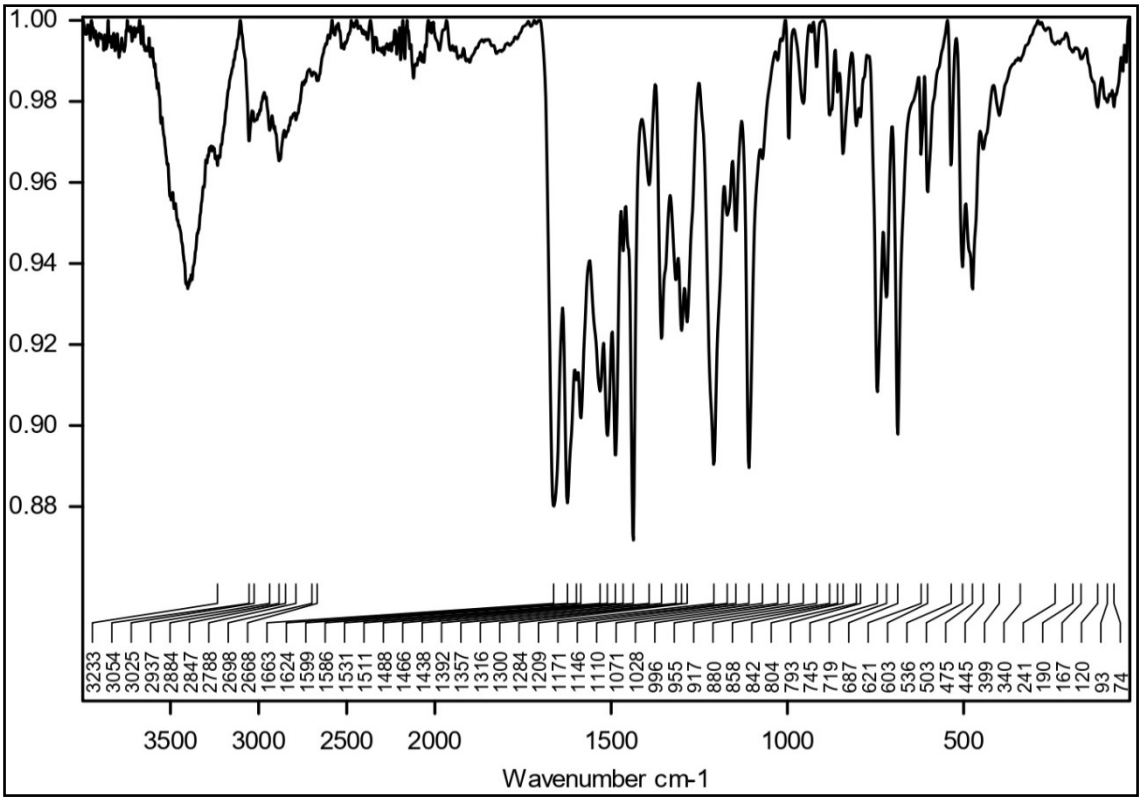

Fig. S19 FT-IR spectrum of **[H_3L4]Cl** (ATR).

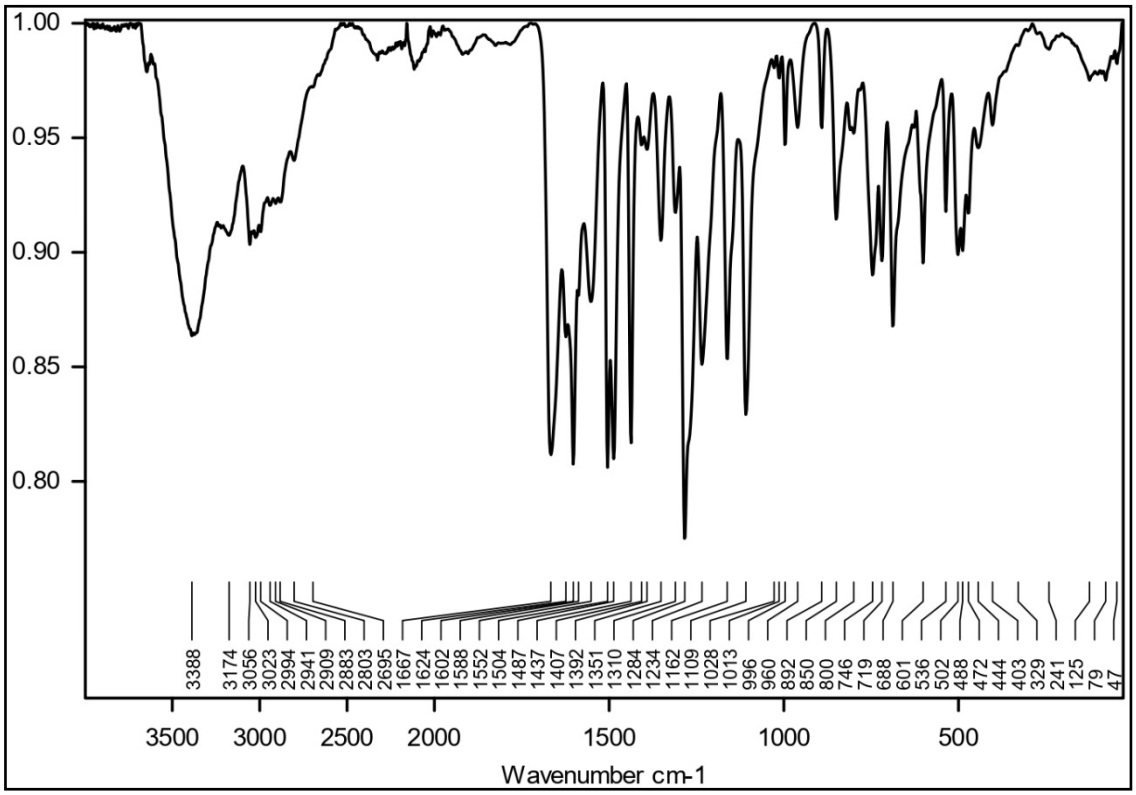

Fig. S20 FT-IR spectrum of **[H_2L5]Cl** (ATR).

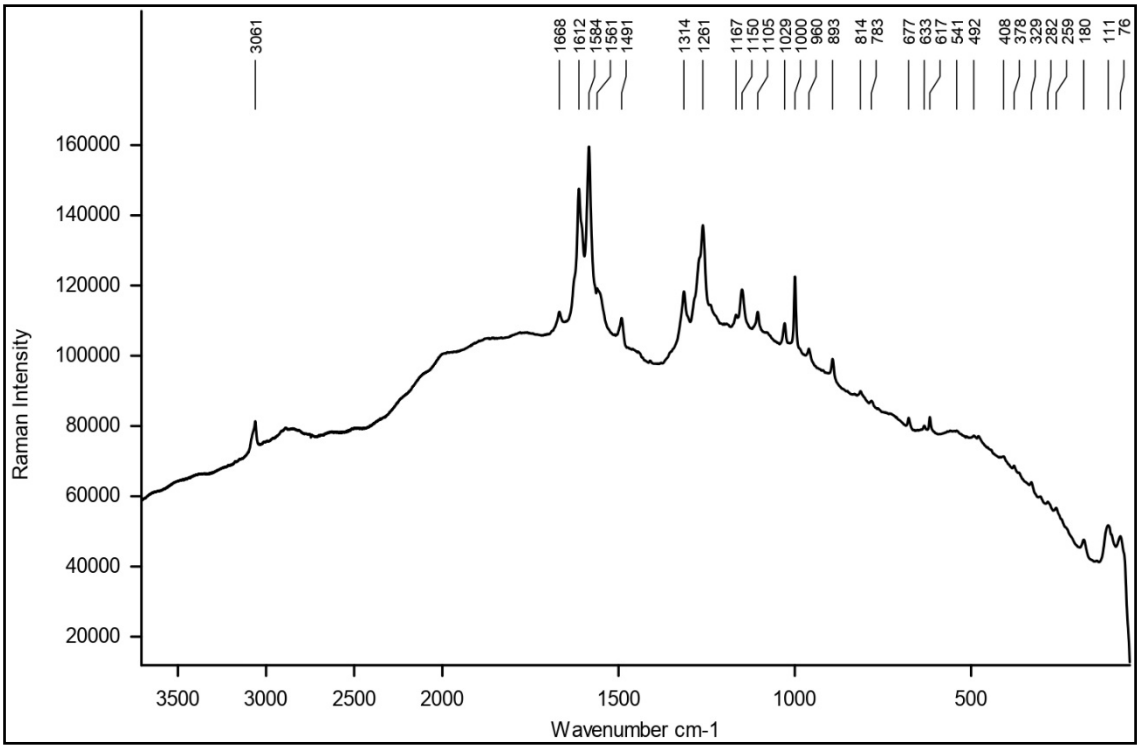

Fig. S21 FT-Raman spectrum of **[H_2L5]Cl** (532 nm, 10mW, 3 coaditions of 10 s).

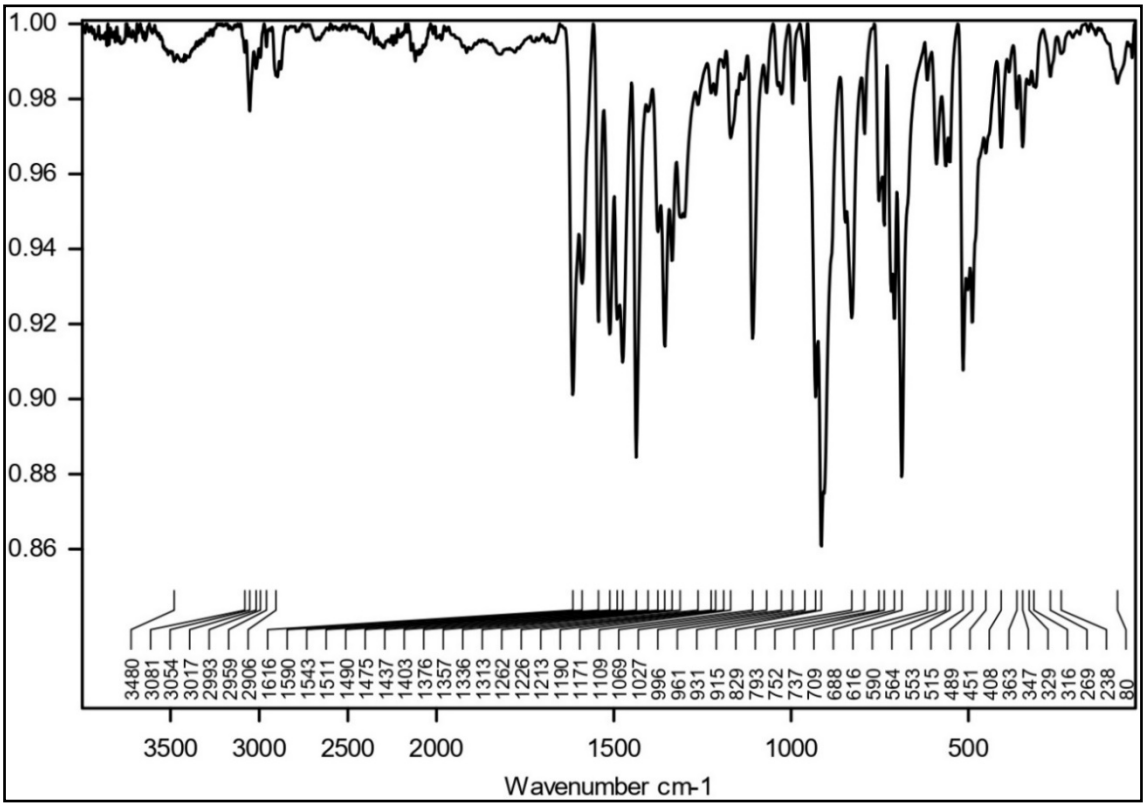

Fig. S22 FT-IR spectrum of $[VO_2L1]\cdot 3H_2O$ (**C1**) (ATR).

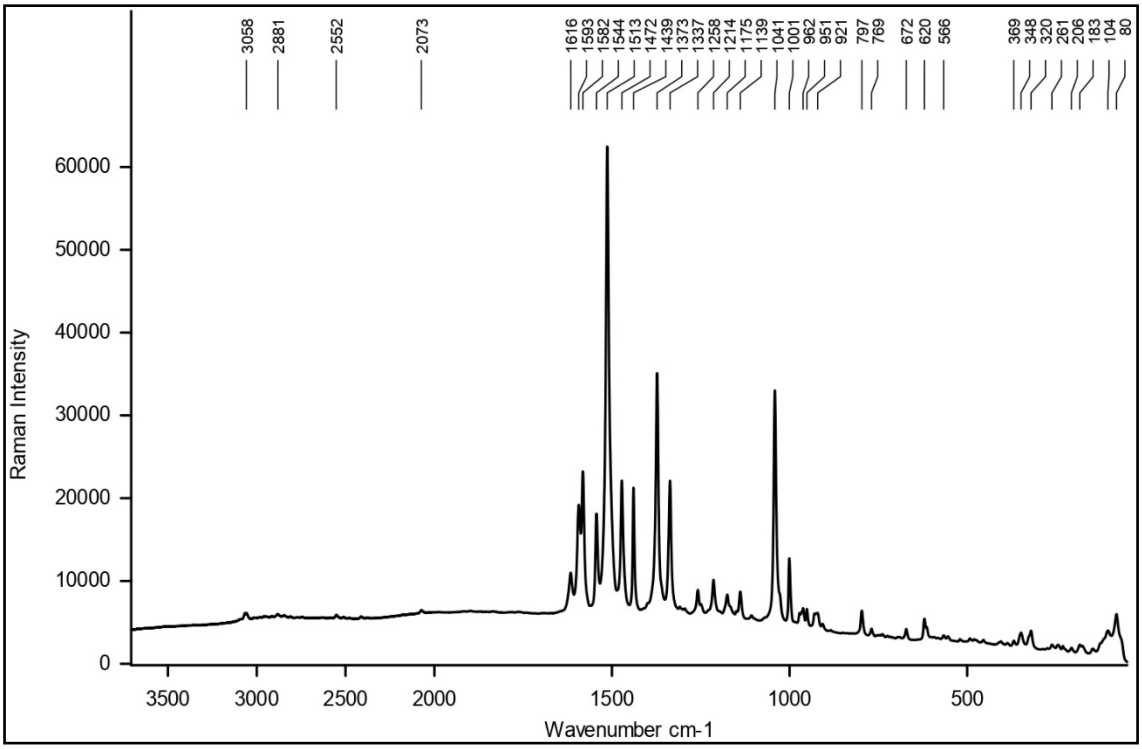

Fig. S23 FT-Raman spectrum of $[VO_2L1]\cdot 3H_2O$ (**C1**) (532 nm, 2mW, 3 coaditions of 10 s).

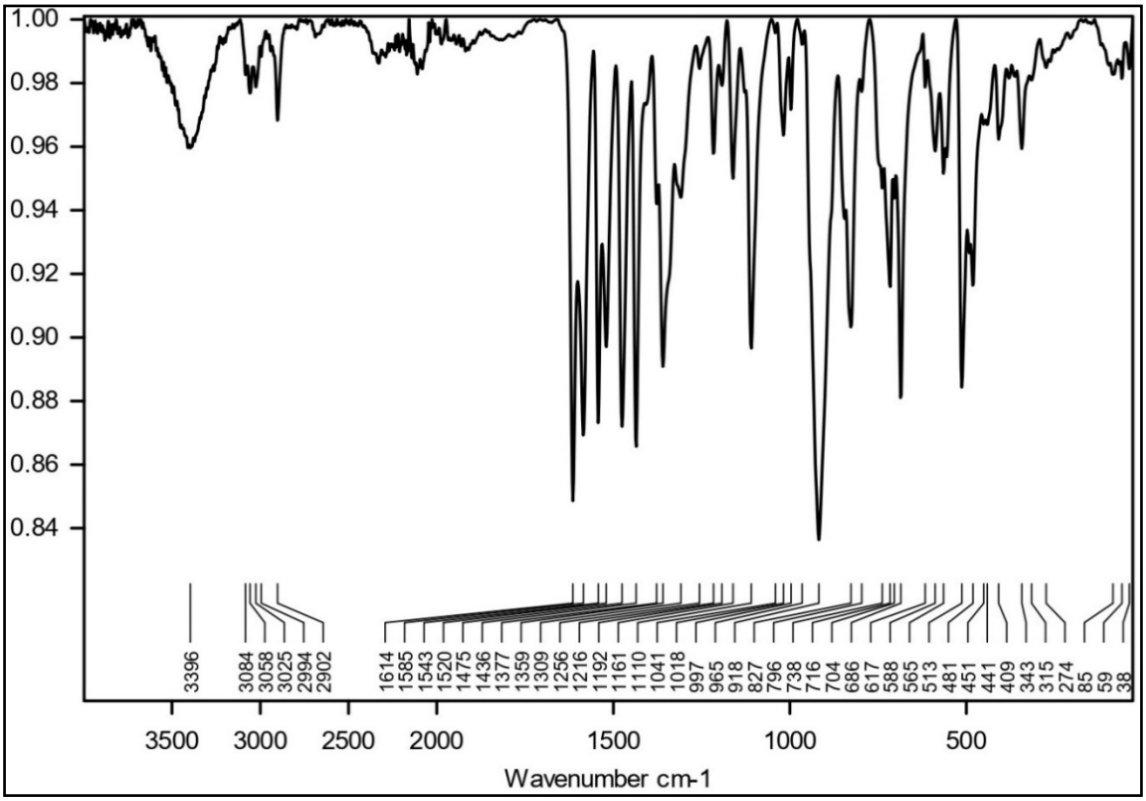

Fig. S24 FT-IR spectrum of $[VO_2L2]\cdot CH_3OH\cdot 4H_2O$ (**C2**) (ATR).

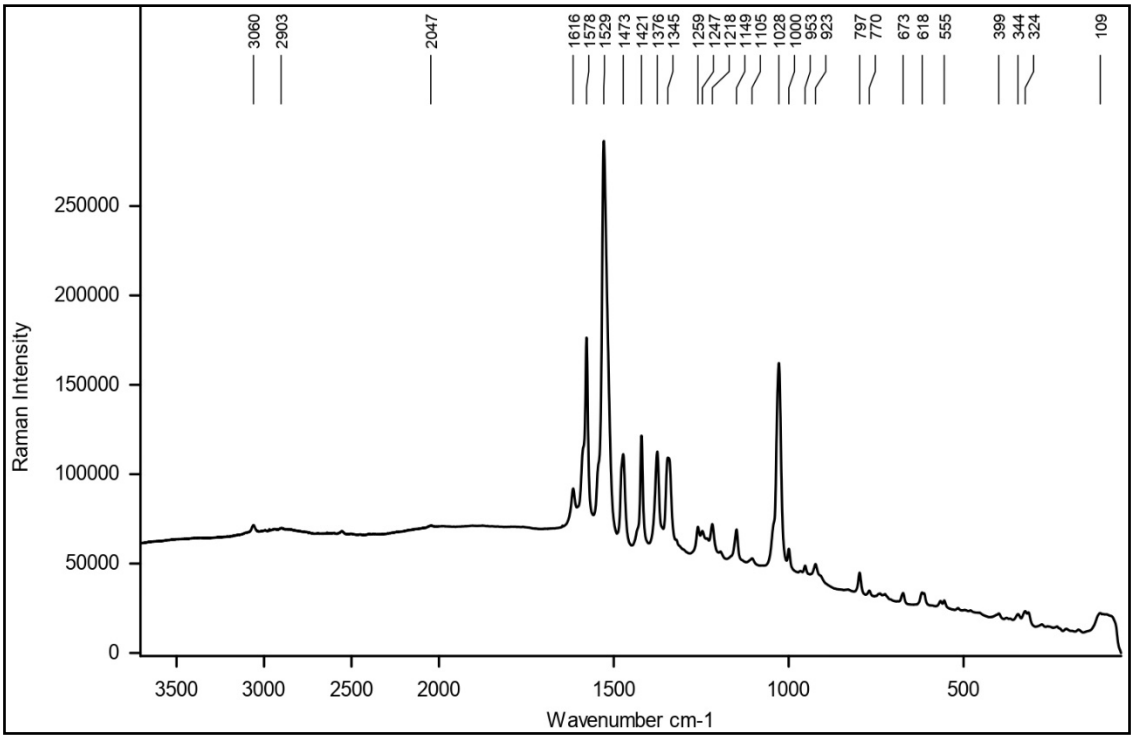

Fig. S25 FT-Raman spectrum of $[VO_2L2]\cdot CH_3OH\cdot 4H_2O$ (**C2**) (532 nm, 0.2mW, 20 coaditions of 30 s).

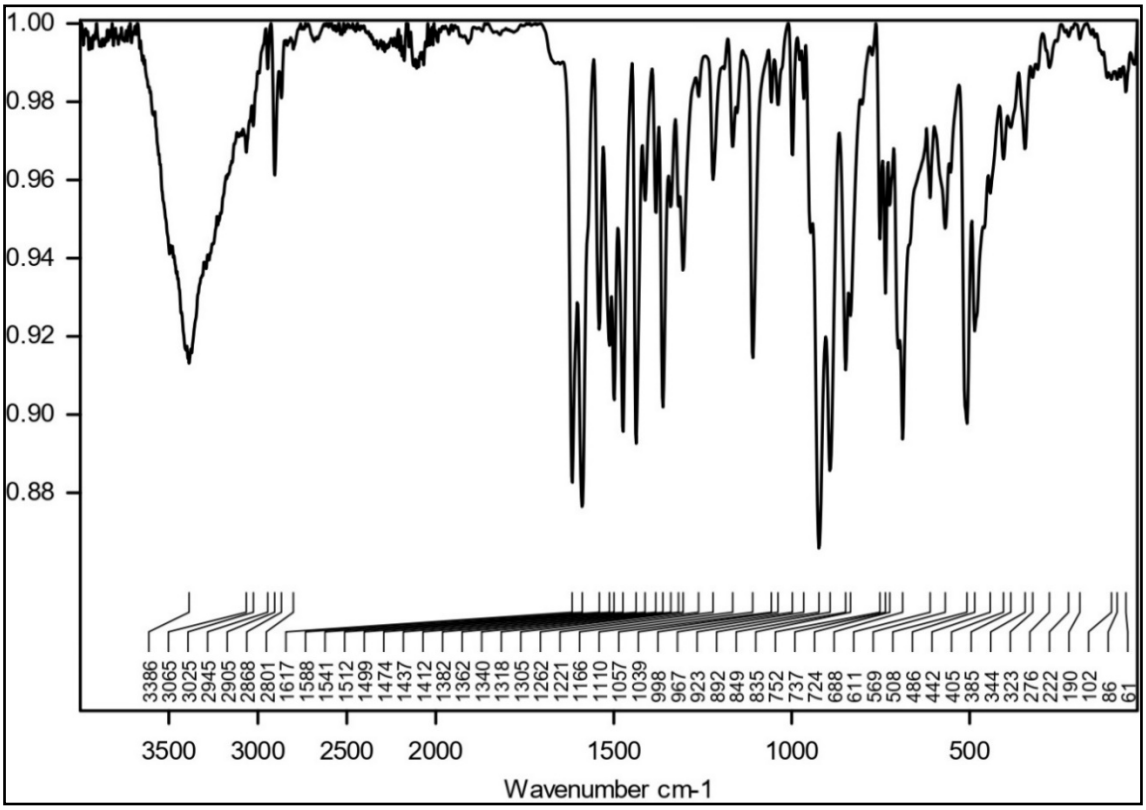

Fig. S26 FT-IR spectrum of $[VO_2L3]\cdot 3.5H_2O$ (**C3**) (ATR).

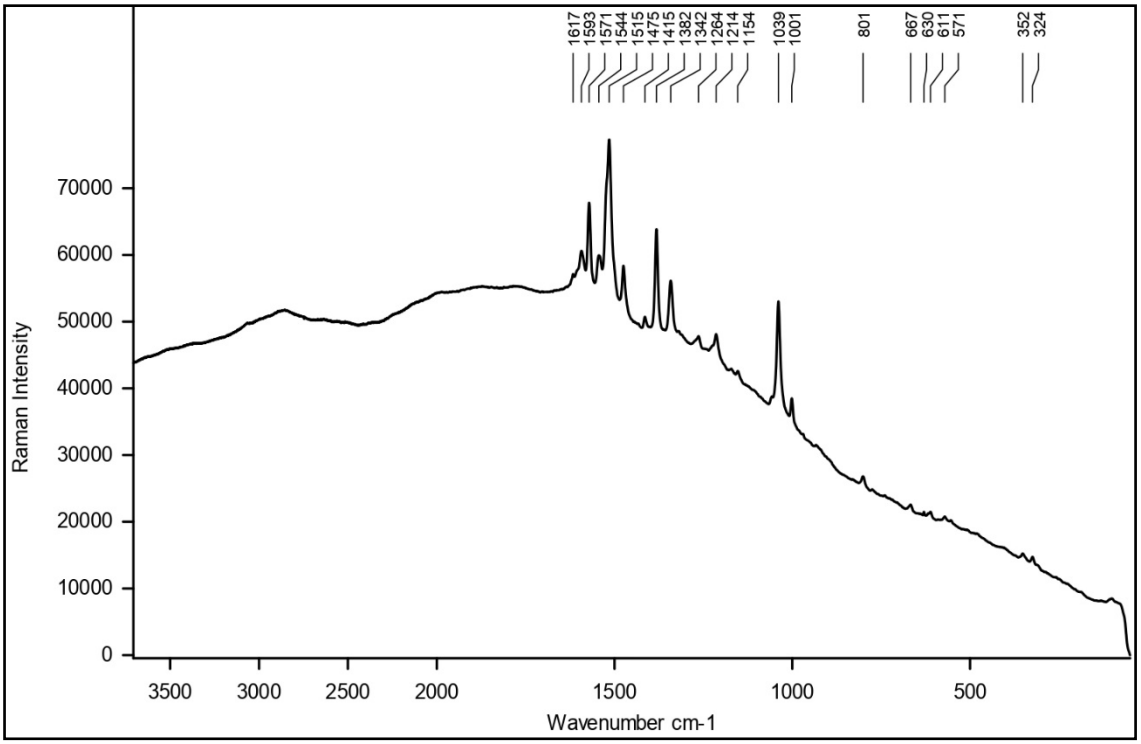

Fig. S27 FT-Raman spectrum of $[VO_2L3]\cdot 3.5H_2O$ (**C3**) (532 nm, 0.2mW, 10 coaditions of 30 s).

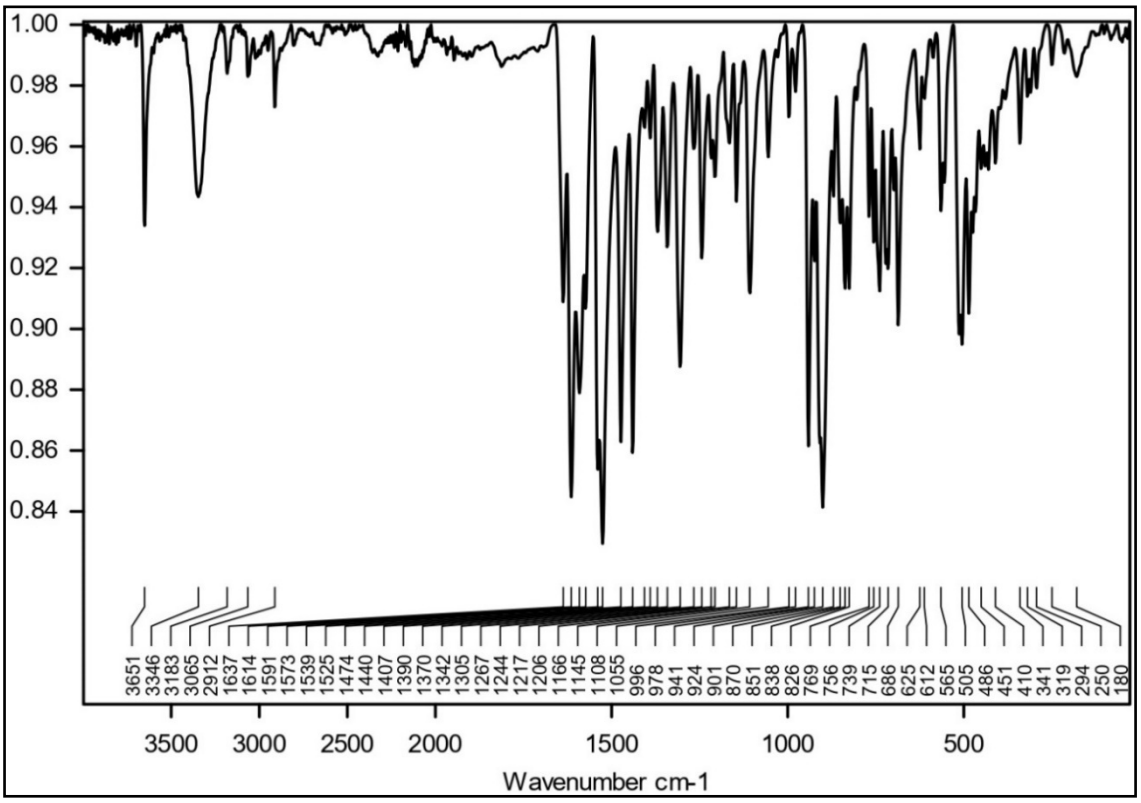

Fig. S28 FT-IR spectrum of $[VO_2HL4]\cdot 2CH_3OH$ (**C4**) (ATR).

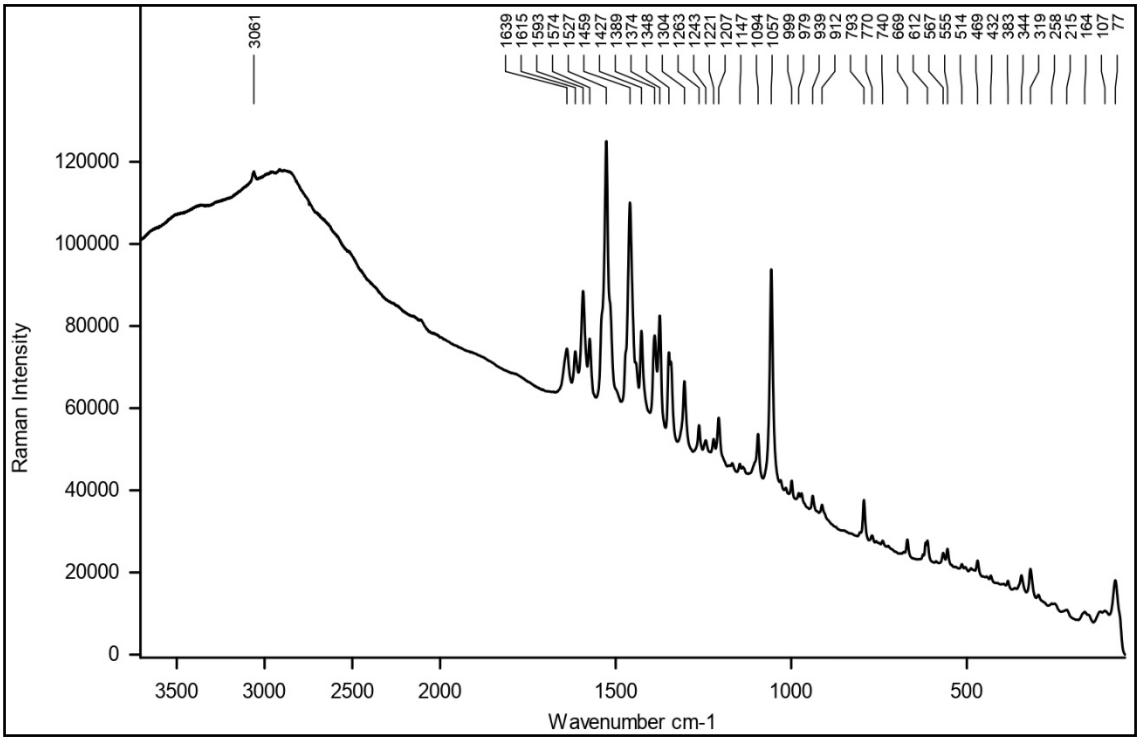

Fig. S29 FT-Raman spectrum of $[VO_2HL4]\cdot 2CH_3OH$ (**C4**) (532 nm, 2mW, 3 coaditions of 10 s).

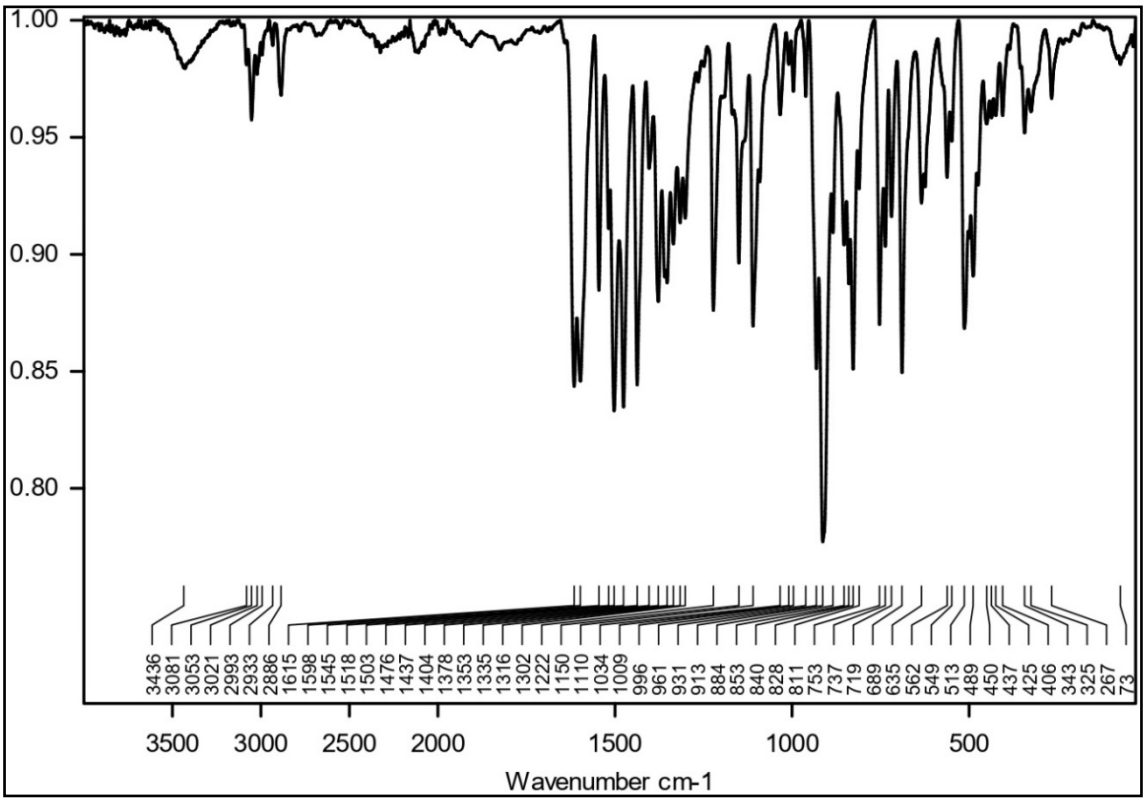

Fig. S30 FT-IR spectrum of $[VO_2L5]\cdot CH_3OH\cdot H_2O$ (**C5**) (ATR).

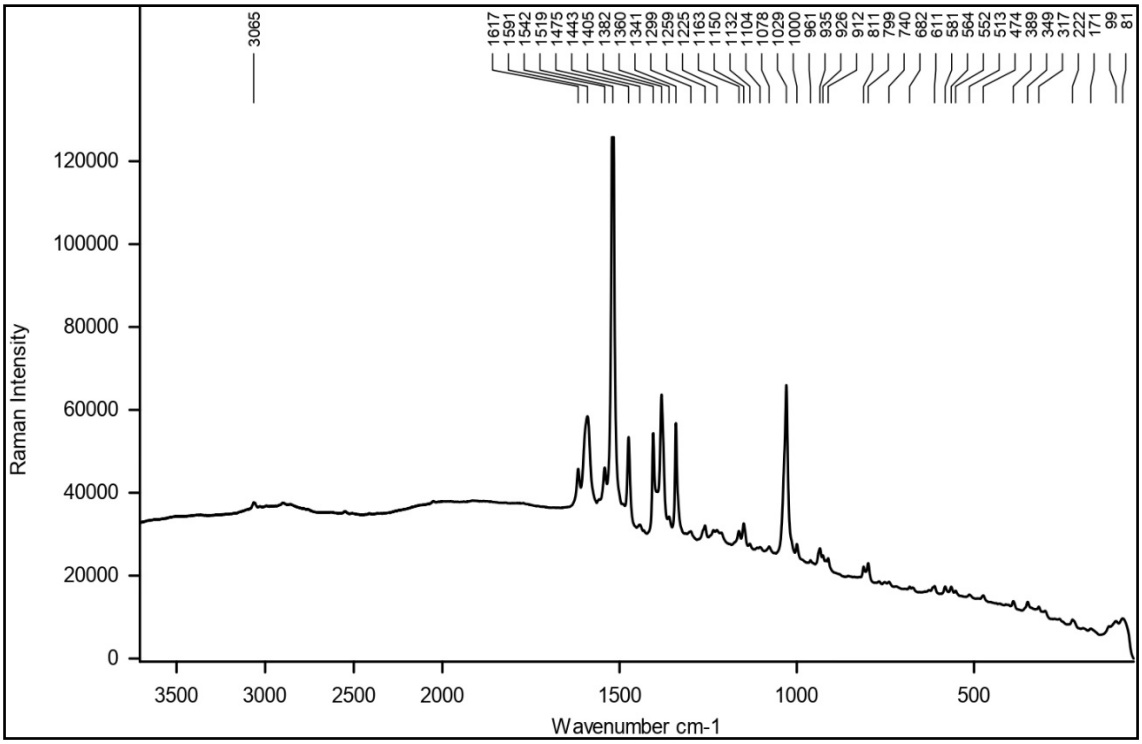

Fig. S31 FT-Raman spectrum of $[VO_2L5]\cdot CH_3OH\cdot H_2O$ (**C5**) (532 nm, 2mW, 3 coaditions of 10 s).

^{1}H, ^{13}C, ^{19}F, ^{31}P, and ^{51}V-NMR spectra of the compounds

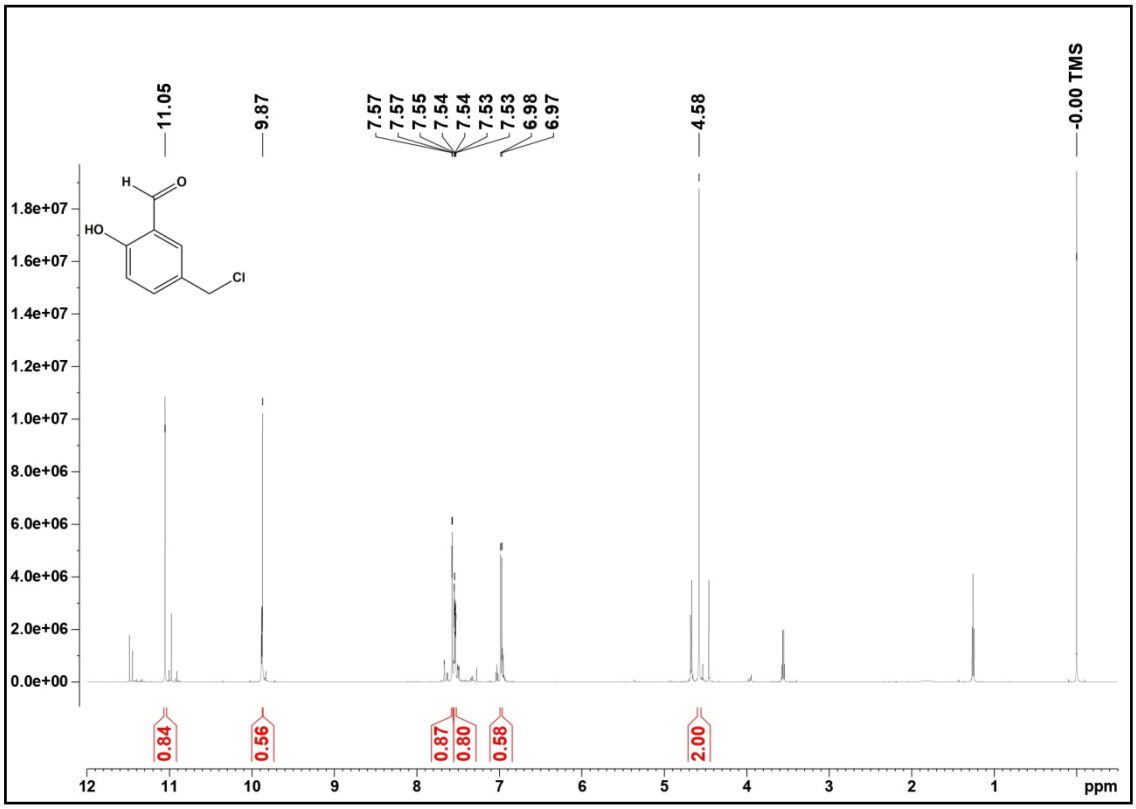

Fig. S32 ^{1}H-NMR spectra of 5-(chloromethyl)-2-hydroxybenzaldehyde (600 MHz, $CDCl_3$).

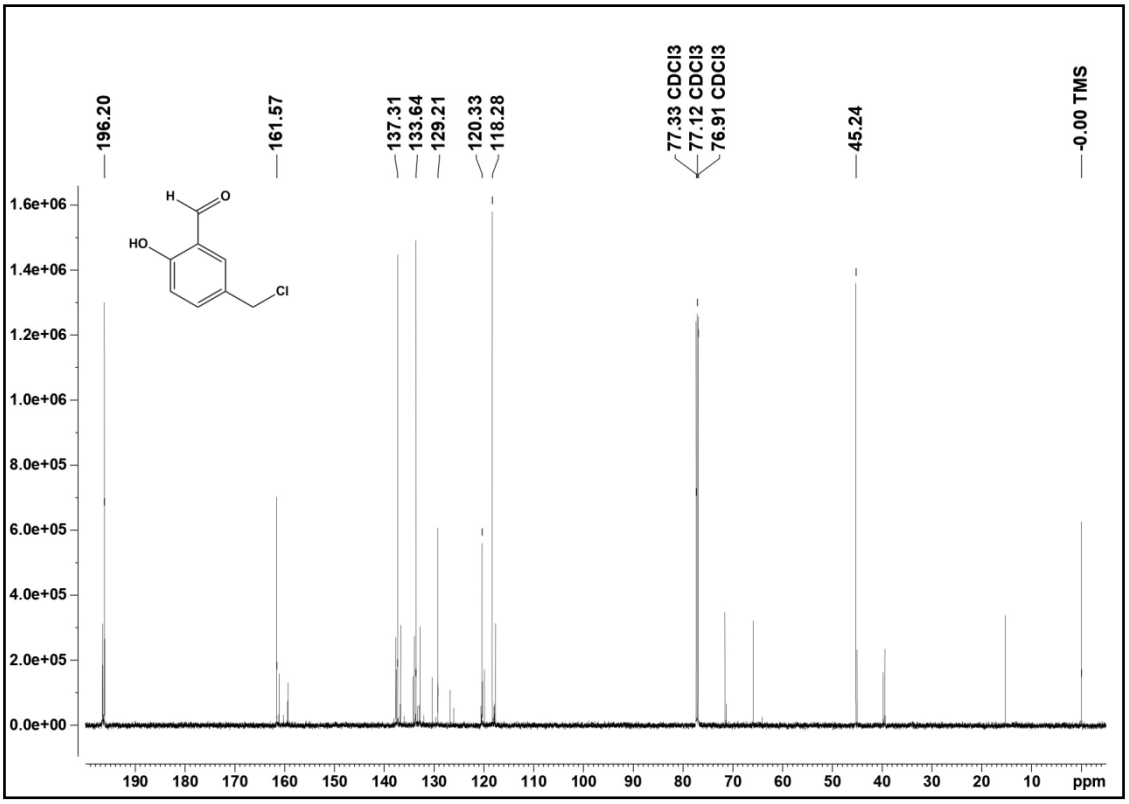

Fig. S33 ^{13}C-NMR spectra of 5-(chloromethyl)-2-hydroxybenzaldehyde (151 MHz, $CDCl_3$).

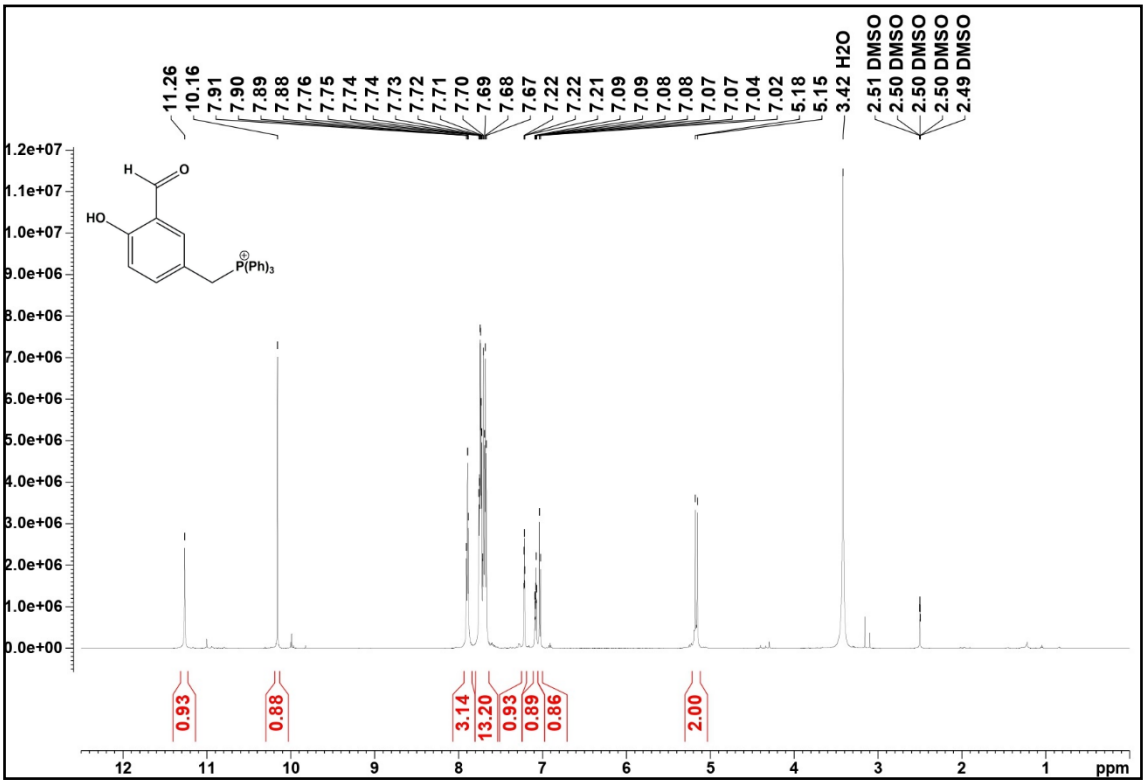

Fig. S34 ^{1}H-NMR spectra of **[AH]Cl** (600 MHz, DMSO-d_6).

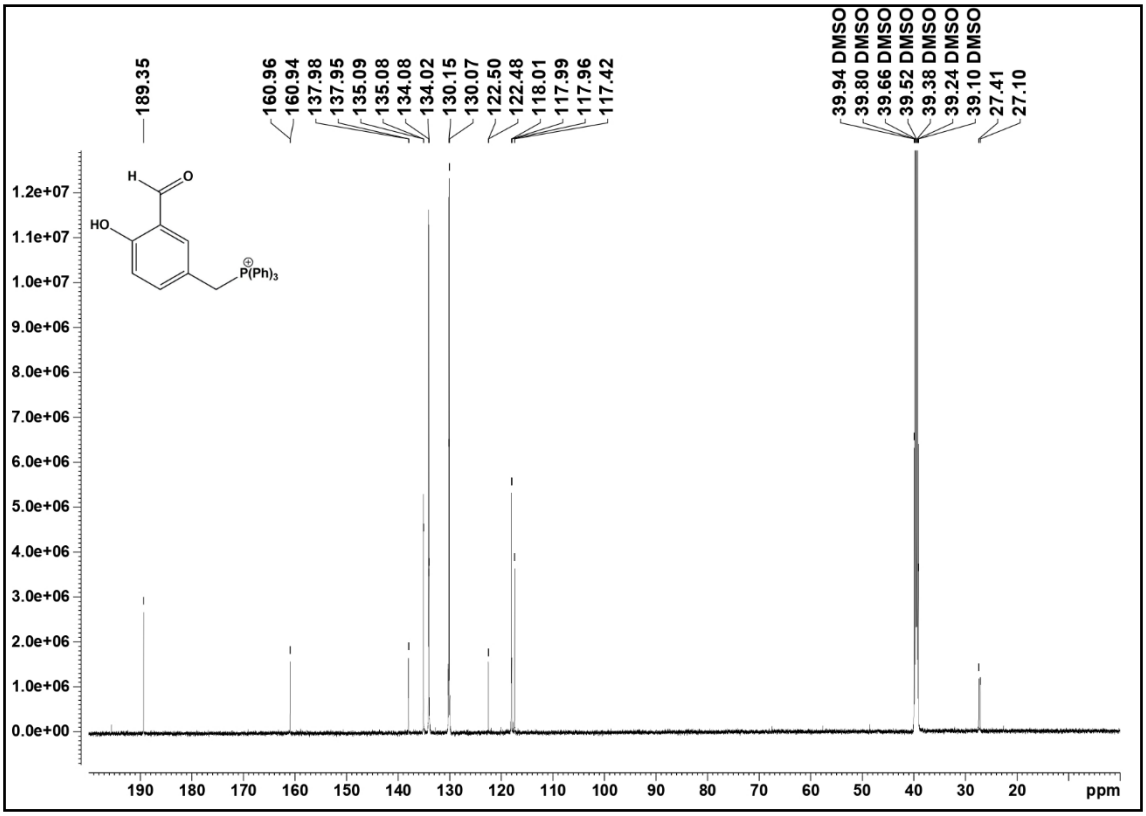

Fig. S35 ^{13}C-NMR spectra of **[AH]Cl** (151 MHz, DMSO-d_6).

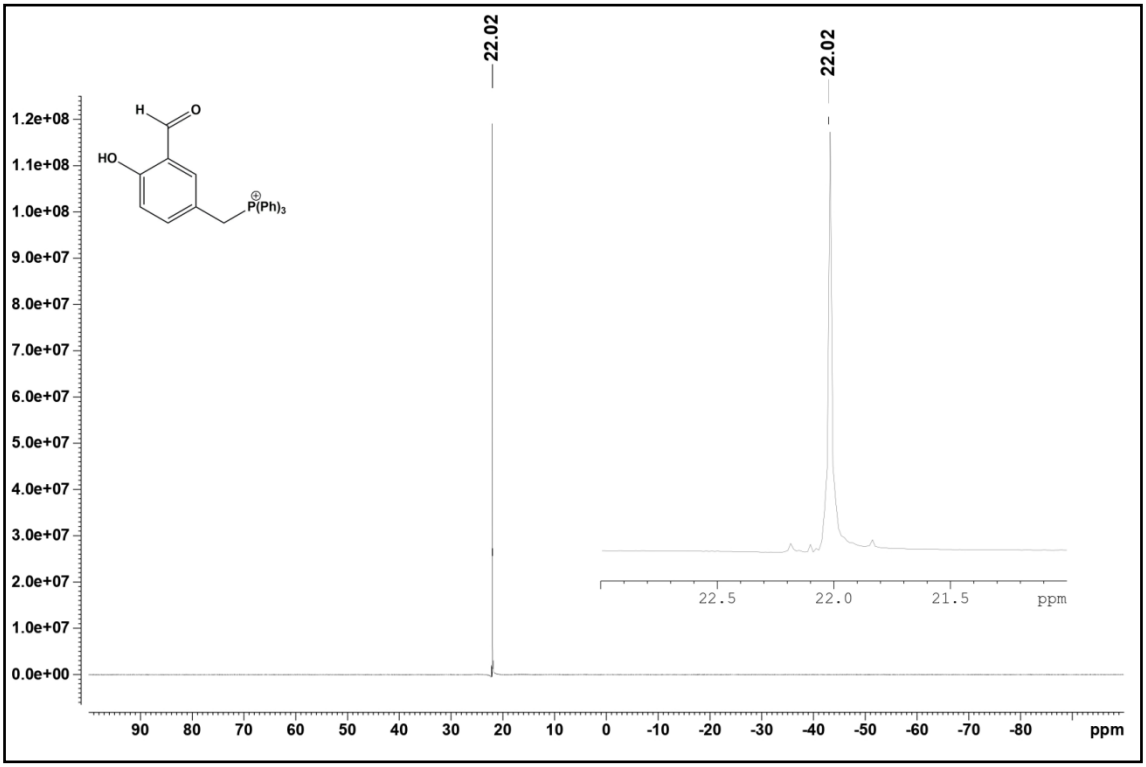

Fig. S36 ^{31}P-NMR spectra of **[AH]Cl** (243 MHz, DMSO-d_6).

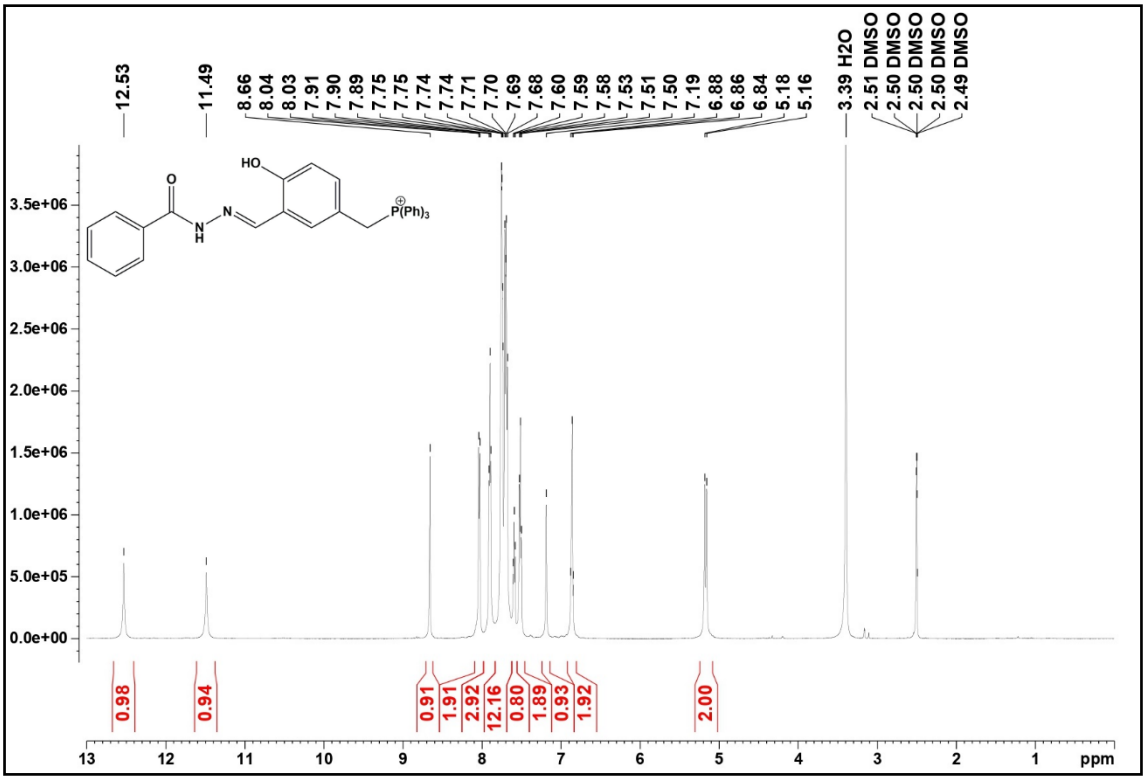

Fig. S37 ^{1}H-NMR spectra of **[H_2L1]Cl** (600 MHz, DMSO-d_6).

Fig. S38 ^{13}C-NMR spectra of **[H_2L1]Cl** (151 MHz, DMSO-d_6).

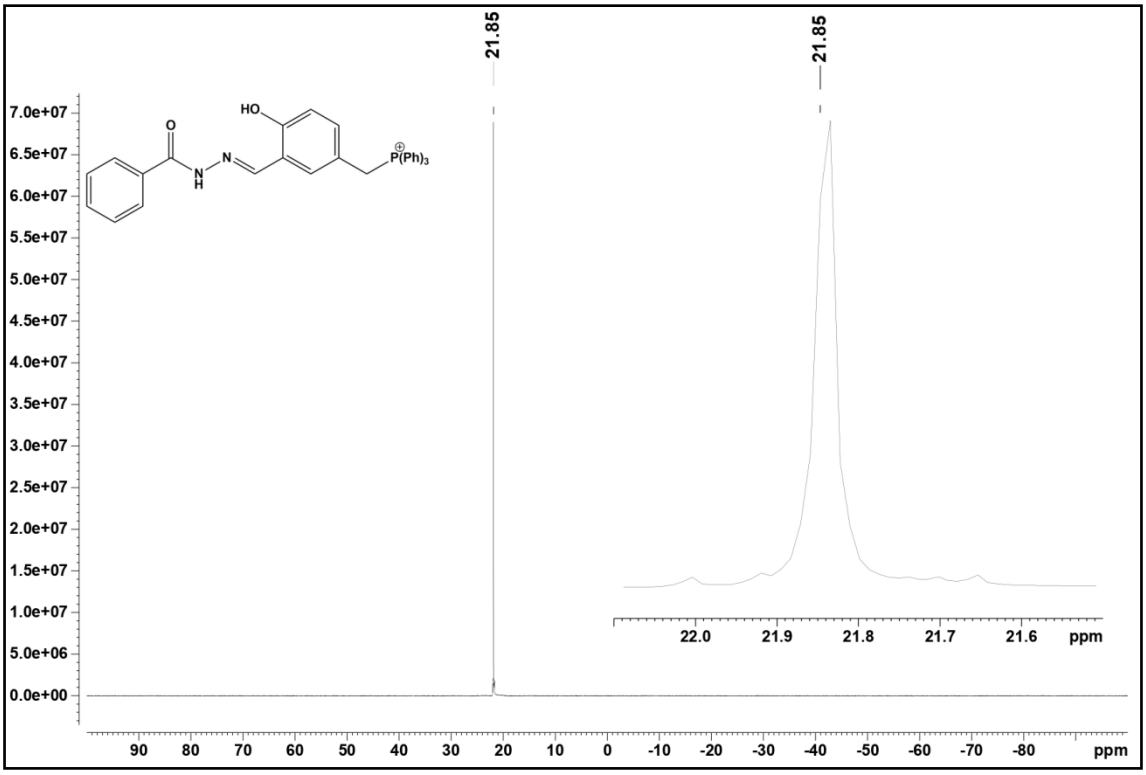

Fig. S39 ^{31}P-NMR spectra of **[H_2L1]Cl** (243 MHz, DMSO-d_6).

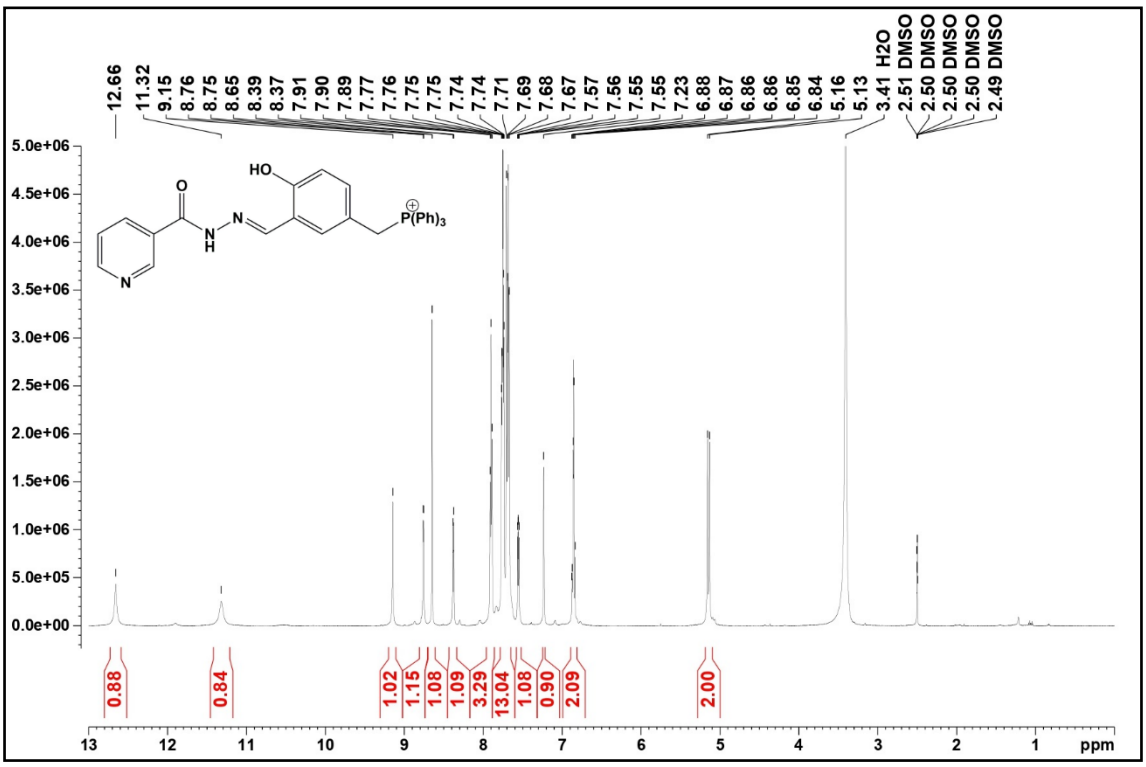

Fig. S40 ^{1}H-NMR spectra of **[H_2L2]Cl** (600 MHz, DMSO-d_6).

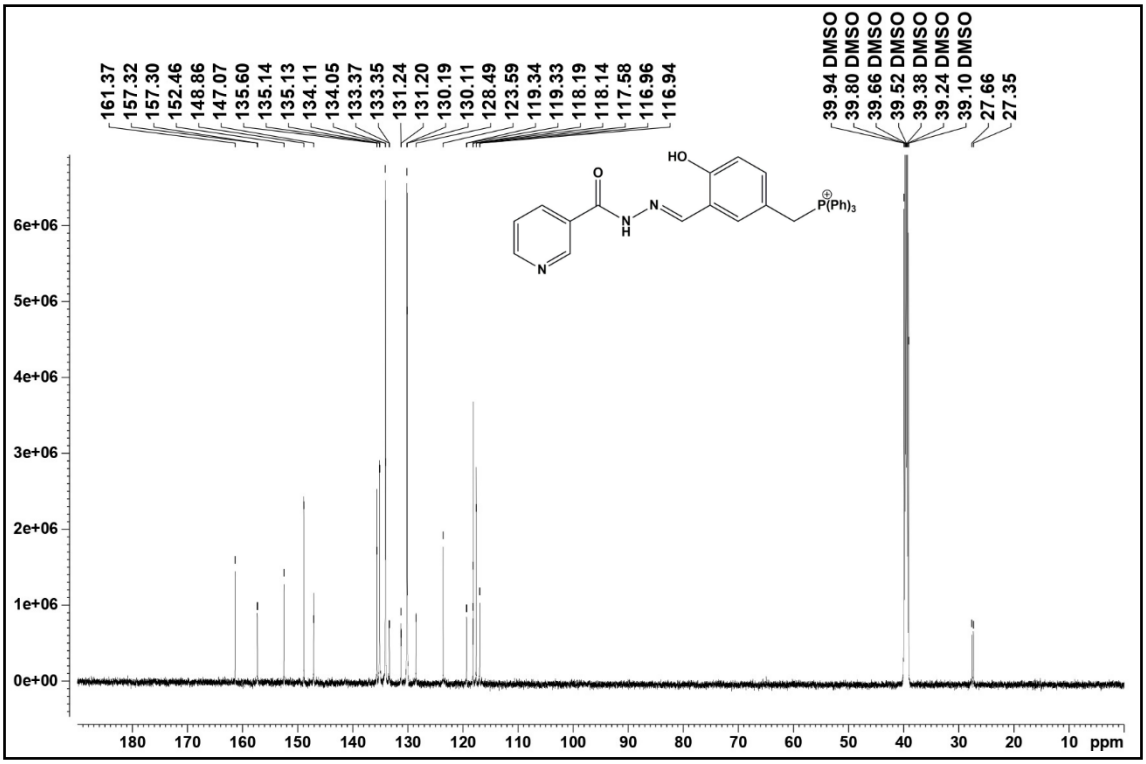

Fig. S41 ^{13}C-NMR spectra of **[H_2L2]Cl** (151 MHz, DMSO-d_6).

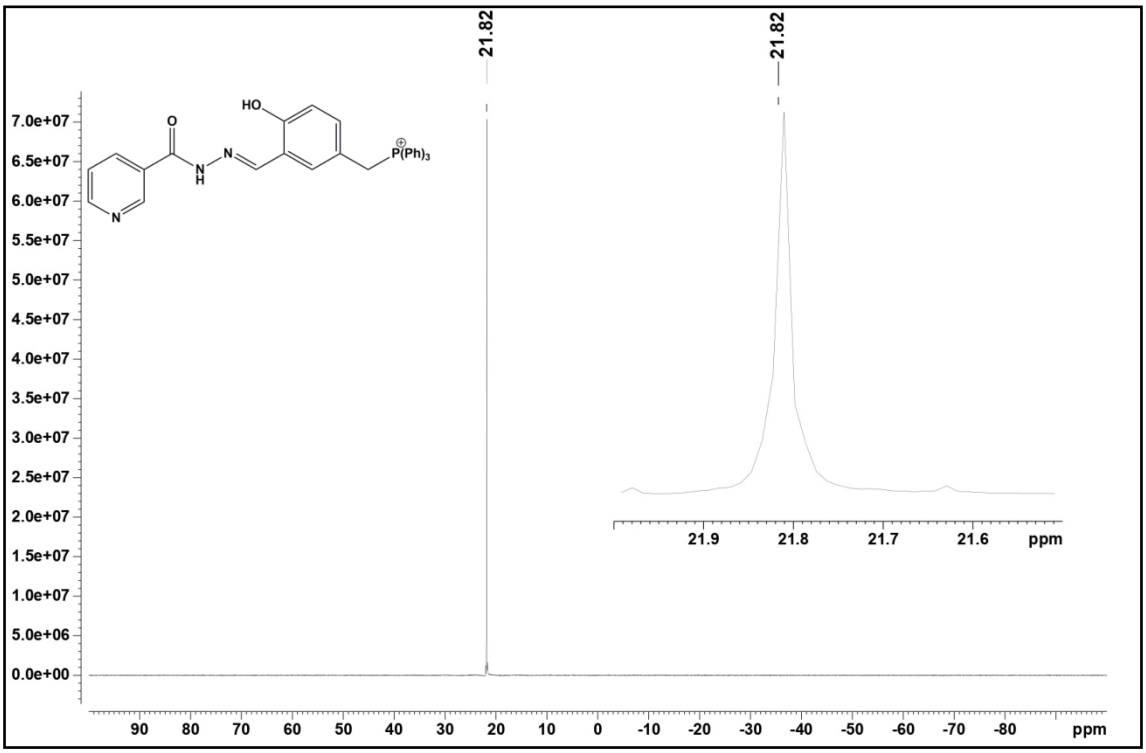

Fig. S42 ^{31}P-NMR spectra of **[H_2L2]Cl** (243 MHz, DMSO-d_6).

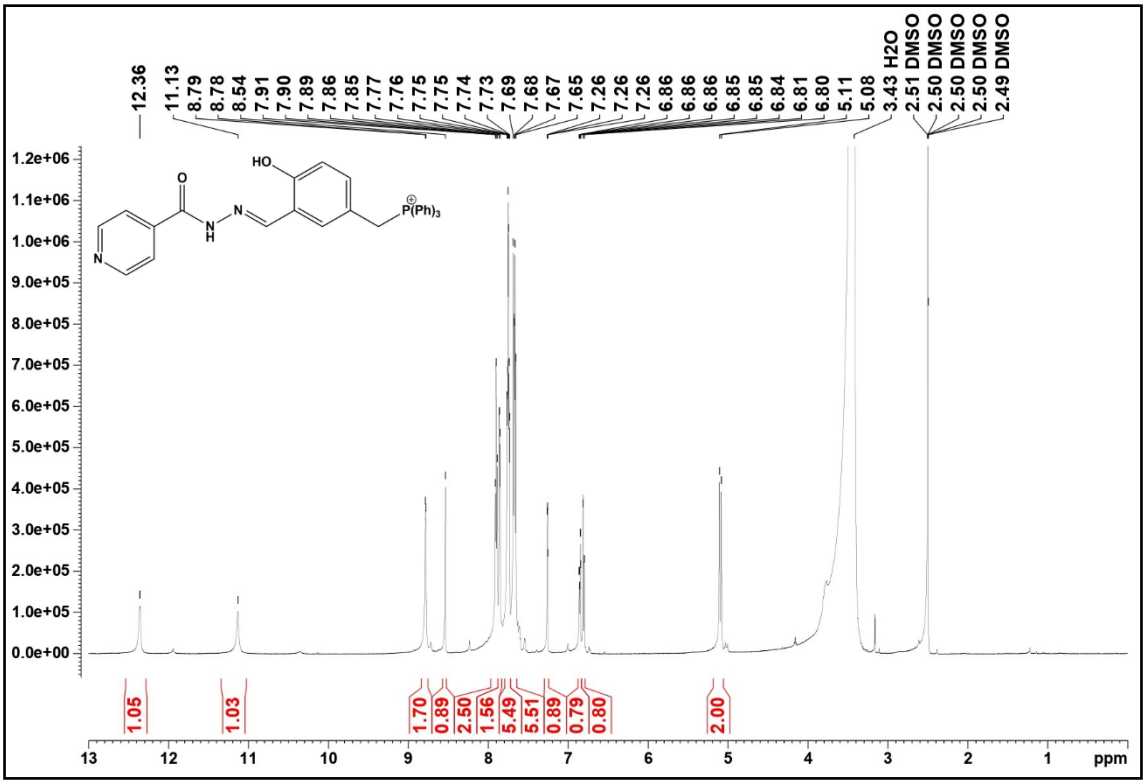

Fig. S43 ^{1}H-NMR spectra of **[H_2L3]Cl** (600 MHz, DMSO-d_6).

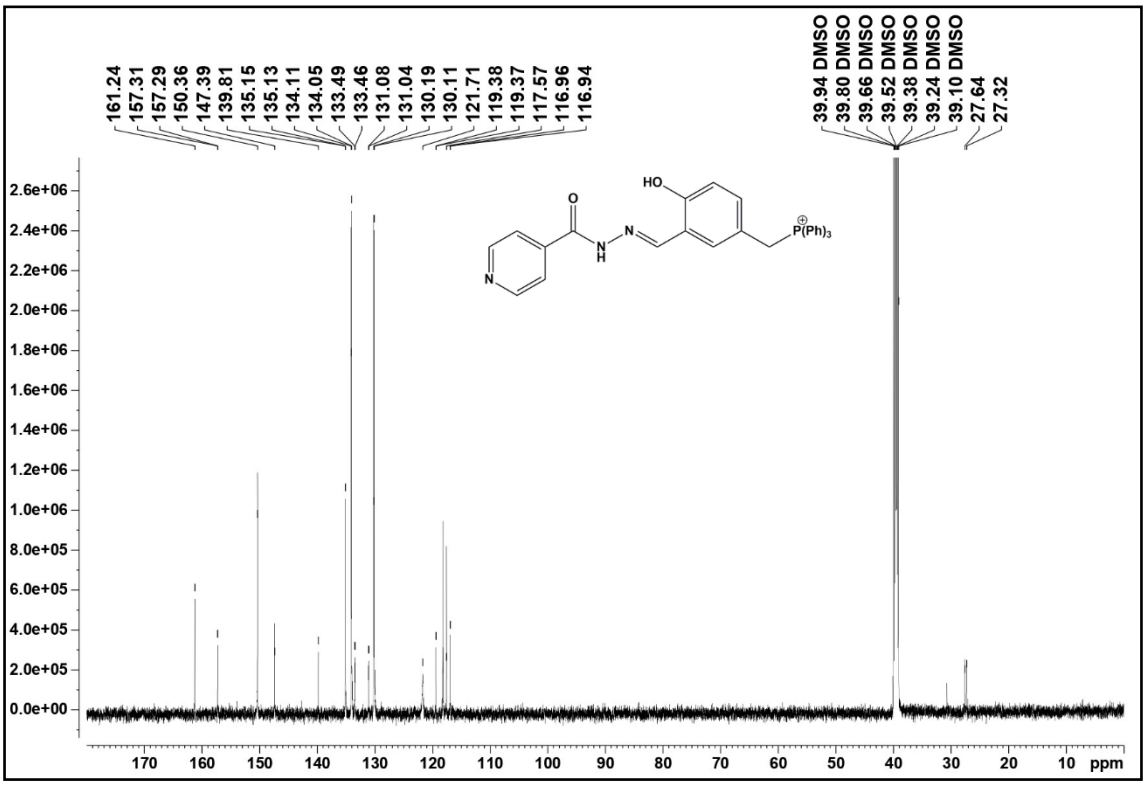

Fig. S44 ^{13}C-NMR spectra of **[H_2L3]Cl** (151 MHz, DMSO-d_6).

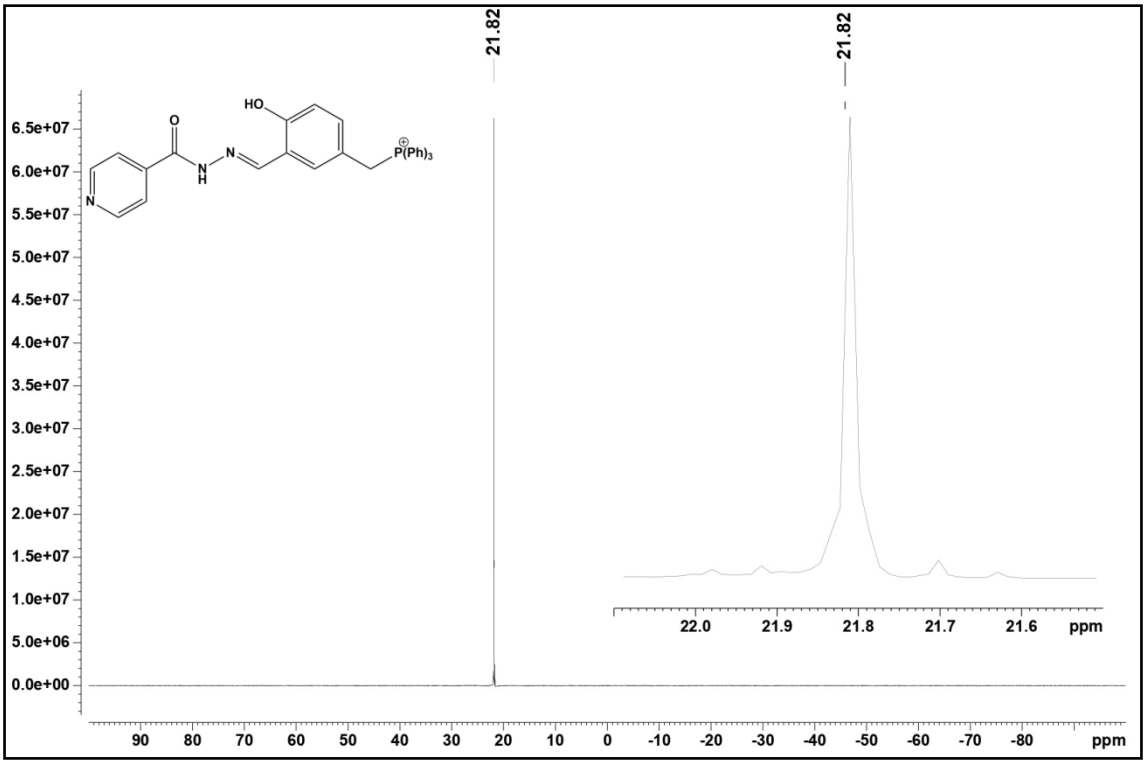

Fig. S45 ^{31}P-NMR spectra of **[H_2L3]Cl** (243 MHz, DMSO-d_6).

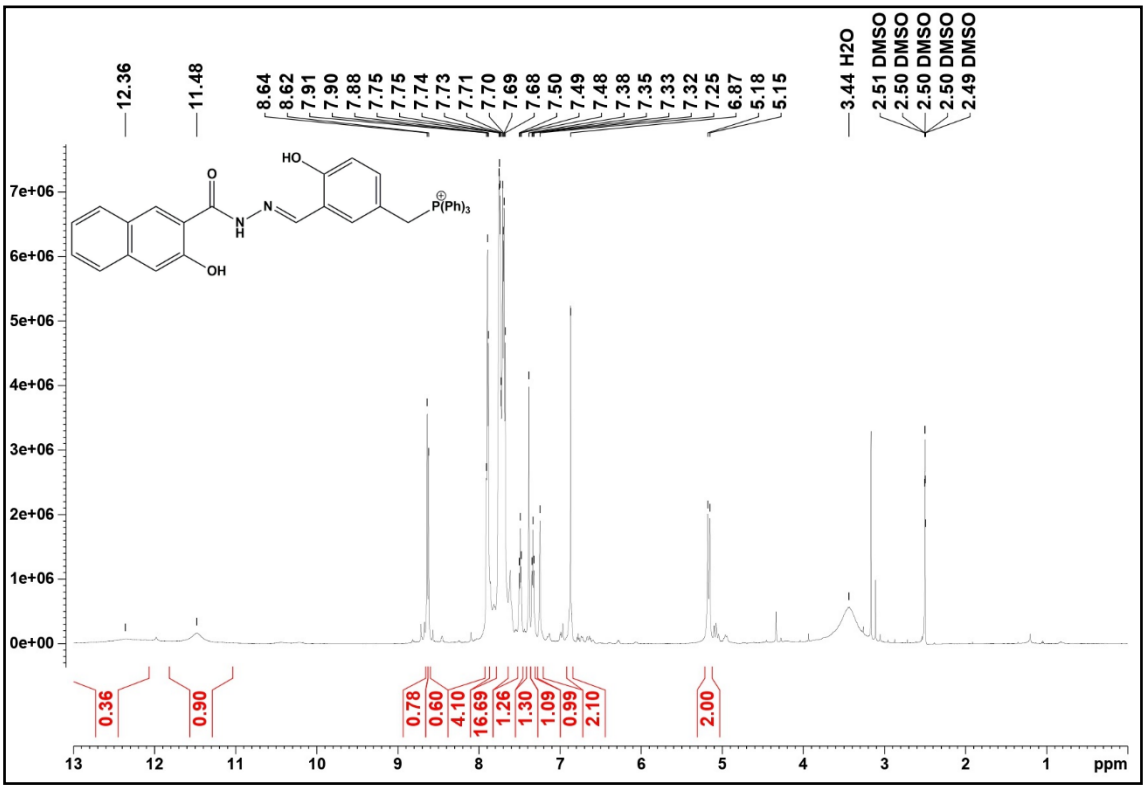

Fig. S46 ^{1}H-NMR spectra of the ligand **[H_3L4]Cl** (600 MHz, DMSO-d_6).

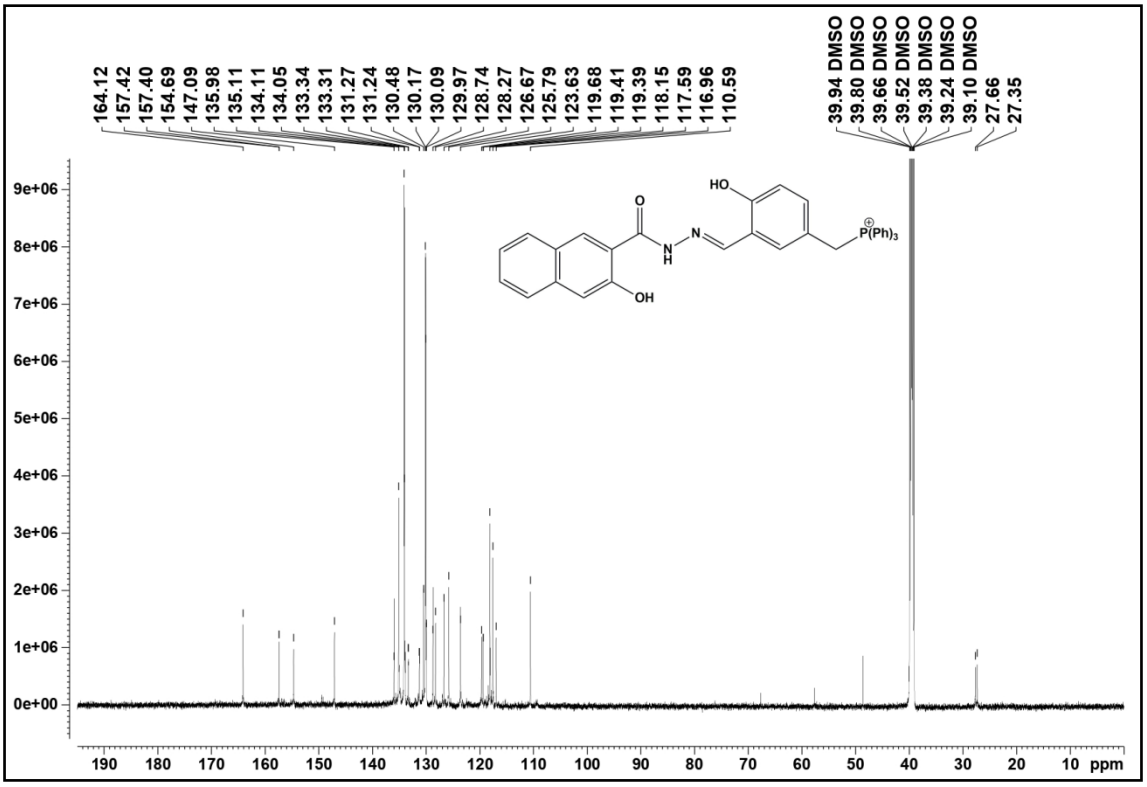

Fig. S47 ^{13}C-NMR spectra of the ligand **[H_3L4]Cl** (151 MHz, DMSO-d_6).

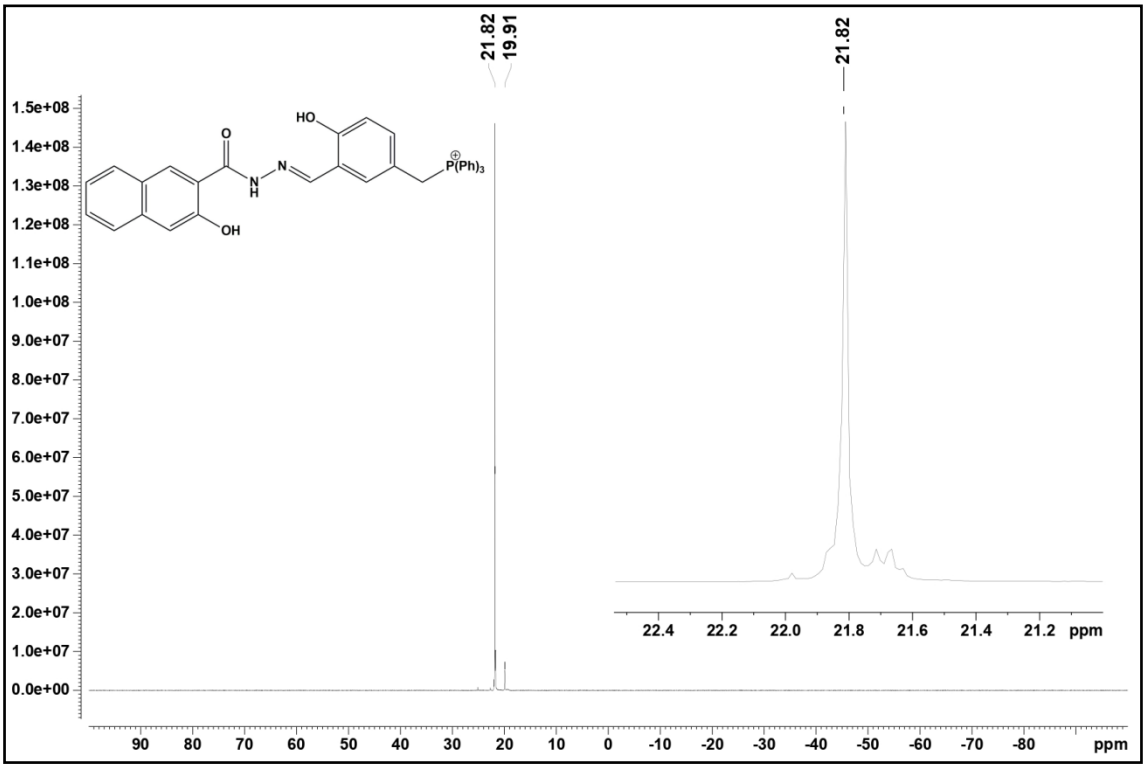

Fig. S48 ^{31}P-NMR spectra of the ligand **[H_3L4]Cl** (243 MHz, DMSO-d_6).

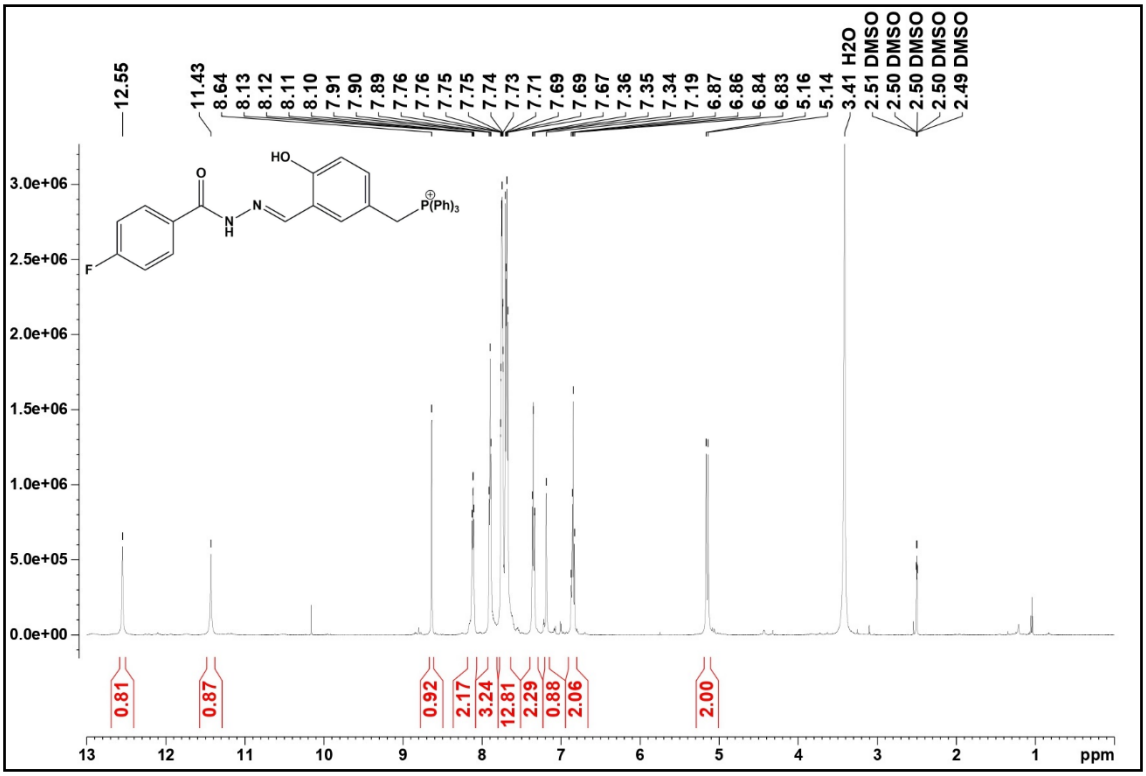

Fig. S49 ^{1}H-NMR spectra of **[H_2L5]Cl** (600 MHz, DMSO-d_6).

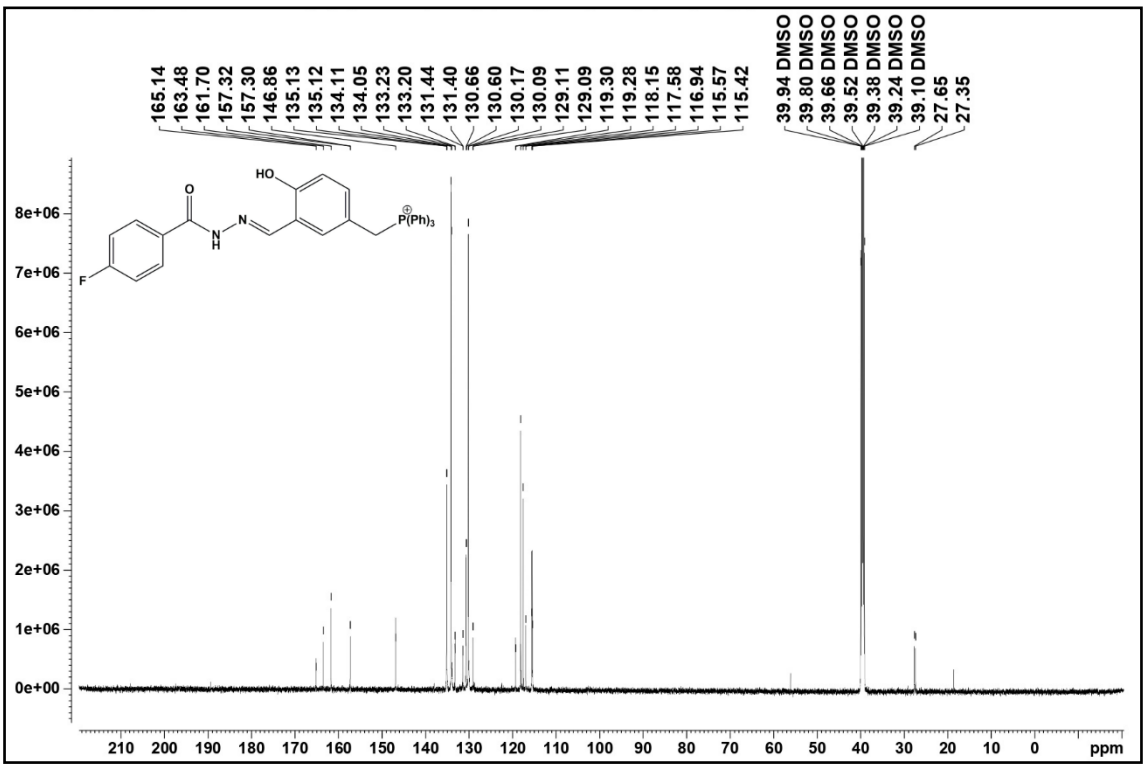

Fig. S50 ^{13}C-NMR spectra of **[H_2L5]Cl** (151 MHz, DMSO-d_6).

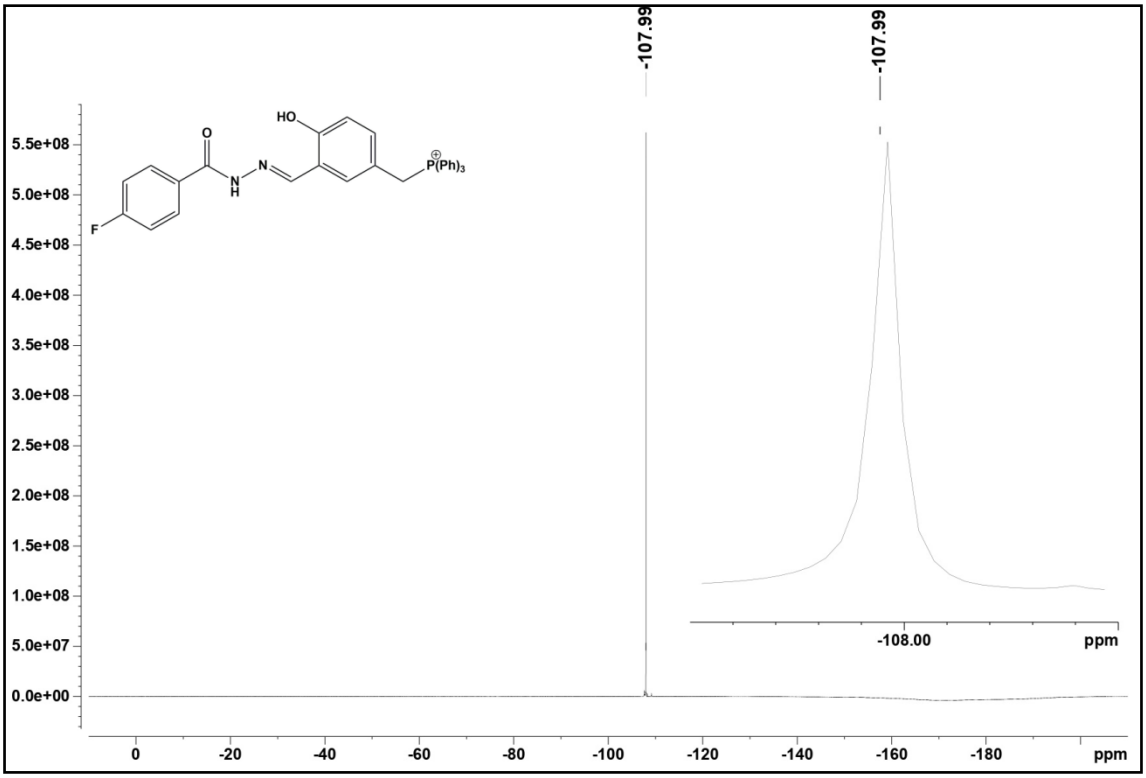

Fig. S51 ^{19}F-NMR spectra of **[H_2L5]Cl** (565 MHz, DMSO-d_6).

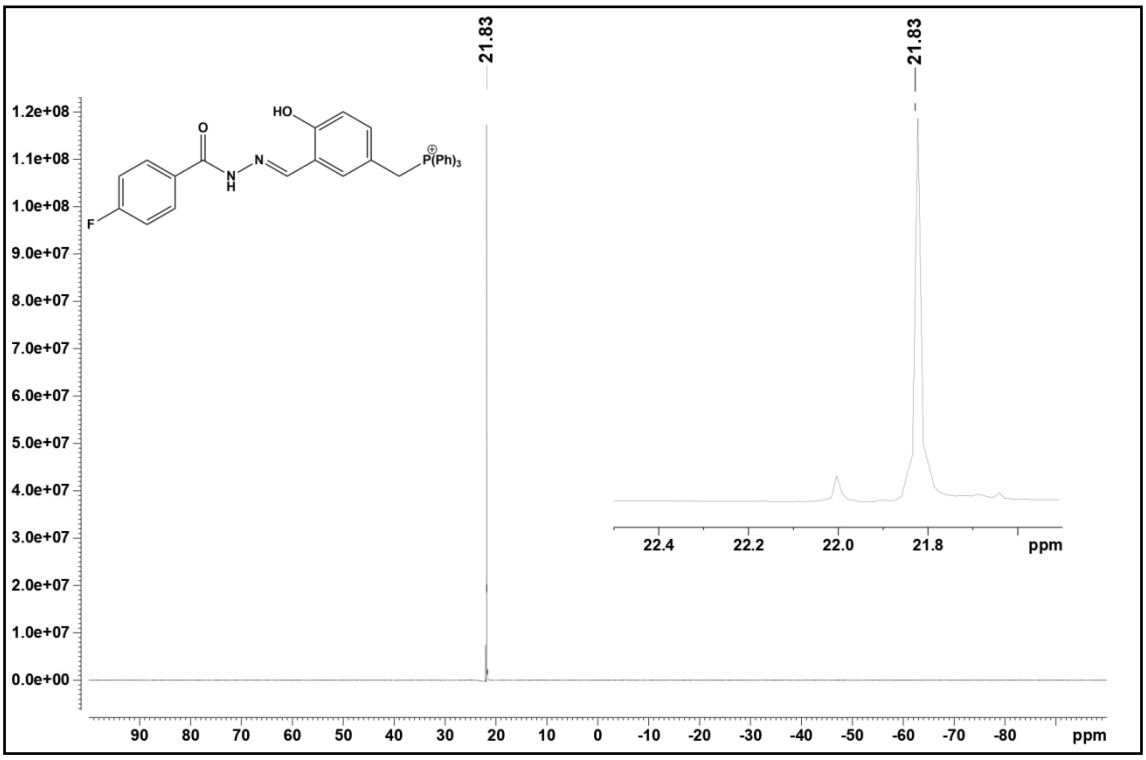

Fig. S52 ^{31}P-NMR spectra of **[H_2L5]Cl** (243 MHz, DMSO-d_6).

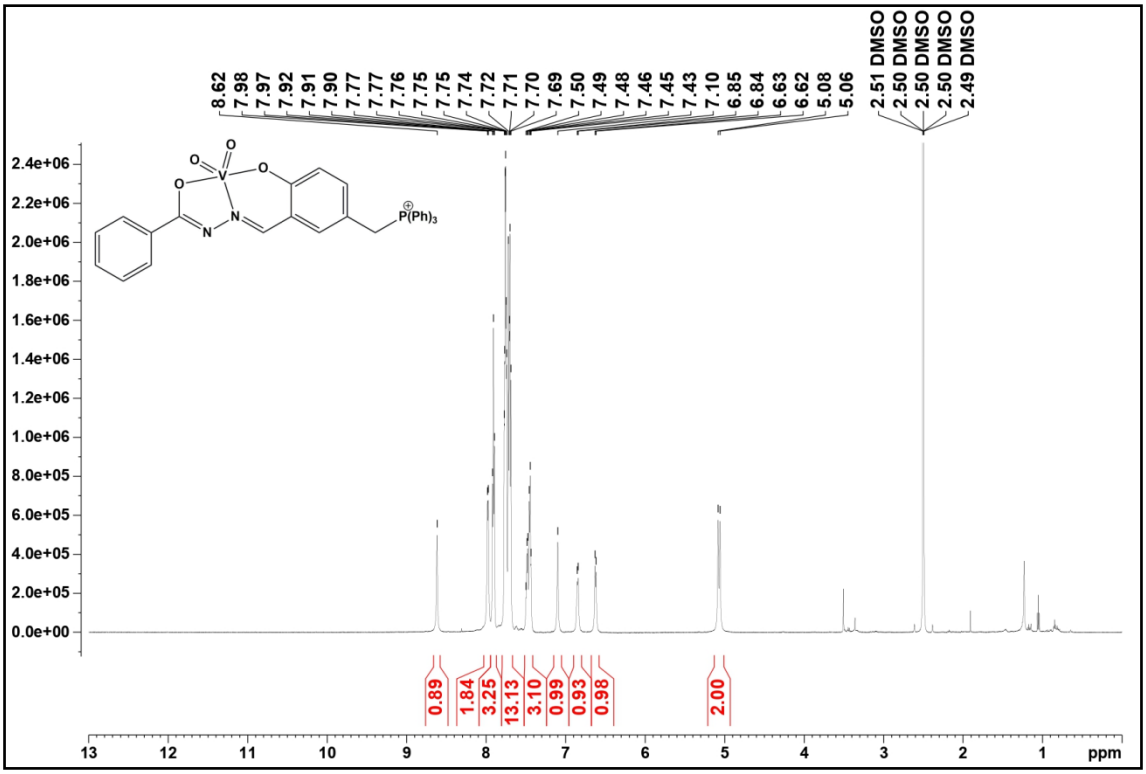

Fig. S53 ^{1}H-NMR spectra of [VO_2**L1**]·3H_2O (**C1**) (600 MHz, DMSO-d_6).

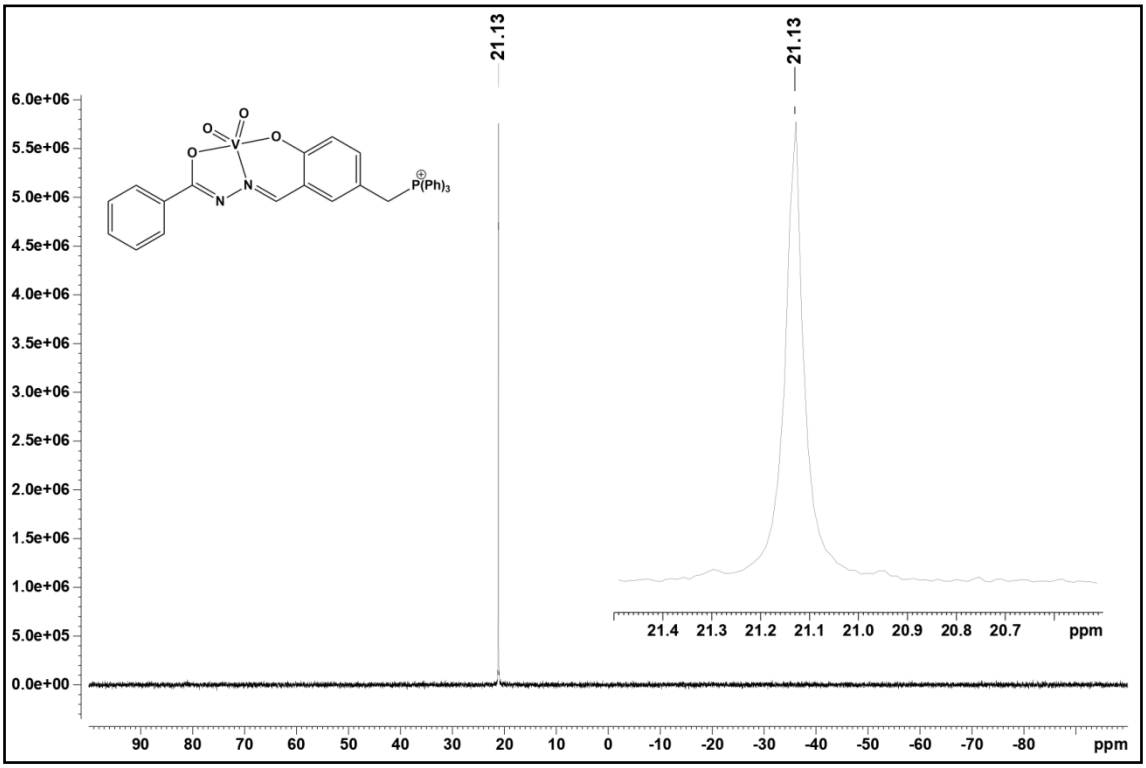

Fig. S54 ^{31}P-NMR spectra of [VO_2**L1**]·3H_2O (**C1**) (243 MHz, DMSO-d_6).

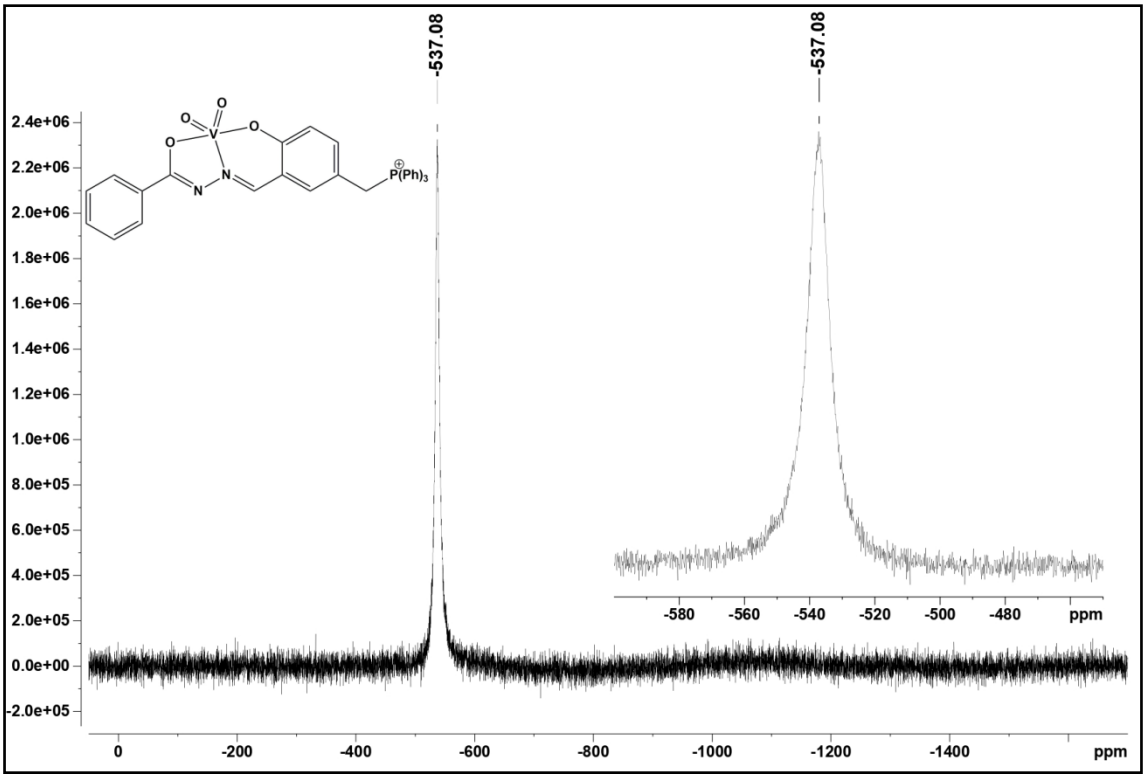

Fig. S55 ^{51}V-NMR spectra of [VO_2**L1**]·3H_2O (**C1**) (158 MHz, DMSO-d_6).

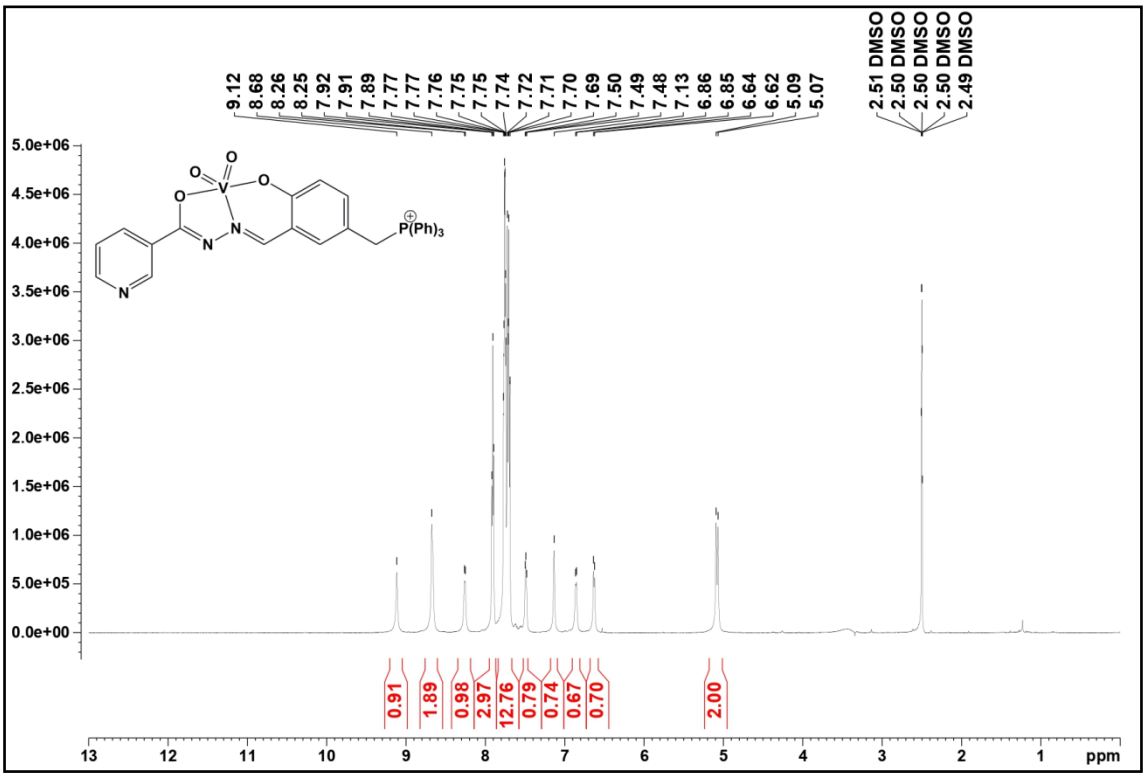

Fig. S56 ^{1}H-NMR spectra of [VO_2**L2**]·CH_3OH·4H_2O (**C2**) (600 MHz, DMSO-d_6).

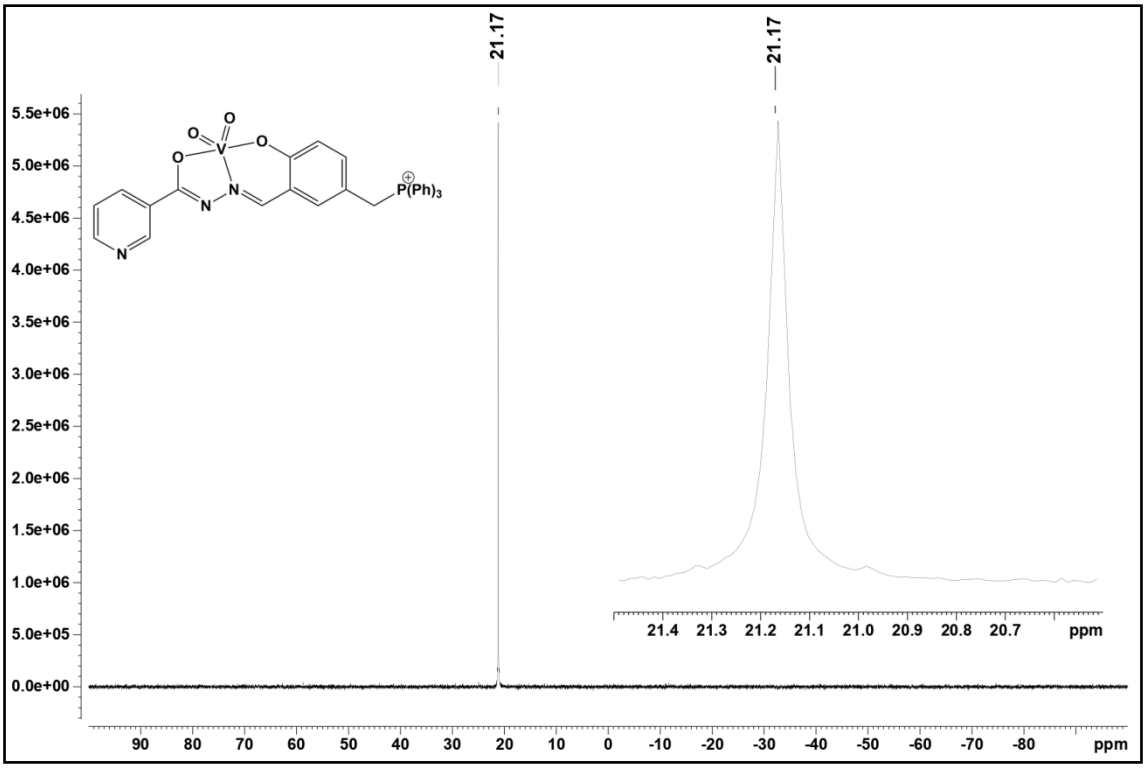

Fig. S57 ^{31}P-NMR spectra of [VO_2**L2**]·CH_3OH·$4H_2O$ (**C2**) (243 MHz, DMSO-d_6).

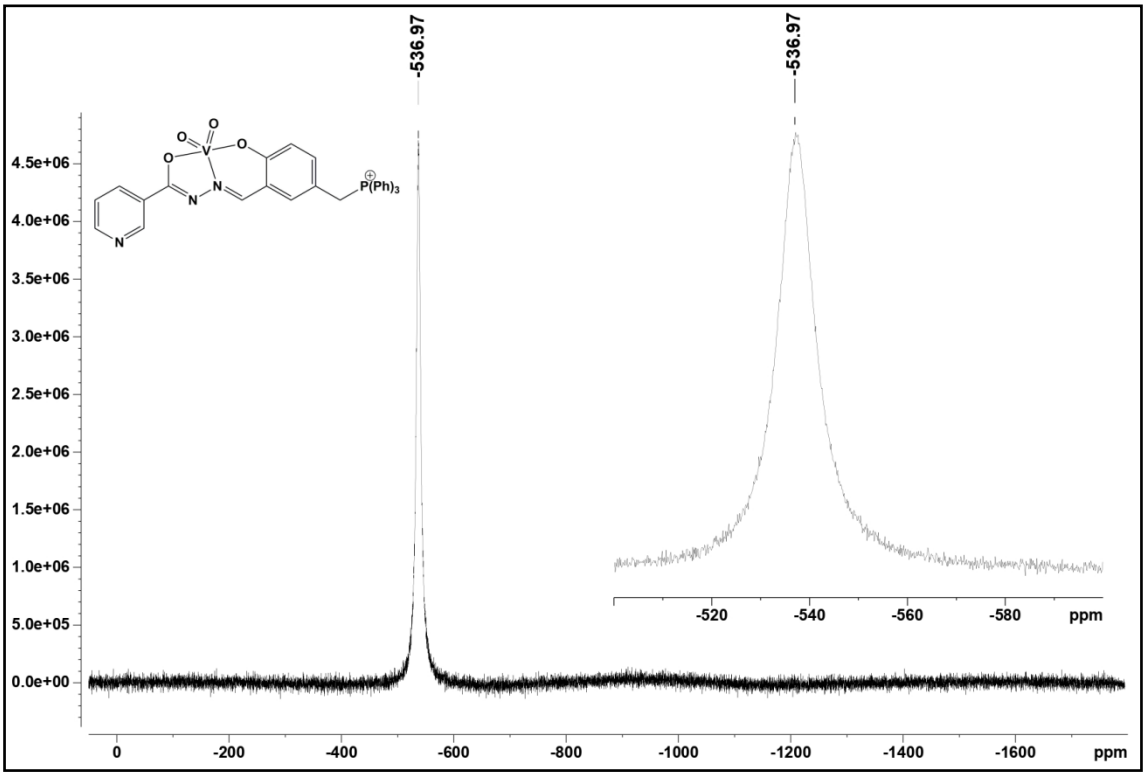

Fig. S58 ^{51}V-NMR spectra of [VO_2**L2**]·CH_3OH·$4H_2O$ (**C2**) (158 MHz, DMSO-d_6).

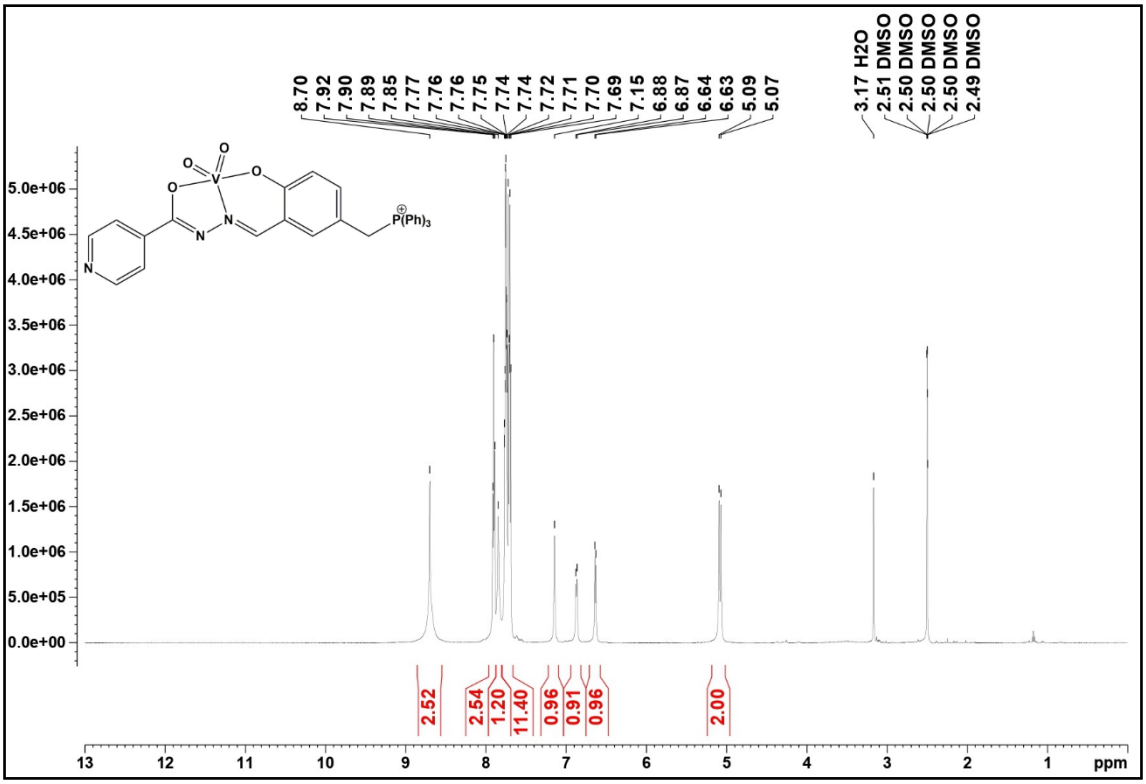

Fig. S59 ^{1}H-NMR spectra of [VO_2**L3**]·3,5H_2O (**C3**) (600 MHz, DMSO-d_6).

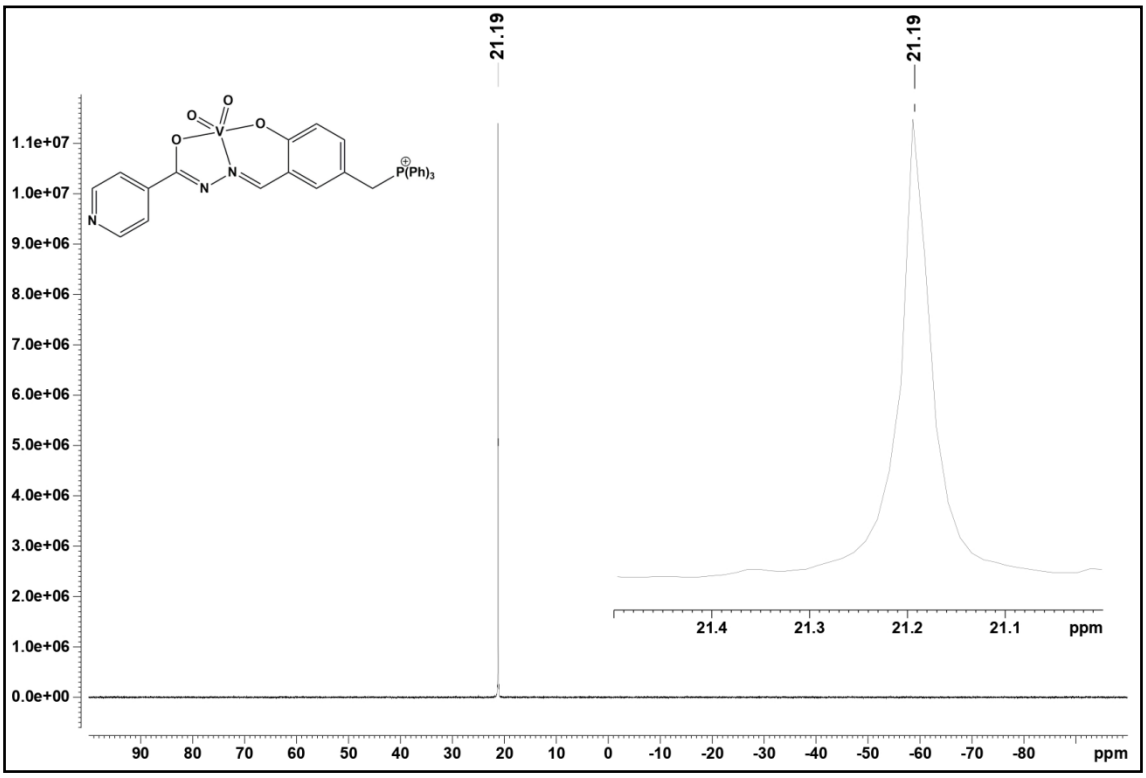

Fig. S60 ^{31}P-NMR spectra of [VO_2**L3**]·3,5H_2O (**C3**) (243 MHz, DMSO-d_6).

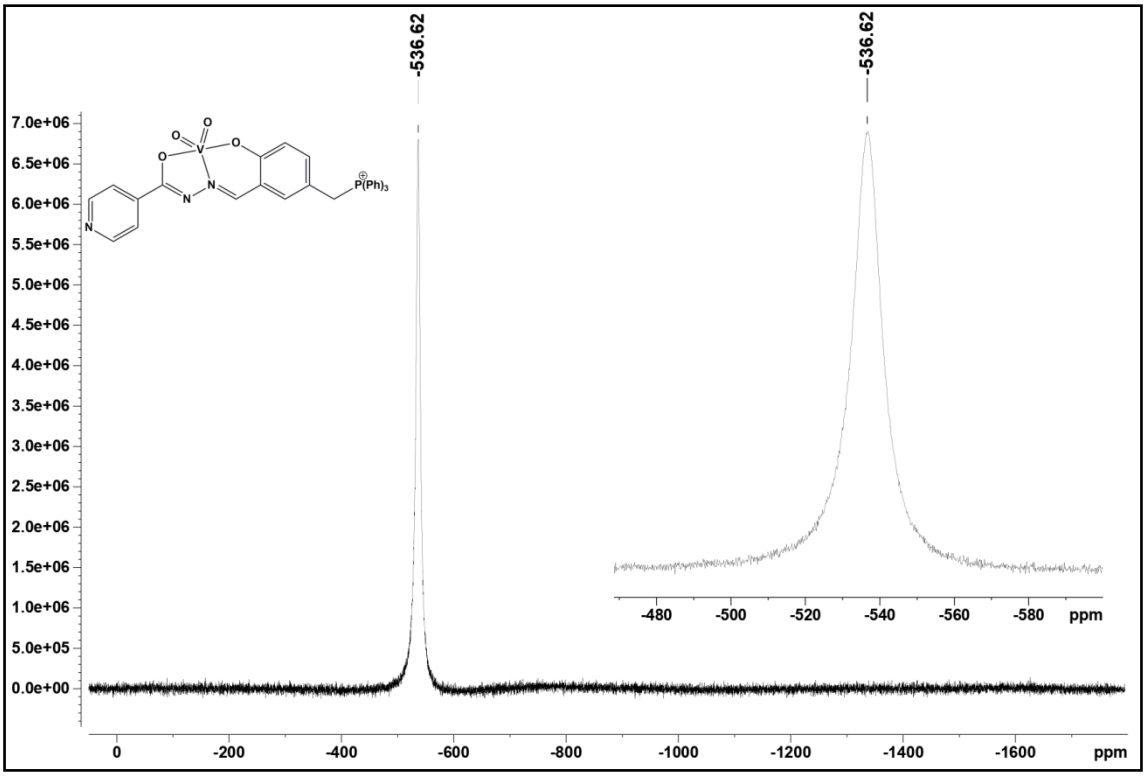

Fig. S61 ^{51}V-NMR spectra of [VO_2**L3**]·3,5H_2O (**C3**) (158 MHz, DMSO-d_6).

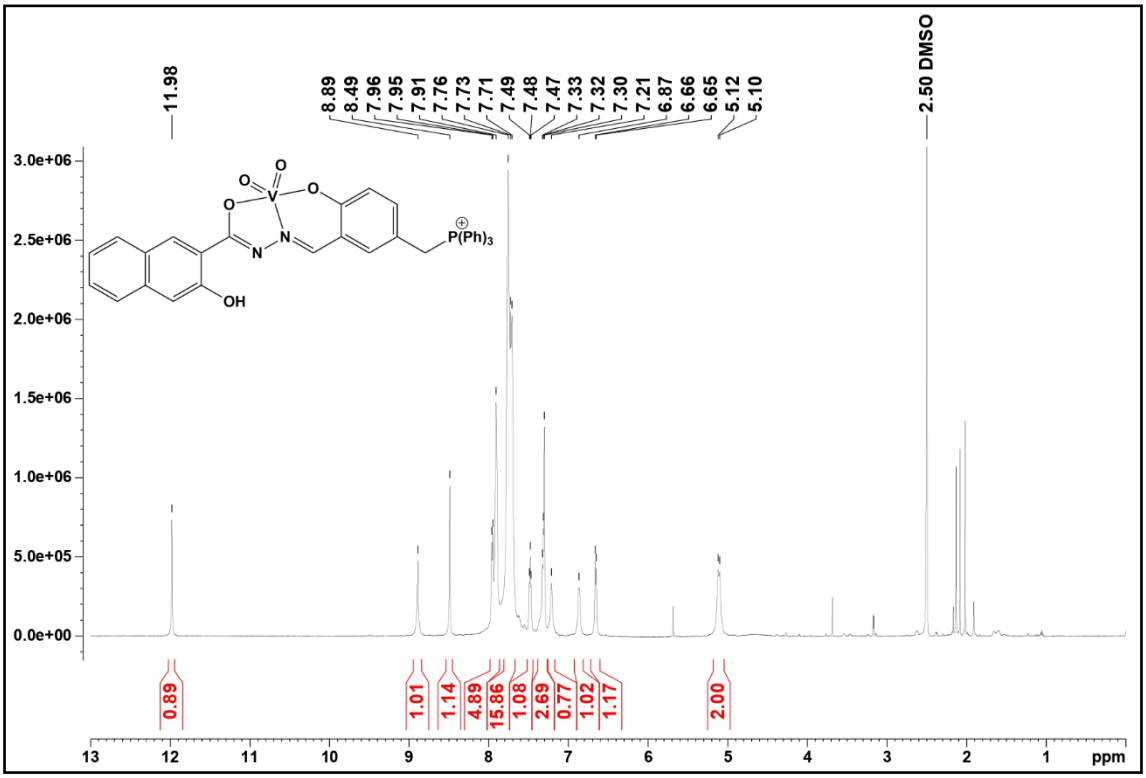

Fig. S62 ^{1}H-NMR spectra of [VO_2**HL4**]·2CH_3OH (**C4**) (600 MHz, DMSO-d_6).

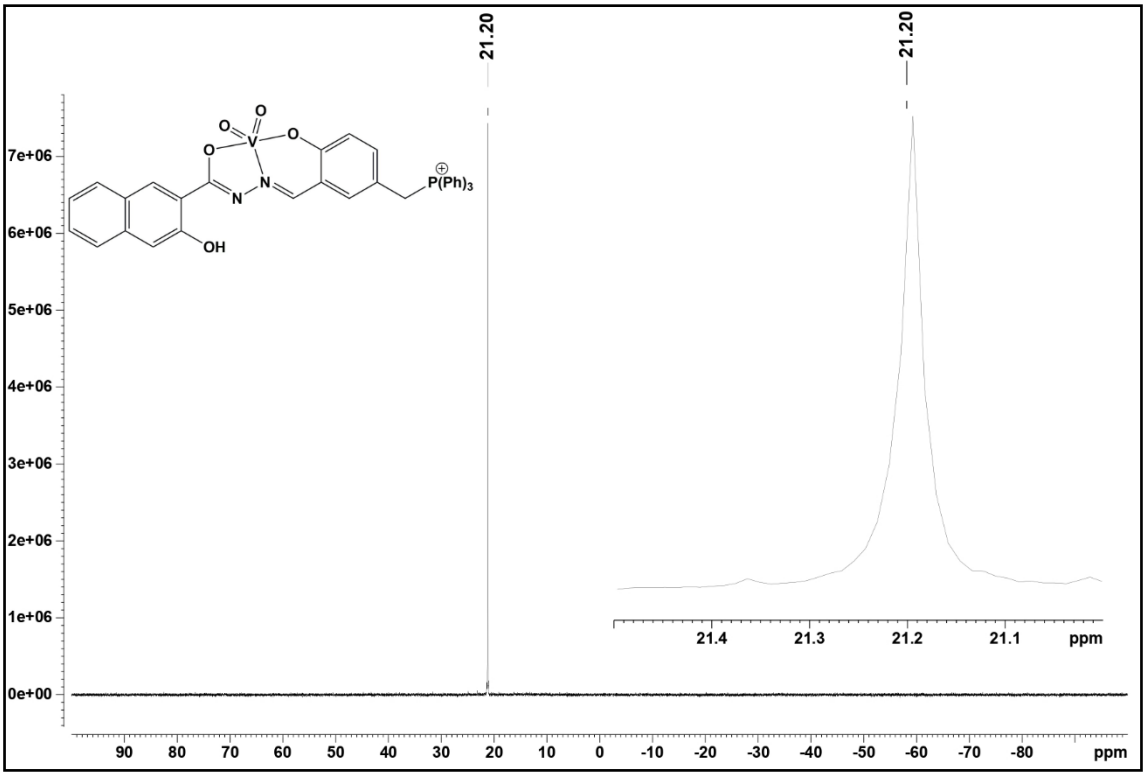

Fig. S63 ^{31}P-NMR spectra of [VO_2**HL4**]·2CH_3OH (**C4**) (243 MHz, DMSO-d_6).

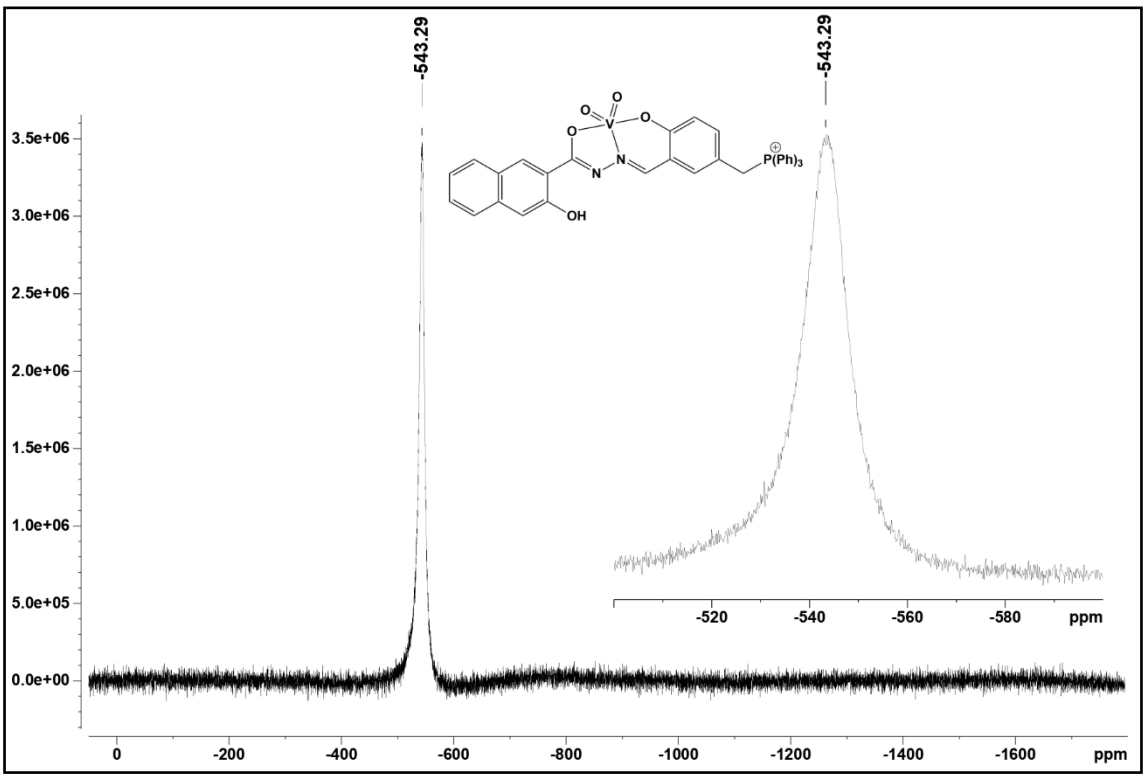

Fig. S64 ^{51}V-NMR spectra of [VO_2**HL4**]·2CH_3OH (**C4**) (158 MHz, DMSO-d_6).

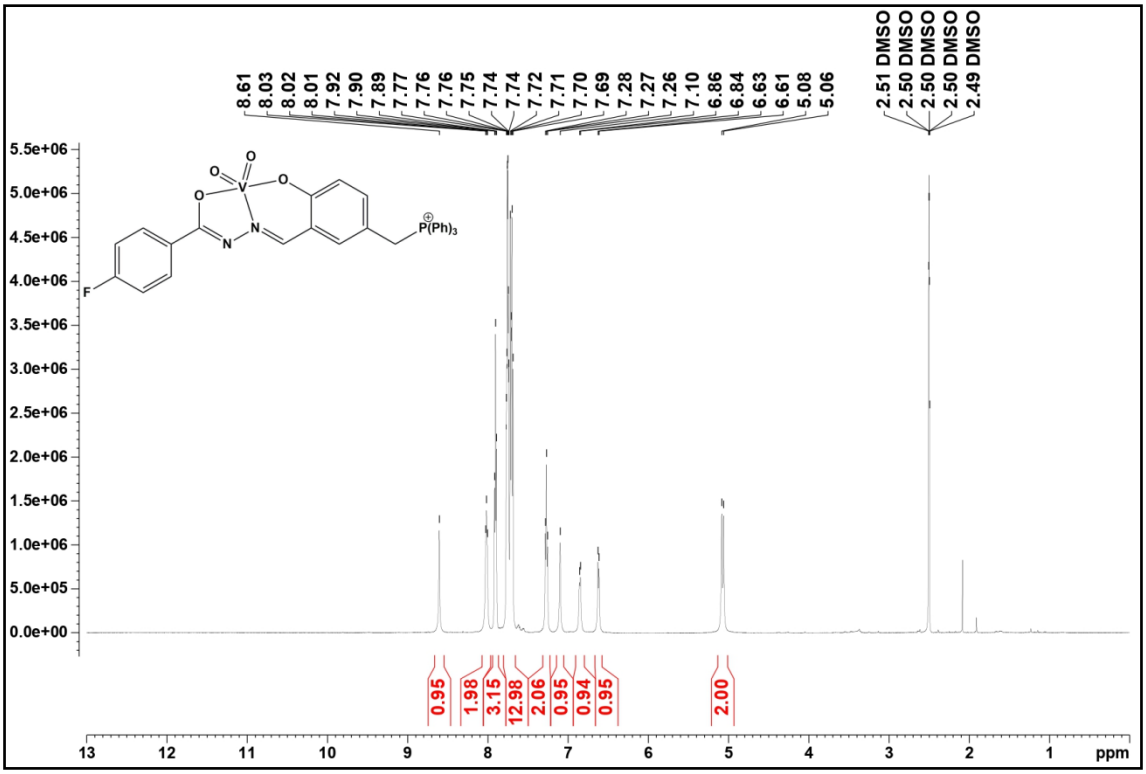

Fig. S65 ^{1}H-NMR spectra of [VO_2**L5**]·CH_3OH·H_2O (**C5**) (600 MHz, DMSO-d_6).

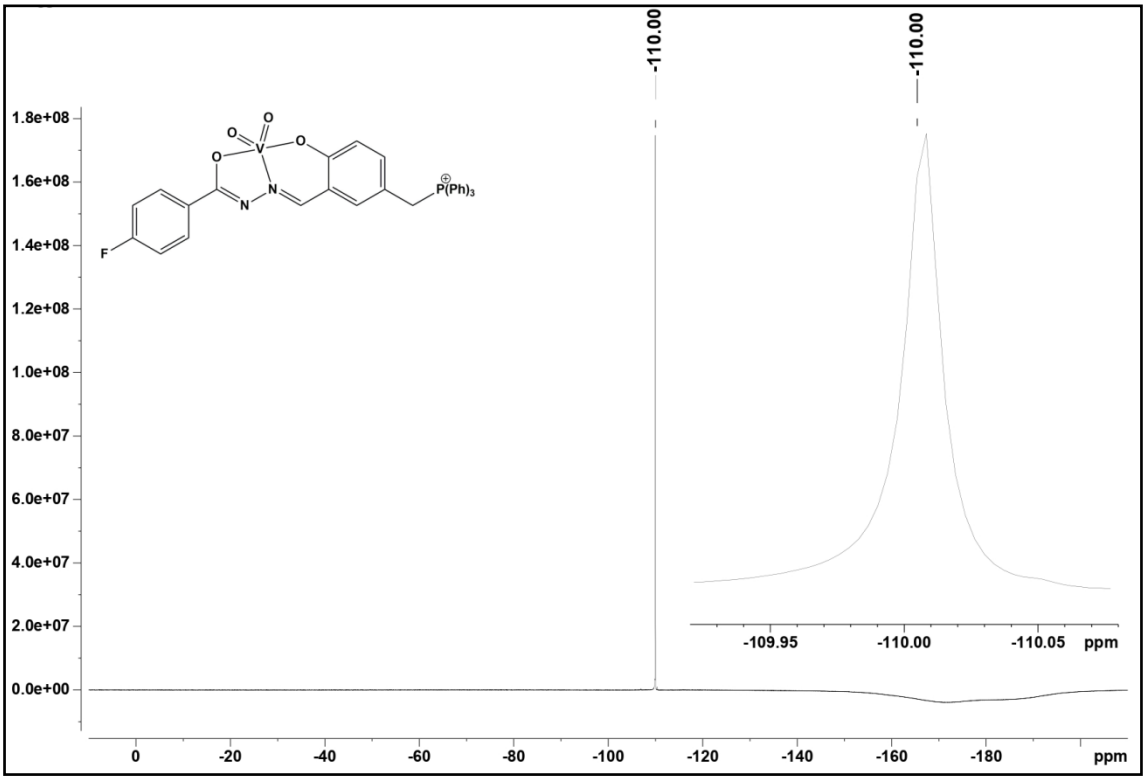

Fig. S66 ^{19}F-NMR spectra of [VO_2**L5**]·CH_3OH·H_2O (**C5**) (565 MHz, DMSO-d_6).

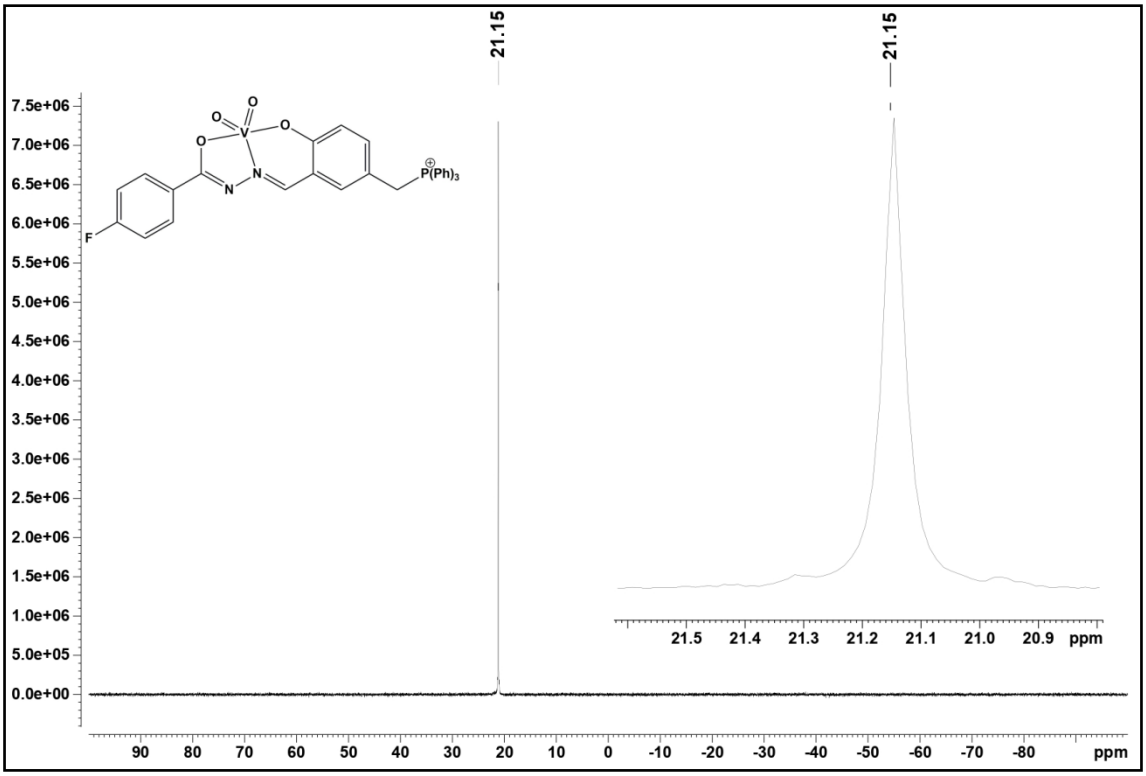

Fig. S67 ^{31}P-NMR spectra of [VO_2**L5**]·CH_3OH·H_2O (**C5**) (243 MHz, DMSO-d_6).

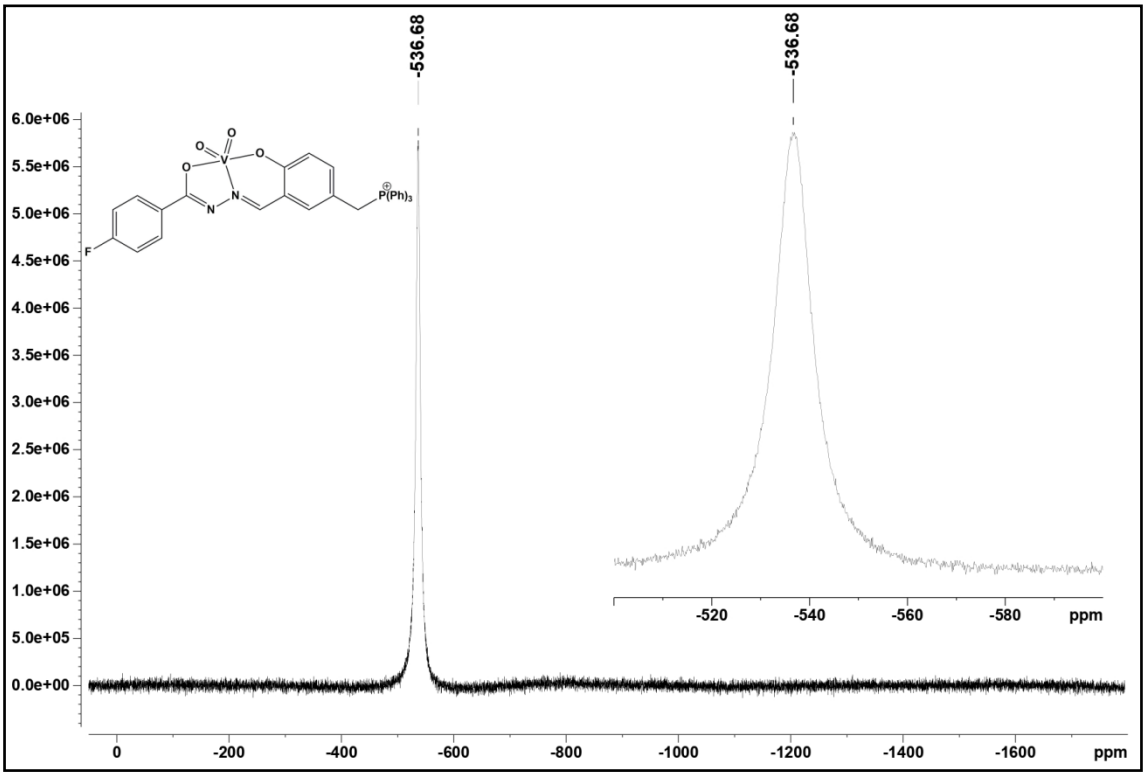

Fig. S68 ^{51}V-NMR spectra of [VO_2**L5**]·CH_3OH·H_2O (**C5**) (158 MHz, DMSO-d_6).

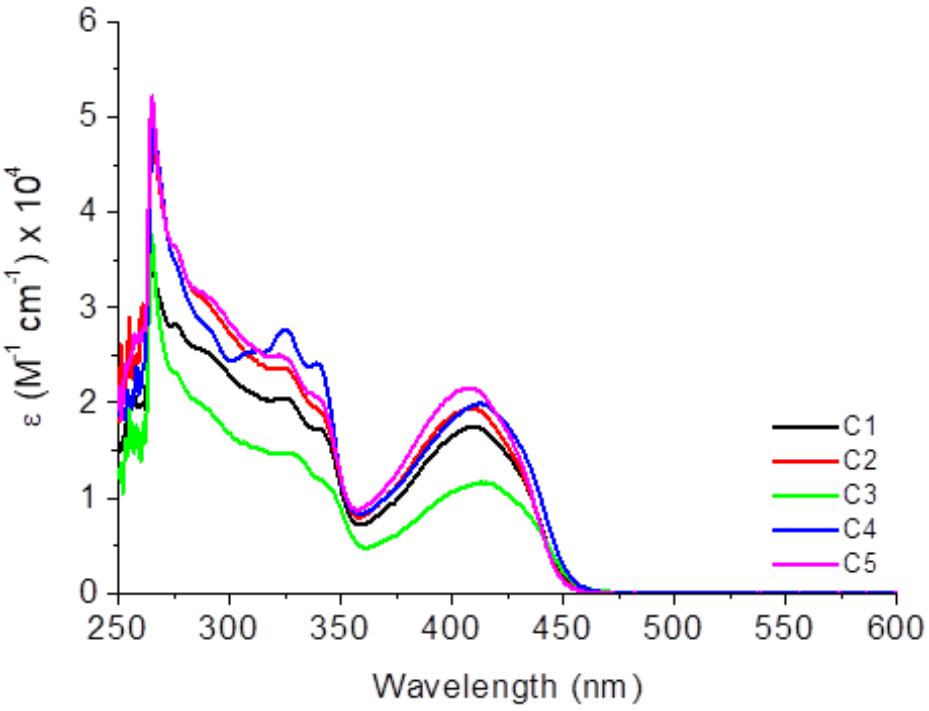

Fig. S69 Absorption UV–Vis electronic spectra of complexes **C1**–**C5** in *N,N*-dimethylformamide solution

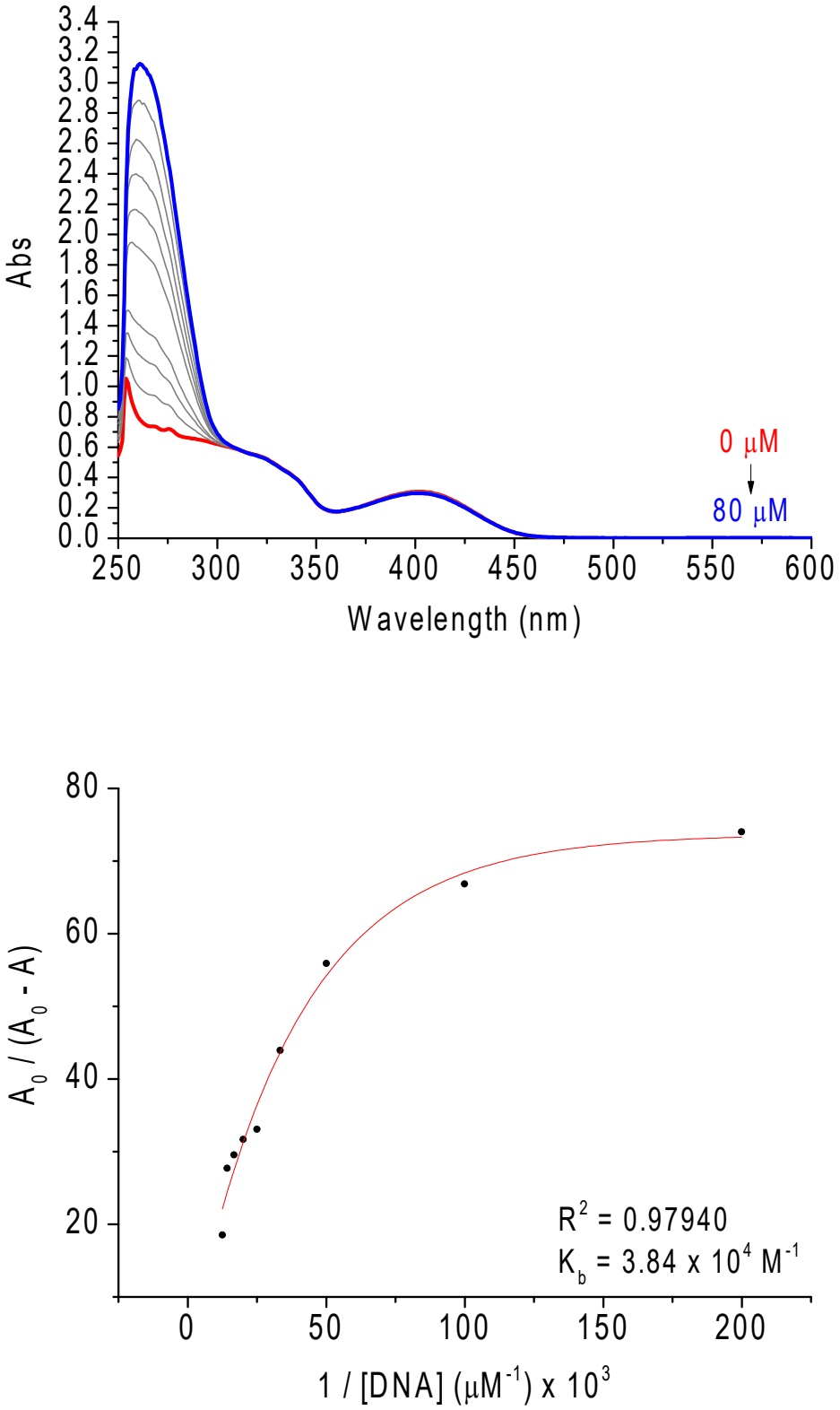

Fig. S70 UV–Vis absorption for **C1** without and upon successive additions of CT-DNA in DMF(5%)/Tris-HCl (pH 7.4) buffer solution and the corresponding plots $A_0/(A_0\text{-}A)$ *versus* 1/[biomolecule] plot.

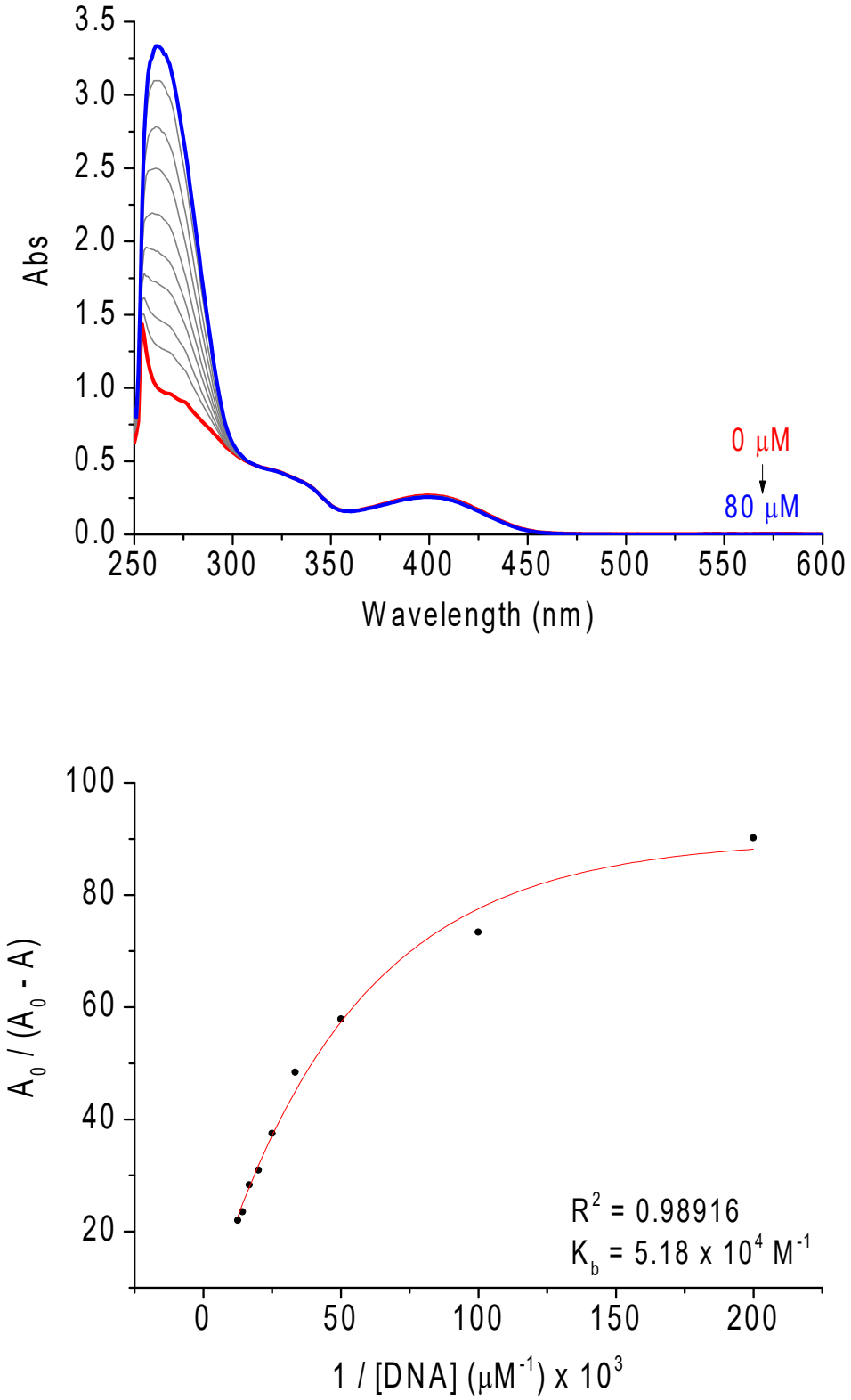

Fig. S71 UV–Vis absorption for **C3** without and upon successive additions of CT-DNA in DMF(5%)/Tris-HCl (pH 7.4) buffer solution and the corresponding plots $A_0/(A_0-A)$ *versus* 1/[biomolecule] plot.

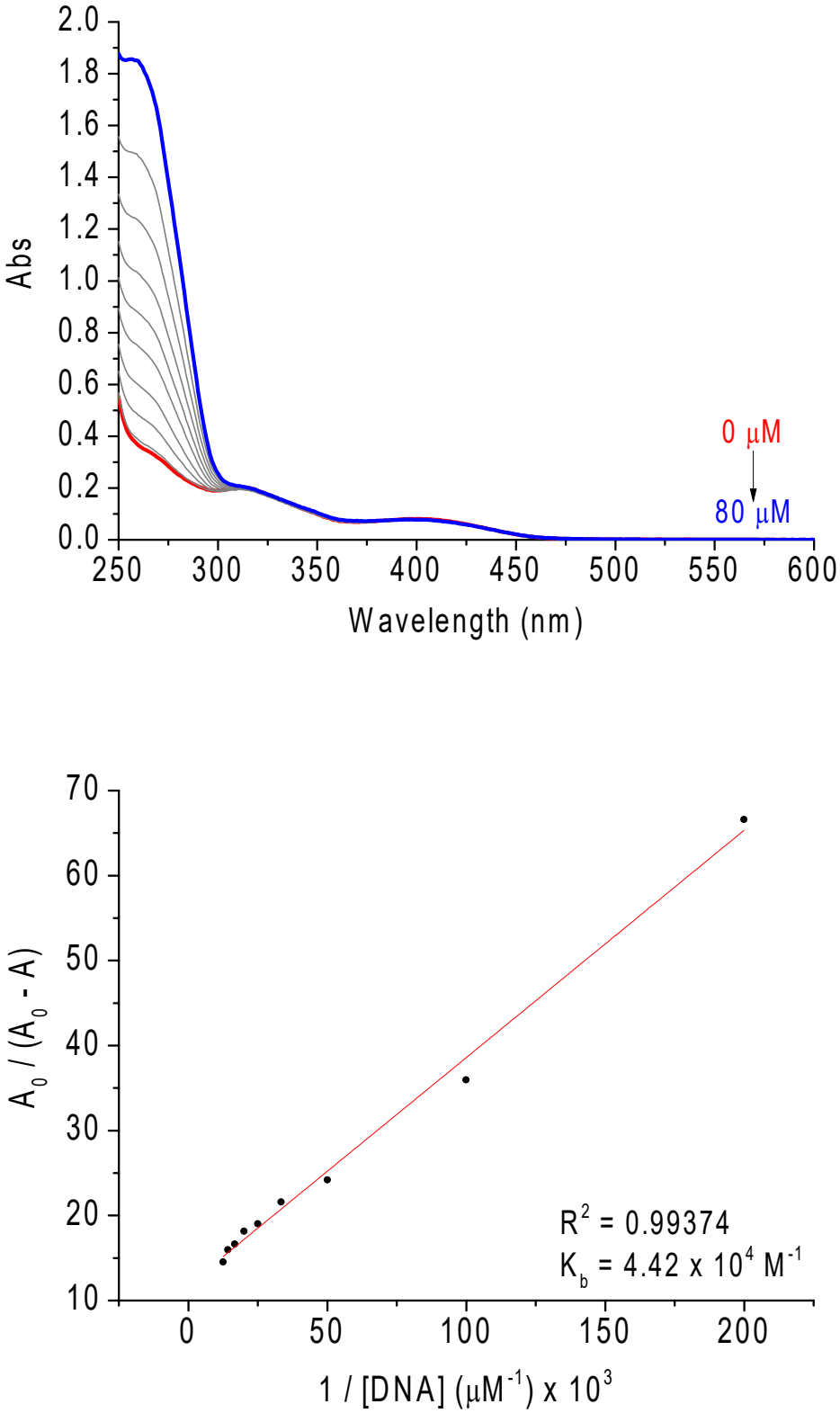

Fig. S72 UV–Vis absorption for **C4** without and upon successive additions of CT-DNA in DMF(5%)/Tris-HCl (pH 7.4) buffer solution and the corresponding plots $A_0/(A_0-A)$ *versus* 1/[biomolecule] plot.

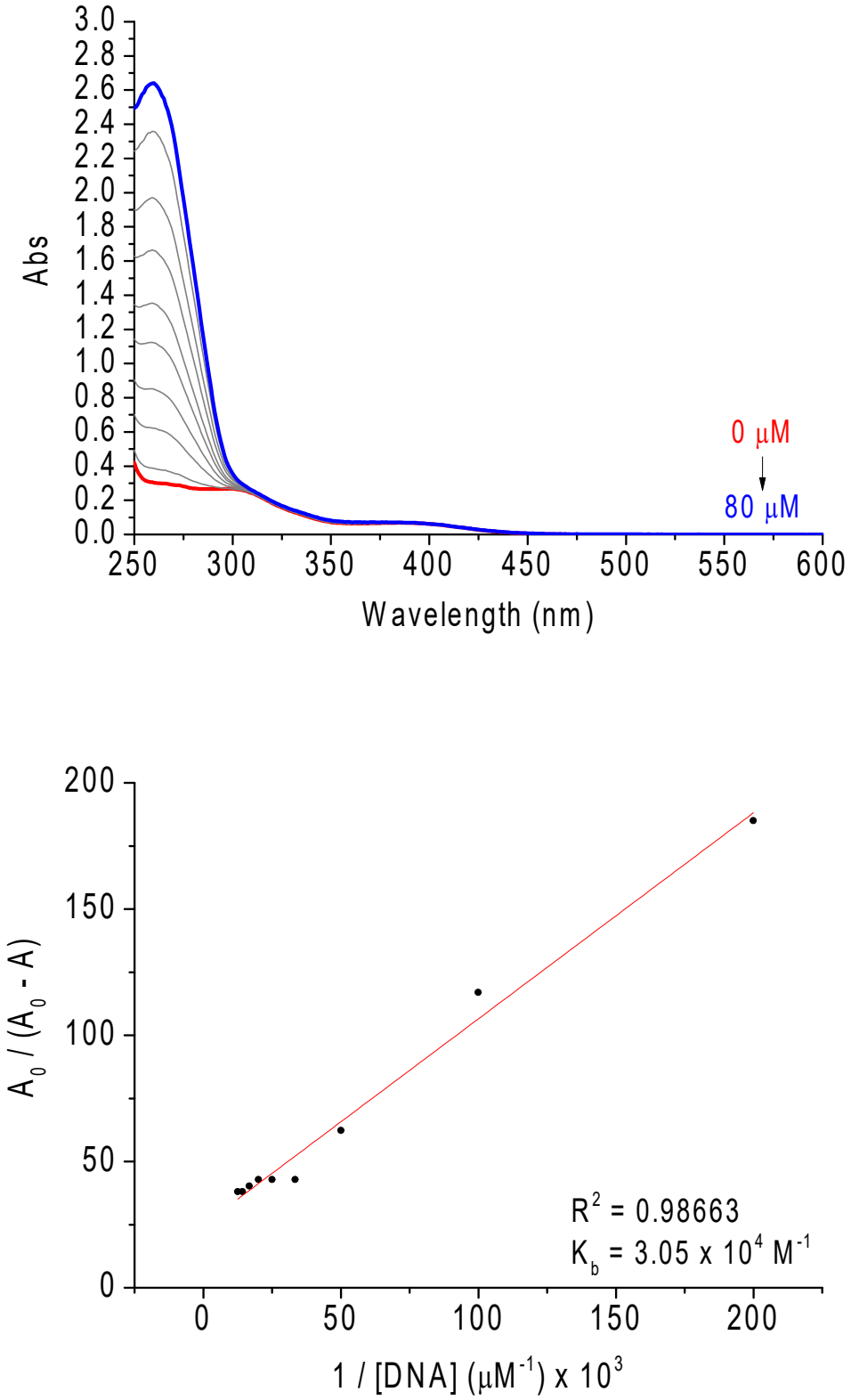

Fig. S73 UV–Vis absorption for **C5** without and upon successive additions of CT-DNA in DMF(5%)/Tris-HCl (pH 7.4) buffer solution and the corresponding plots $A_0/(A_0-A)$ *versus* 1/[biomolecule] plot.

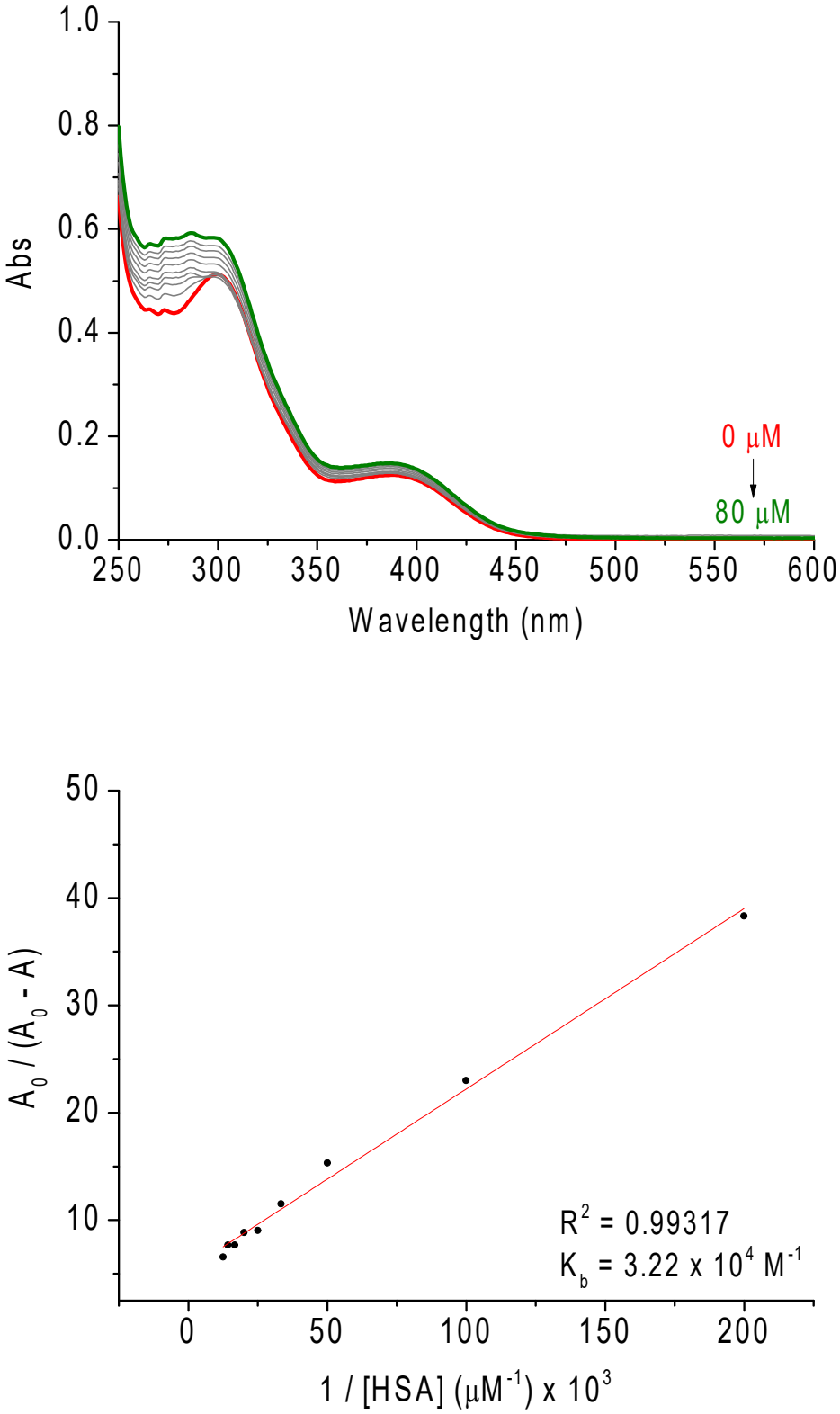

Fig. S74 UV–Vis absorption for **C1** without and upon successive additions of HSA in DMF(5%)/Tris-HCl (pH 7.4) buffer solution and the corresponding plots $A_0/(A_0-A)$ *versus* 1/[biomolecule] plot.

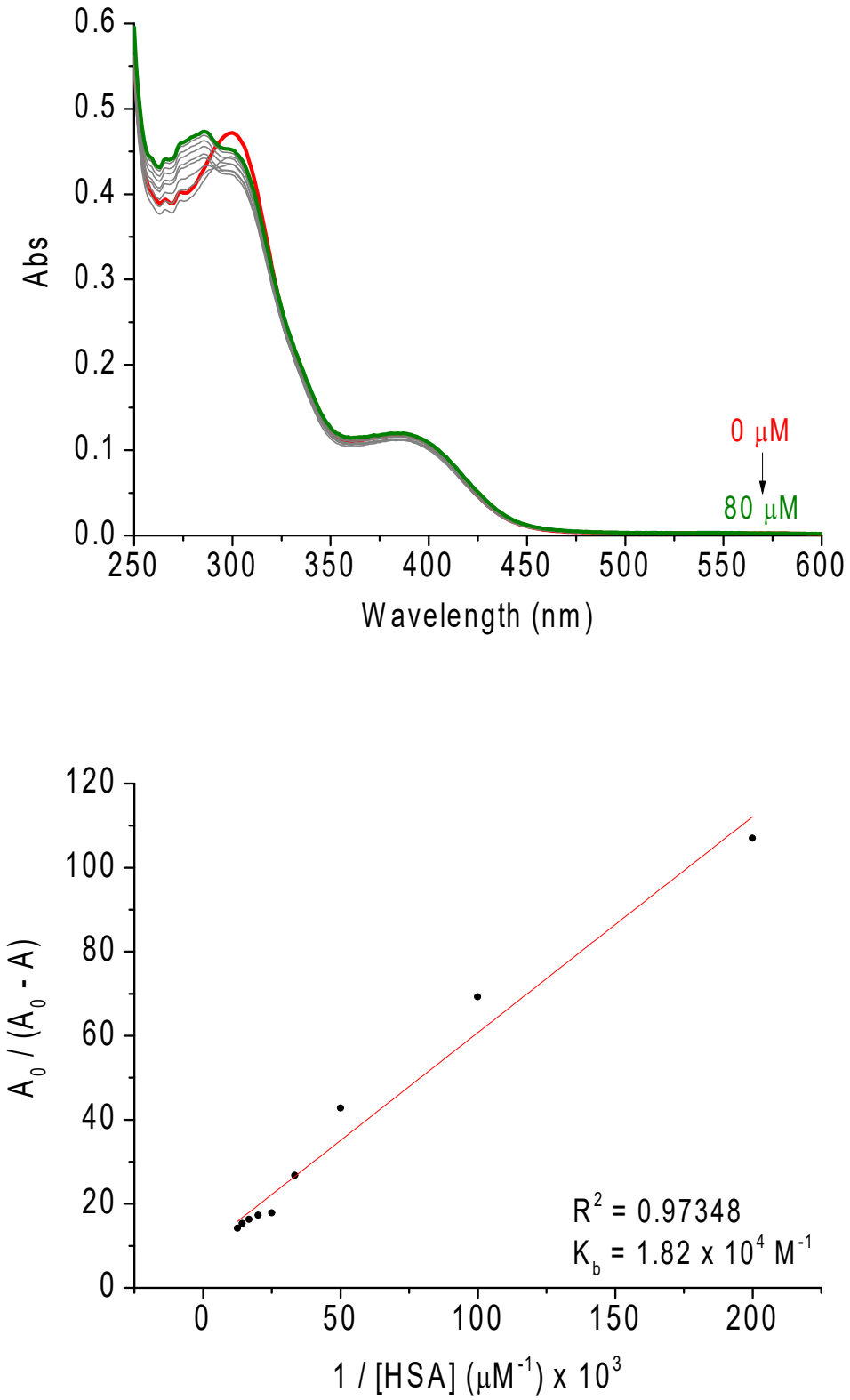

Fig. S75 UV–Vis absorption for **C3** without and upon successive additions of HSA in DMF(5%)/Tris-HCl (pH 7.4) buffer solution and the corresponding plots $A_0/(A_0\text{-}A)$ *versus* 1/[biomolecule] plot.

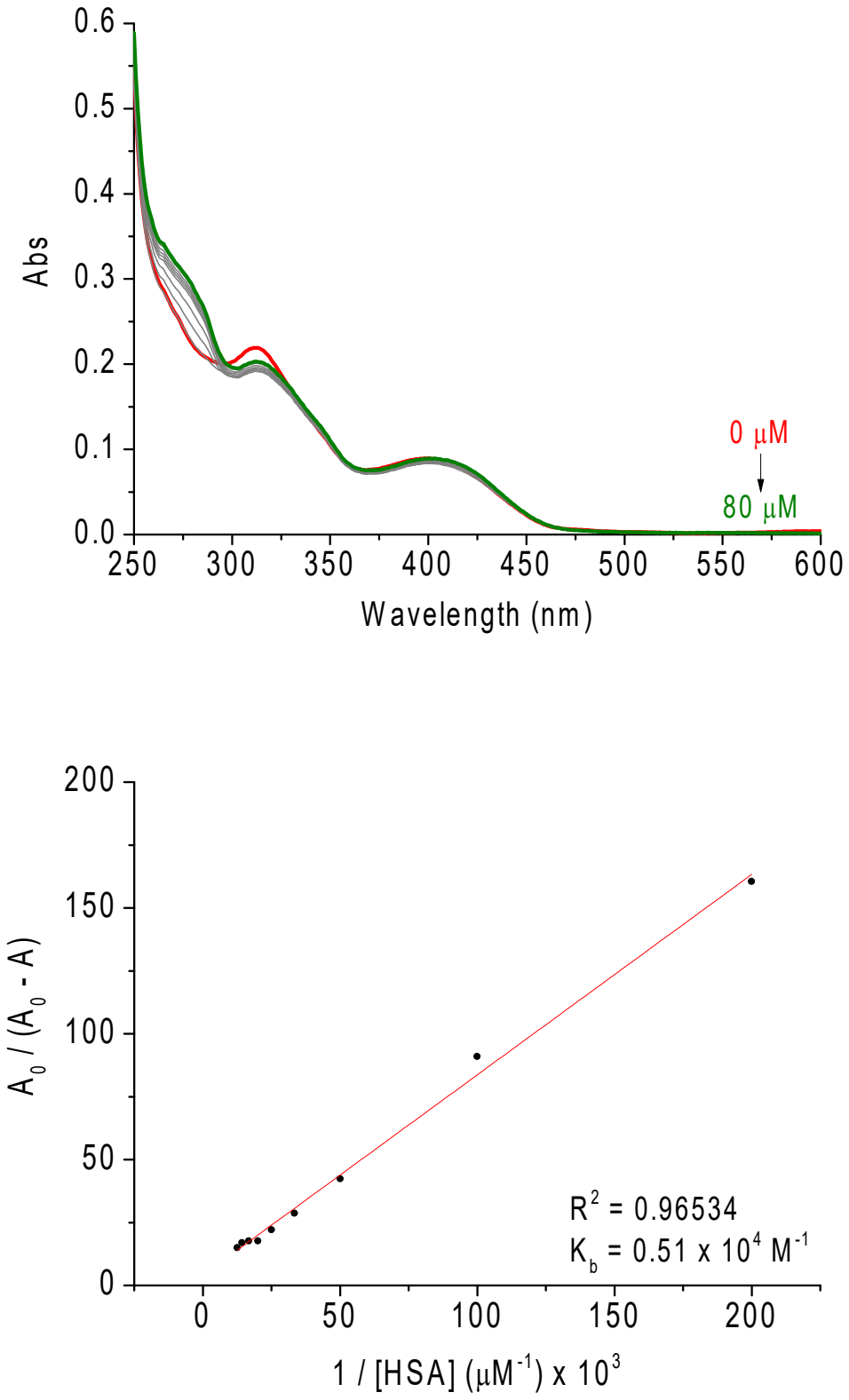

Fig. S76 UV–Vis absorption for **C4** without and upon successive additions of HSA in DMF(5%)/Tris-HCl (pH 7.4) buffer solution and the corresponding plots $A_0/(A_0-A)$ *versus* 1/[biomolecule] plot.

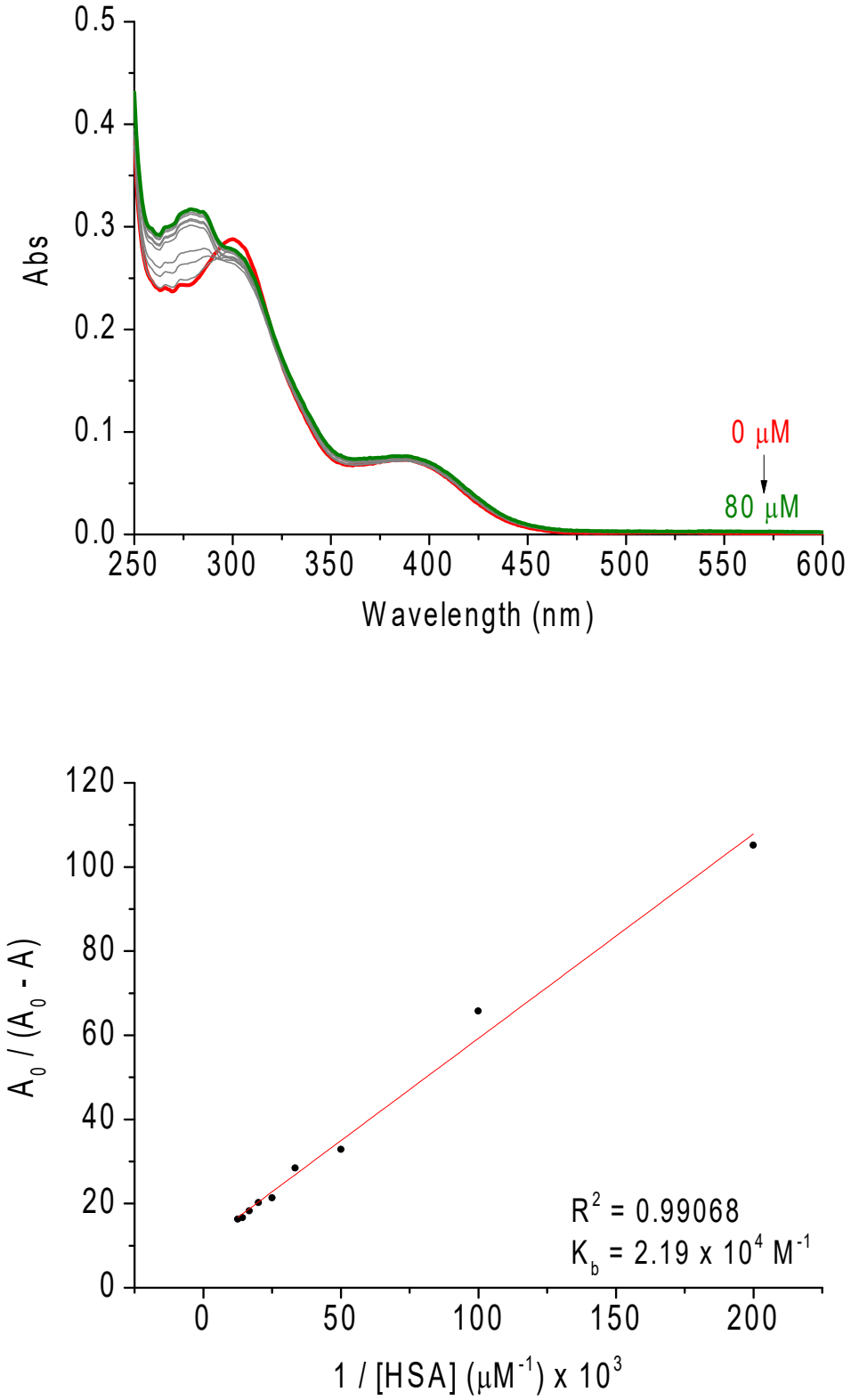

Fig. S77 UV–Vis absorption for **C5** without and upon successive additions of HSA in DMF(5%)/Tris-HCl (pH 7.4) buffer solution and the corresponding plots $A_0/(A_0\text{-}A)$ *versus* 1/[biomolecule] plot.

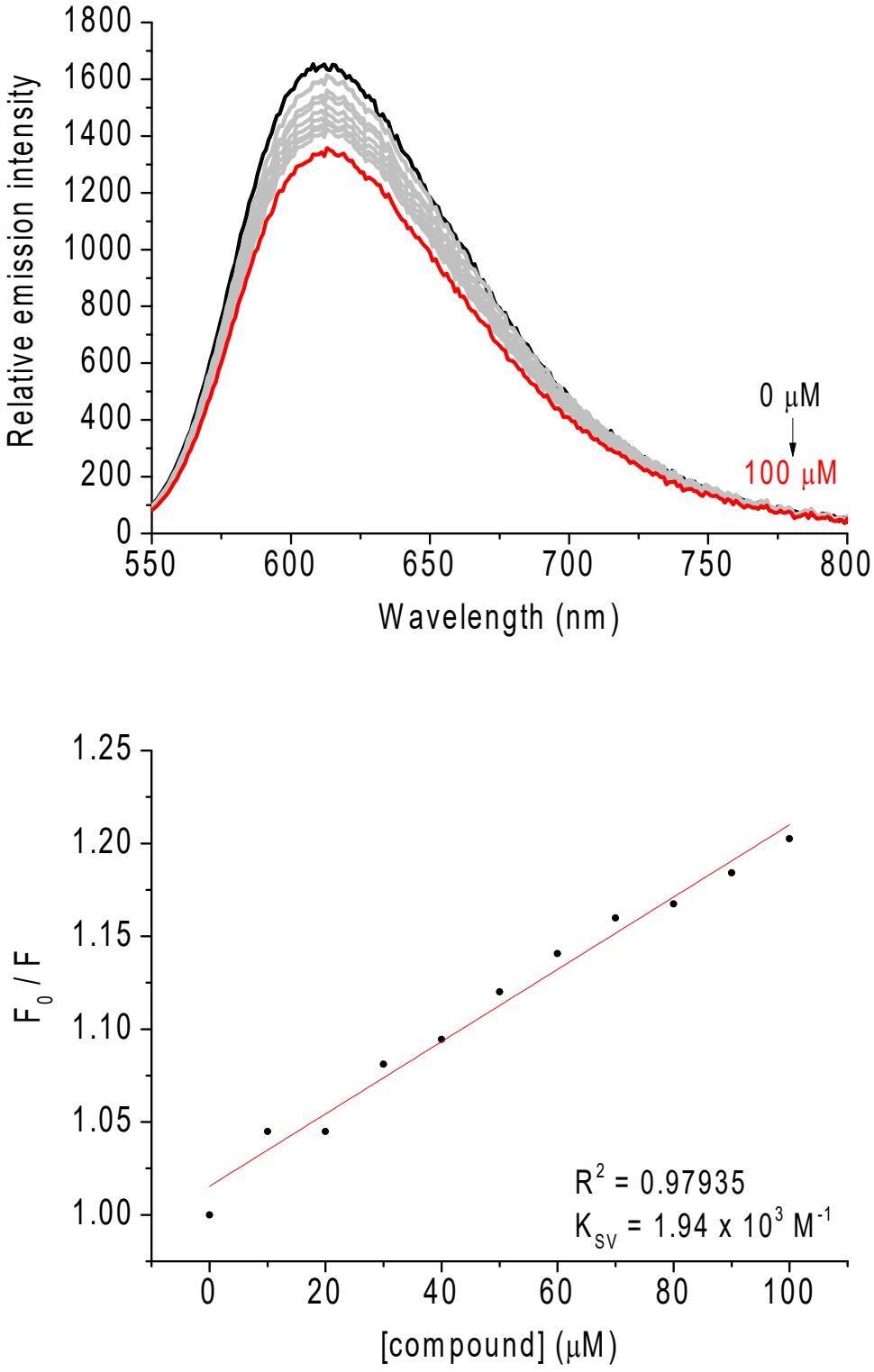

Fig. S78 Competition assays for **C1** in the system CT-DNA:EB in DMF(5%)/Tris-HCl (pH 7.4) buffer solution and the corresponding Stern-Volmer plots F_0/F *versus* [complex].

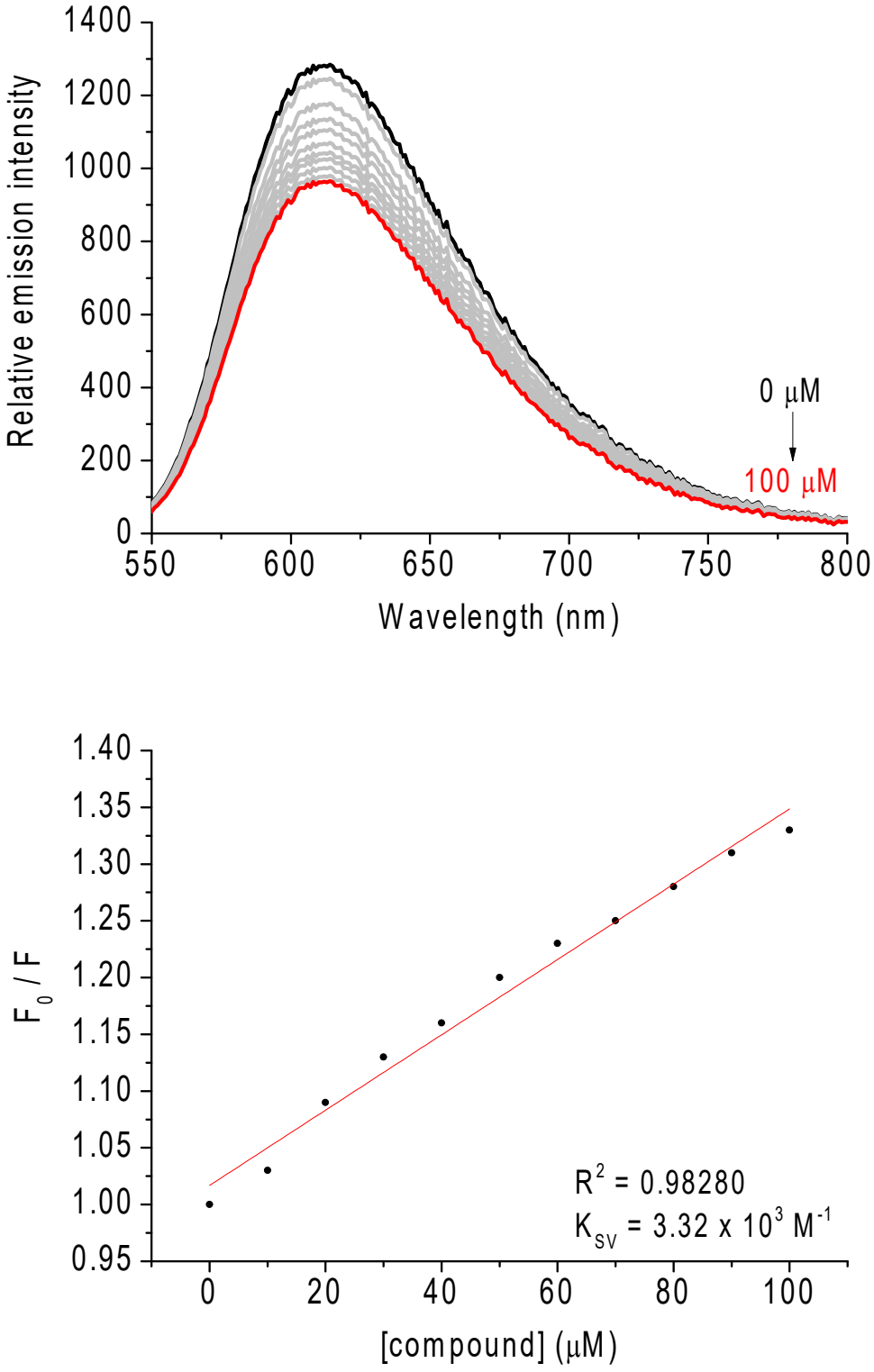

Fig. S79 Competition assays for **C2** in the system CT-DNA:EB in DMF(5%)/Tris-HCl (pH 7.4) buffer solution and the corresponding Stern-Volmer plots F_0/F *versus* [complex].

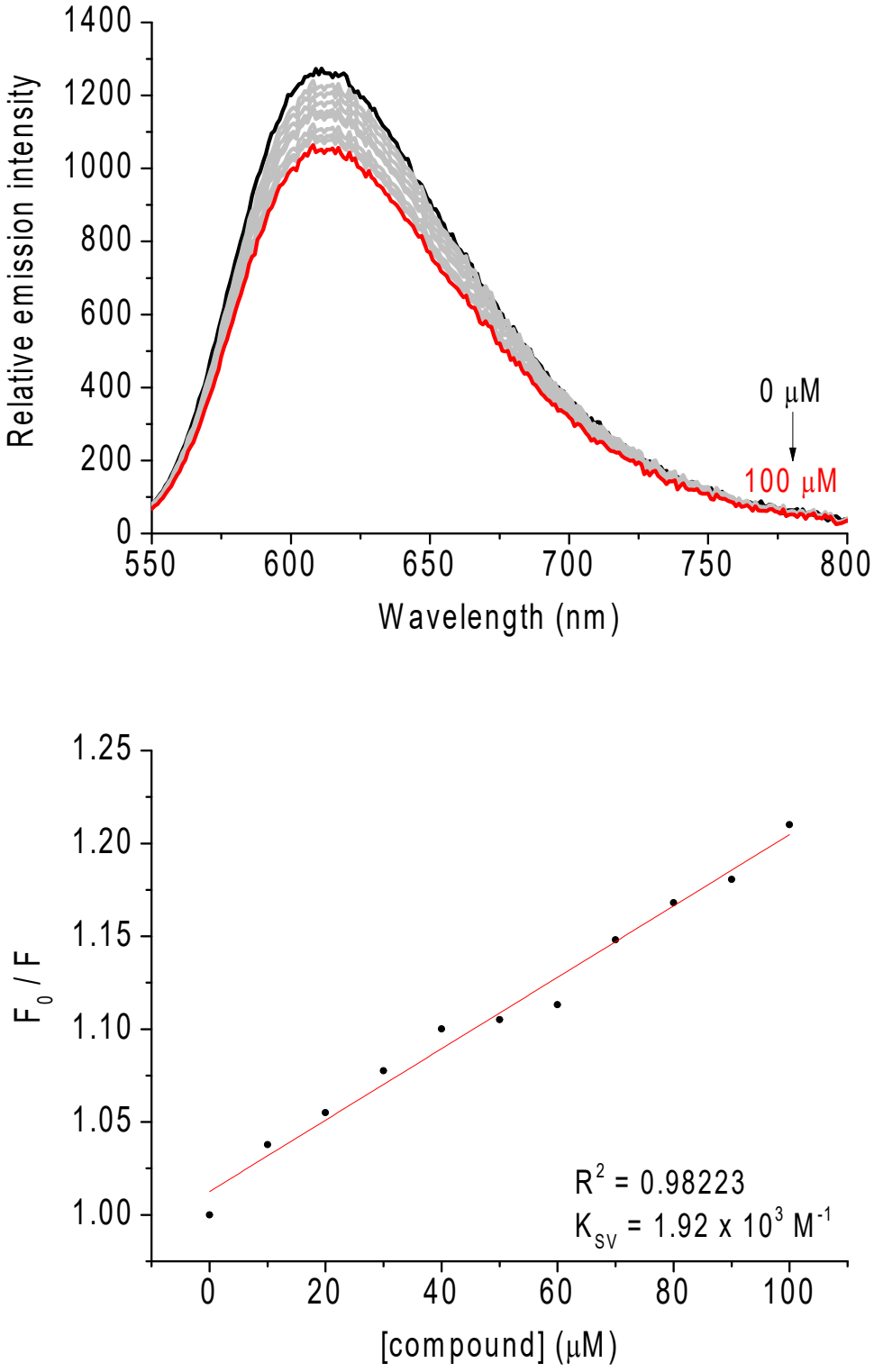

Fig. S80 Competition assays for **C3** in the system CT-DNA:EB in DMF(5%)/Tris-HCl (pH 7.4) buffer solution and the corresponding Stern-Volmer plots F_0/F *versus* [complex].

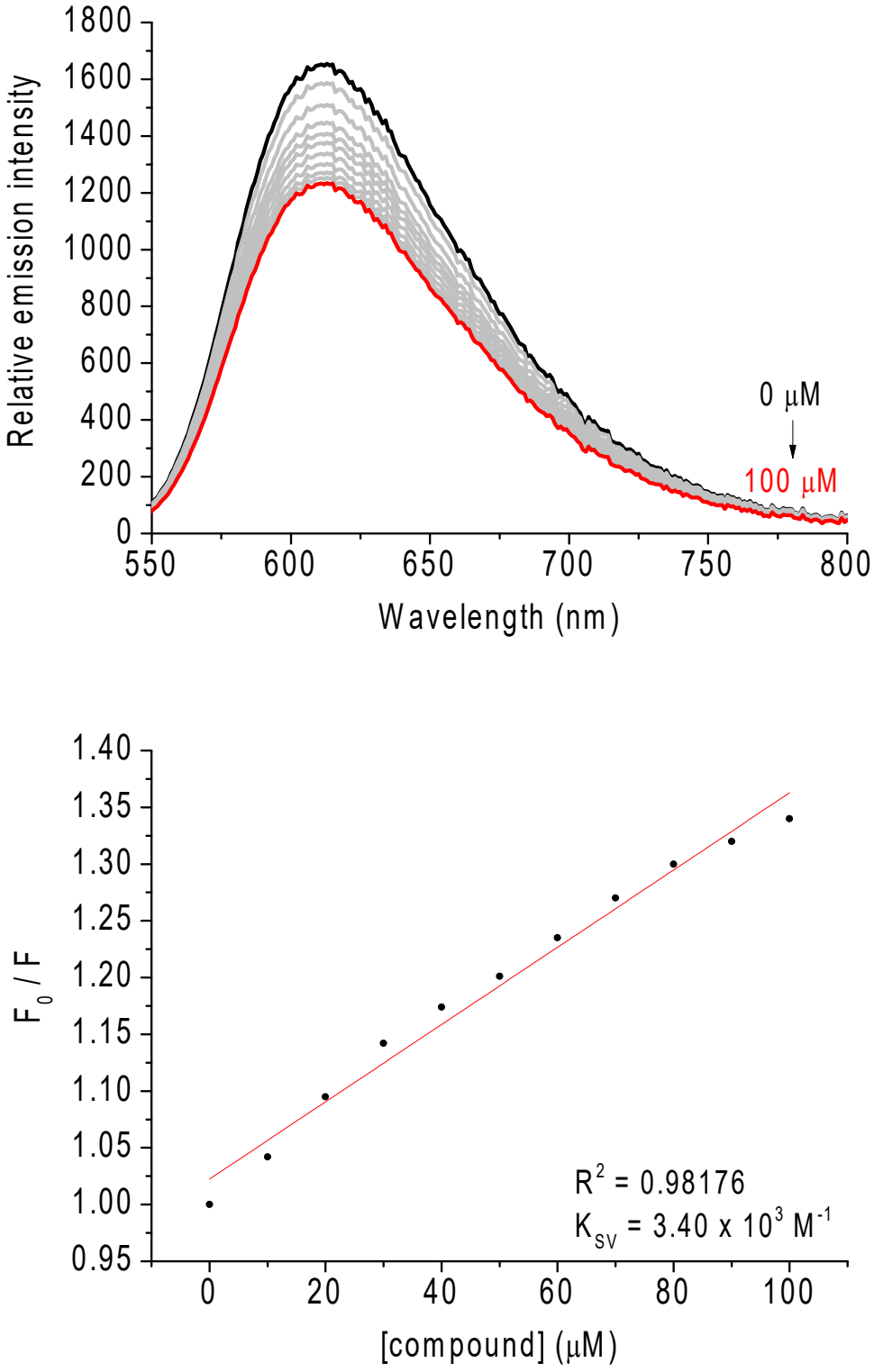

Fig. S81 Competition assays for **C4** in the system CT-DNA:EB in DMF(5%)/Tris-HCl (pH 7.4) buffer solution and the corresponding Stern-Volmer plots F_0/F *versus* [complex].

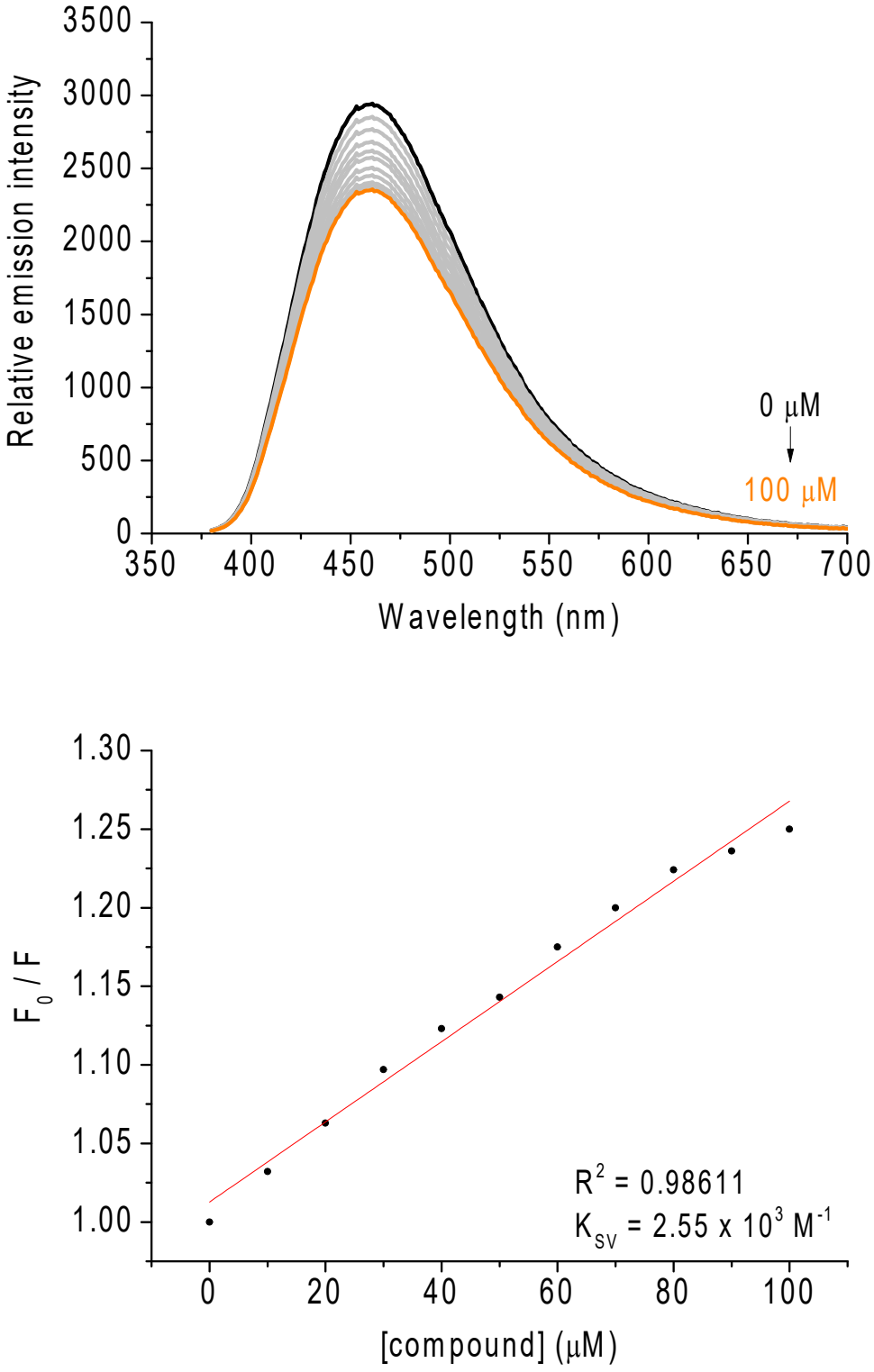

Fig. S82 Competition assays for **C1** in the system CT-DNA:DAPI in DMF(5%)/Tris-HCl (pH 7.4) buffer solution and the corresponding Stern-Volmer plots F_0/F *versus* [complex].

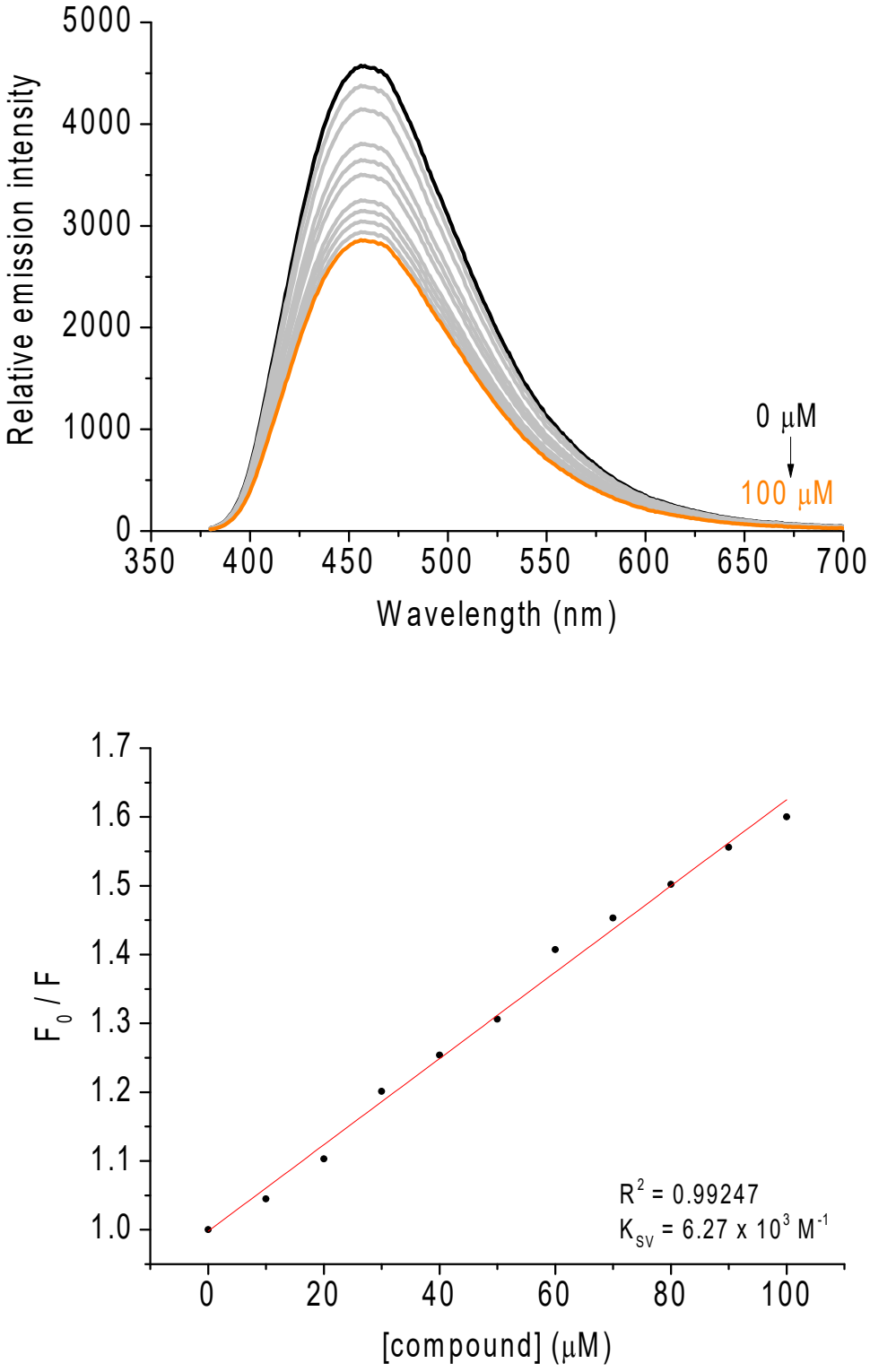

Fig. S83 Competition assays for **C2** in the system CT-DNA:DAPI in DMF(5%)/Tris-HCl (pH 7.4) buffer solution and the corresponding Stern-Volmer plots F_0/F *versus* [complex].

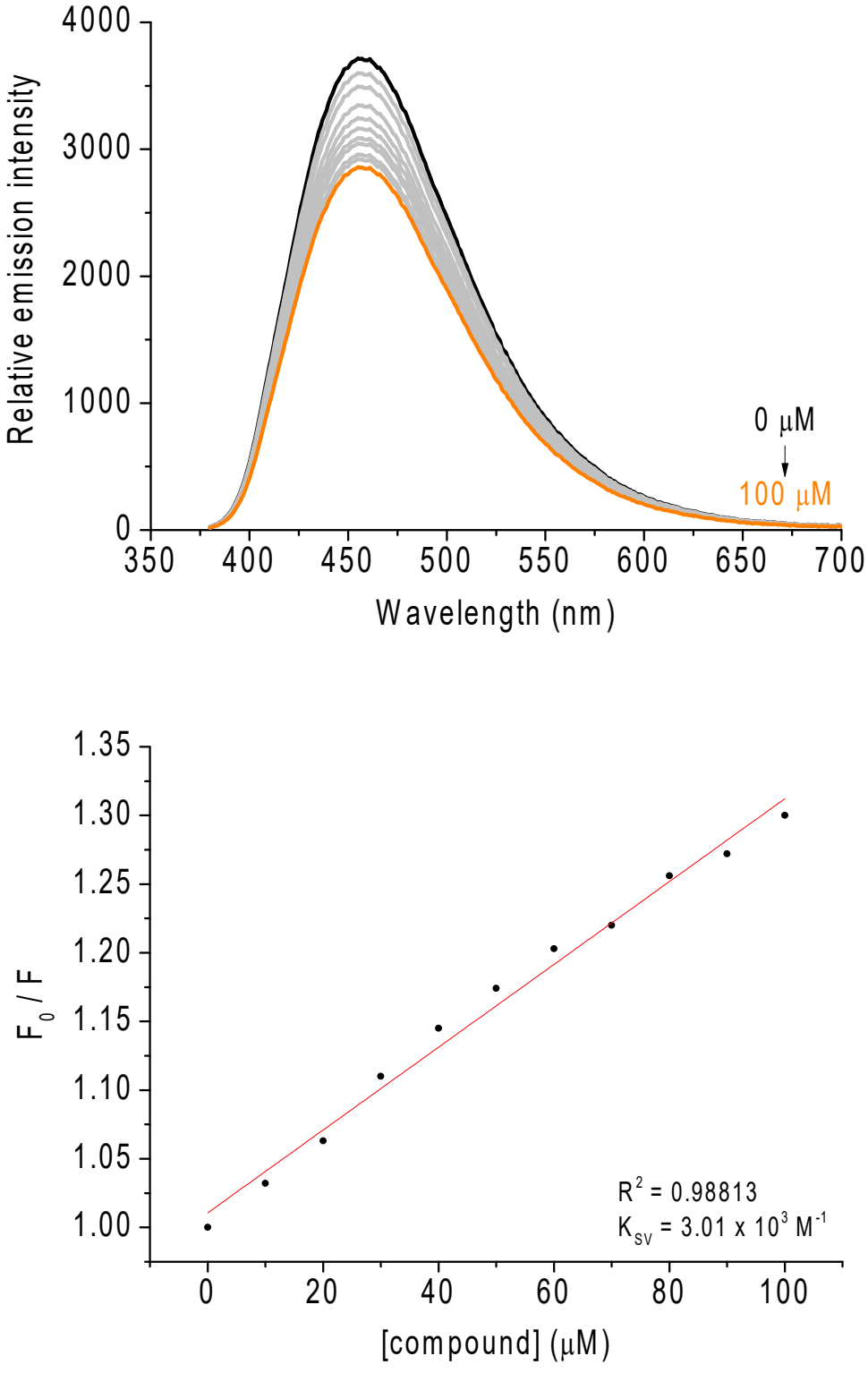

Fig. S84 Competition assays for **C3** in the system CT-DNA:DAPI in DMF(5%)/Tris-HCl (pH 7.4) buffer solution and the corresponding Stern-Volmer plots F_0/F *versus* [complex].

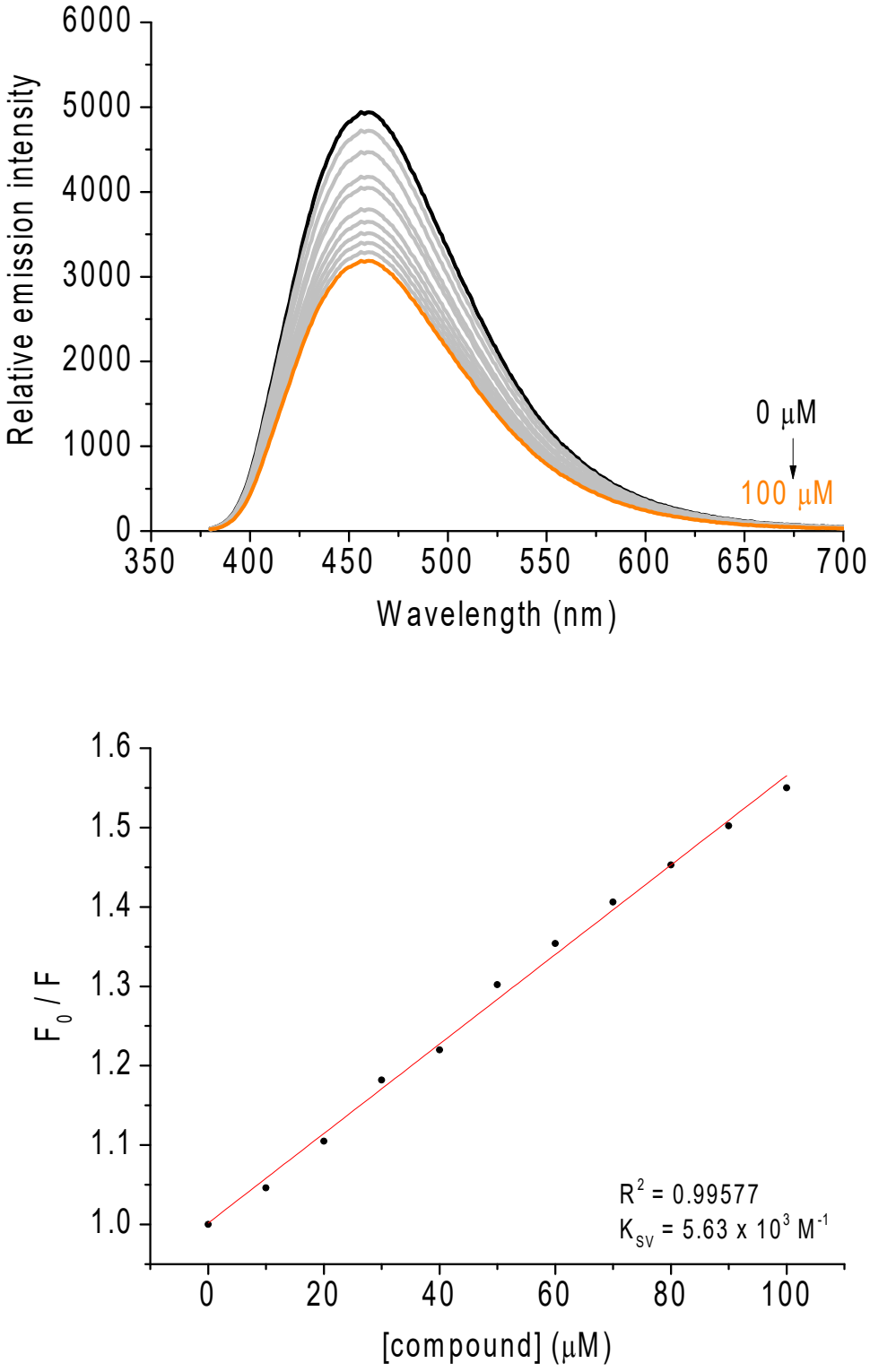

Fig. S85 Competition assays for **C4** in the system CT-DNA:DAPI in DMF(5%)/Tris-HCl (pH 7.4) buffer solution and the corresponding Stern-Volmer plots F_0/F *versus* [complex].

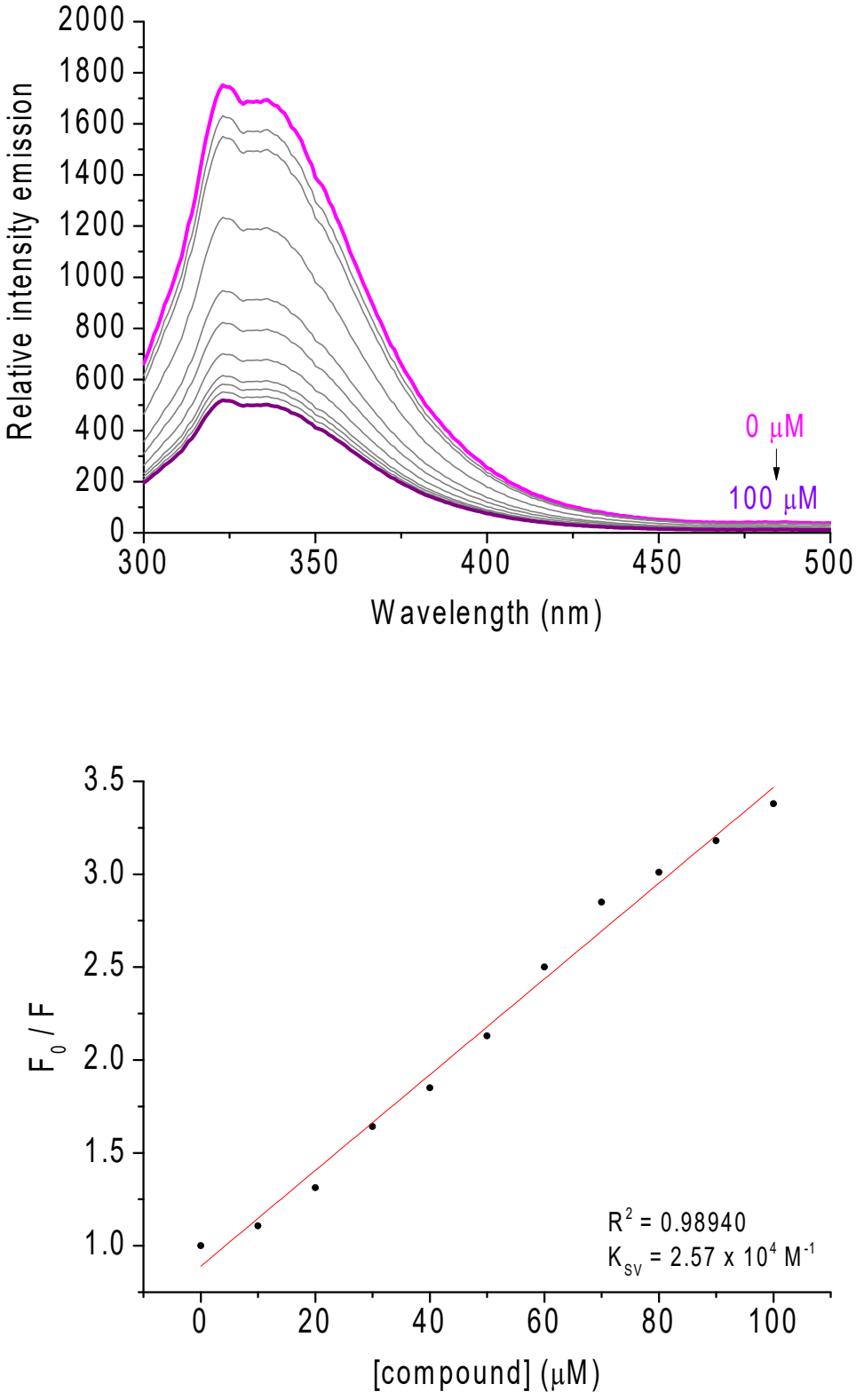

Fig. S86 Steady-state fluorescence emission spectra for HSA without and in the presence of dioxidovanadium(V) derivative **C1**, in DMF(5%)/Tris-HCl (pH 7.4) buffer solution. Graph shown the F_0/F *versus* [complex] plot.

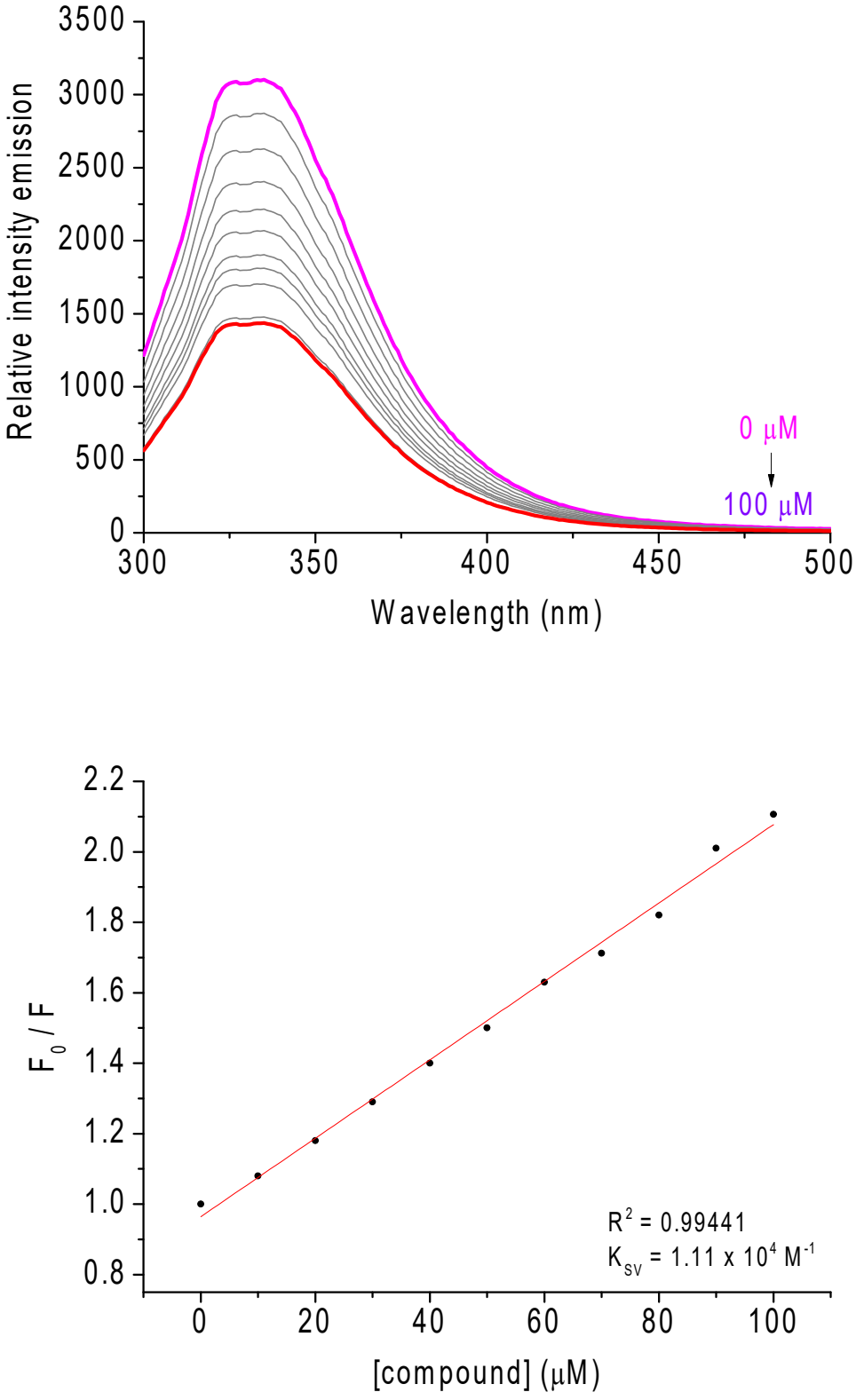

Fig. S87 Steady-state fluorescence emission spectra for HSA without and in the presence of dioxidovanadium(V) derivative **C2**, in DMF(5%)/Tris-HCl (pH 7.4) buffer solution. Graph shown the F_0/F *versus* [complex] plot.

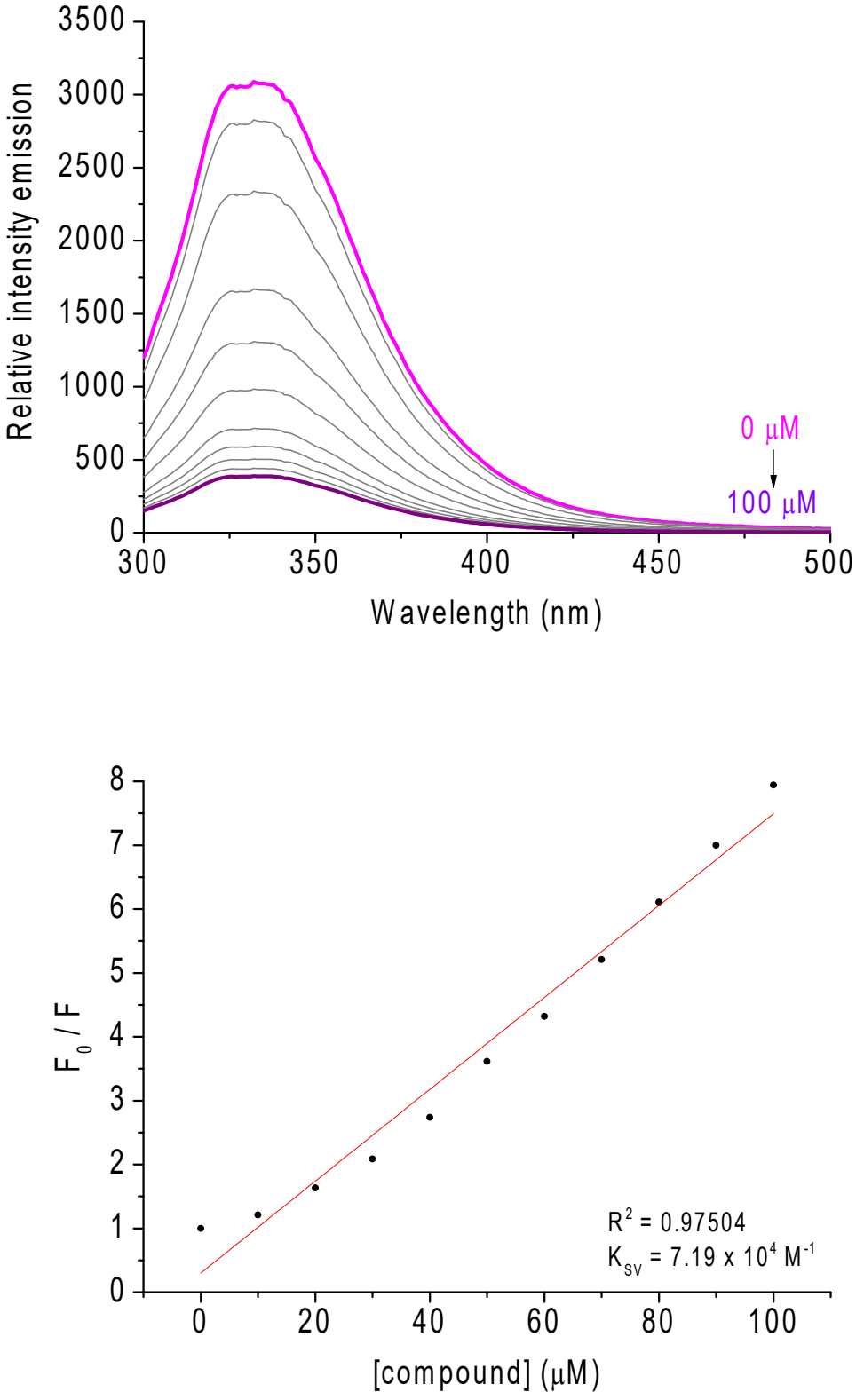

Fig. S88 Steady-state fluorescence emission spectra for HSA without and in the presence of dioxidovanadium(V) derivative **C3**, in DMF(5%)/Tris-HCl (pH 7.4) buffer solution. Graph shown the F_0/F *versus* [complex] plot.

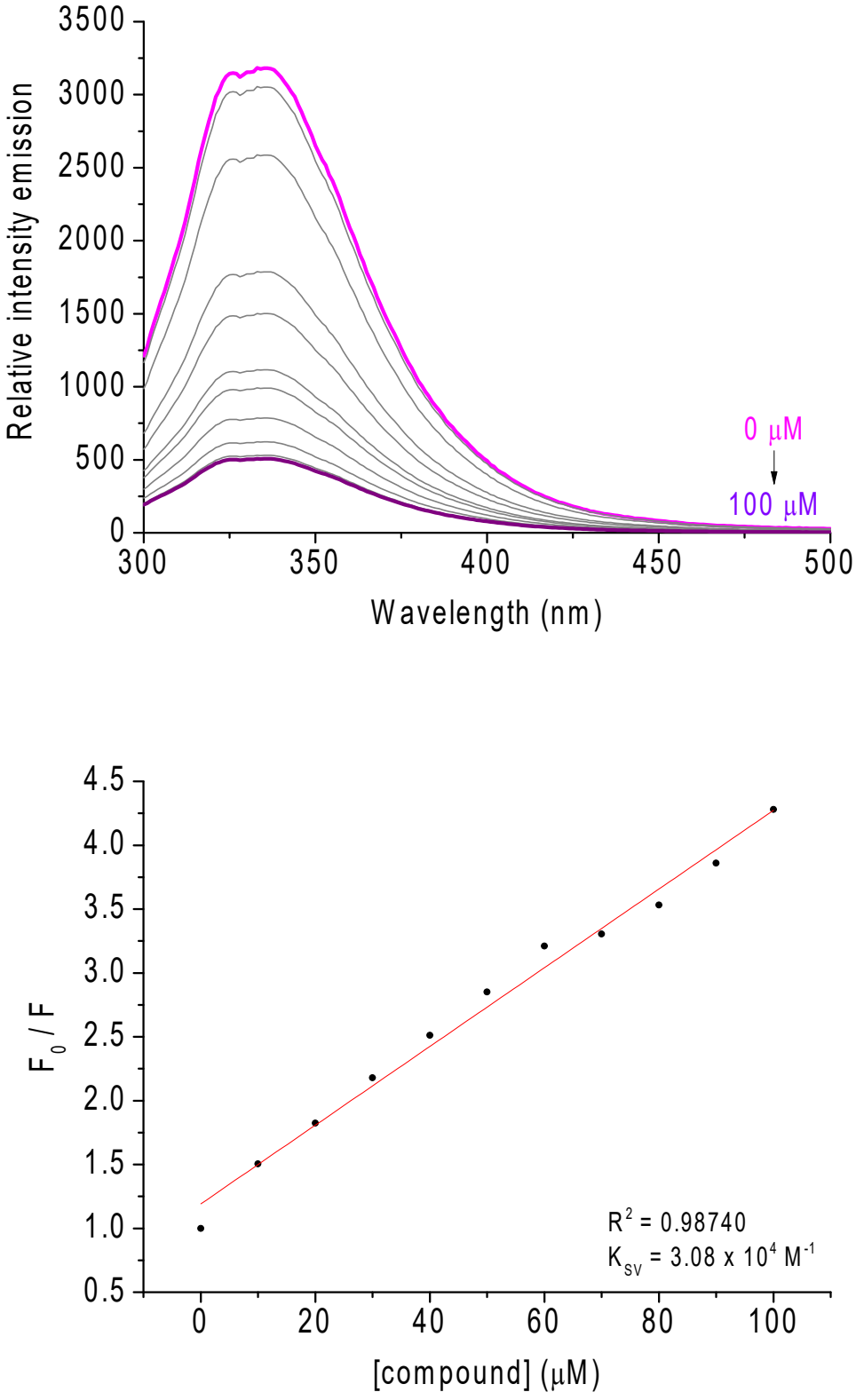

Fig. S89 Steady-state fluorescence emission spectra for HSA without and in the presence of dioxidovanadium(V) derivative **C4**, in DMF(5%)/Tris-HCl (pH 7.4) buffer solution. Graph shown the F_0/F *versus* [complex] plot.

Electronic Supplementary Information references

1 P. G. Kargar, G. Bagherzade and H. Eshghi, *RSC Adv.*, 2020, **10**, 32927–32937.
2 S. K. Sinniah, K. S. Sim, S. W. Ng and K. W. Tan, *J. Mol. Struct.*, 2017, **1137**, 253–259.
3 S. T. Chew, K. M. Lo, S. K. Sinniah, K. S. Sim and K. W. Tan, *RSC Adv.*, 2014, **4**, 61232–61247.
4 S. T. Chew, K. M. Lo, S. K. Lee, M. P. Heng, W. Y. Teoh, K. S. Sim and K. W. Tan, *Eur. J. Med. Chem.*, 2014, **76**, 397–407.
5 M. Mohanty, S. K. Maurya, A. Banerjee, S. A. Patra, M. R. Maurya, A. Crochet, K. Brzezinski and R. Dinda, *New J. Chem.*, 2019, **43**, 17680–17695.
6 N. Patel, A. K. Prajapati, R. N. Jadeja, R. N. Patel, S. K. Patel, I. P. Tripathi, N. Dwivedi, V. K. Gupta and Raymond. J. Butcher, *Polyhedron*, 2020, **180**, 114434.
7 S. P. Dash, A. K. Panda, S. Pasayat, R. Dinda, A. Biswas, E. R. T. Tiekink, Y. P. Patil, M. Nethaji, W. Kaminsky, S. Mukhopadhyay and S. K. Bhutia, *Dalton Trans.*, 2014, **43**, 10139.
8 S. D. Kurbah and R. A. Lal, *New J. Chem.*, 2020, **44**, 5410–5418.